TECHNISCHE UNIVERSITÄT MÜNCHEN

Fakultät für Chemie

Catalytic and electrocatalytic routes for hydrogenation of carbonyl compounds in aqueous phase

Laura Chantal Anna Meyer

Vollständiger Abdruck der von der Fakultät für Chemie der Technischen Universität München zur Erlangung des akademischen Grades einer

Doktorin der Naturwissenschaften (Dr. rer. nat)

genehmigten Dissertation.

Vorsitzender	Prof. Dr.-Ing. Kai-Olaf M. Hinrichsen
Prüfer der Dissertation	1. Prof. Dr. Johannes A. Lercher
	2. Hon.-Prof. Dr. Richard W. Fischer

Die Dissertation wurde am 09.05.2022 bei der Technischen Universität München eingereicht und durch die Fakultät für Chemie am 14.07.2022 angenommen.

Für meine Eltern.

Acknowledgments

I want to express my sincere gratitude to my advisor, Prof. Dr. Johannes A. Lercher for giving me the opportunity to perform my doctoral work at Pacific Northwest National Laboratory and the tremendous support throughout the course of the PhD. Your patient guidance, knowledge, and feedback during the often intense scientific group discussions made me learn and grow in my professional and personal life.

Furthermore, I want to thank my mentor Dr. Oliver Gutierrez, who helped me throughout these years. Thank you for pushing me forward, patiently listening to my worries and being there for answering any questions. You were always helping to understand any phenomena in the lab and supporting with corrections of drafts and presentation preparation.

My appreciation also goes to Dr. Udishnu Sanyal, who over time became a mentor. Your scientific motivation and many advice as well as our numerous electrochemical and catalytic discussions were very valuable. You always had an open ear and supported me, which I am thankful for.

Next, I would like to appreciate the kindness and guidance from Prof. Dr. Miroslaw Derewinski at the beginning and the help and discussions in catalysis, reaction engineering and EXAFS with Dr. Don Camaioni, Dr. Abhi Karkamkar, Dr. Juan Lopez-Ruiz and Dr. John Fulton. Further, I would like to thank Dr. John Linehan and Dr. Jon Egbert for any practical help in the lab. Also, thank you to my managers at PNNL throughout this time Dr. Aaron Appel, Dr. Janos Szanyi, Dr. Nancy Washton, and Dr. Wendy Shaw, as well as the PNNL administrative staff.

I also want to appreciate some of the great people I met, had many discussions and collaborations with and spent time off work: Prof. Dr. Manish Shetty, Dr. Lillian Hale, Julia Moreira, Cristina Padilla-Cintron, Dr. Thuy Le, Dr. Yang Qiu, Dr. Linxiao Chen, Dr. Honghong (Crystal) Shi, Dr. Katherine Koh, Dr. Amnon Ortoll-Bloch, Dr. Wesley Gillis, and Dr. Sebastian Prodinger. I had a fabulous time with you guys!

I also would like to thank my lab mates throughout the time in PSL 1603/1504, who always had a helping hand and made it an enjoyable working atmosphere, that is Dr. Yifeng Zhu, Dr. Meng Wang, Dr. Feng Chen, Dr. Jian Zheng, Dr. Sungmin Kim and Julian Schmid.

Furthermore, I am grateful for the senior scientists and administrative staff in TCII at TUM right at the beginning of this work, Prof. Dr. Andreas Jentys, Dr. Erika Ember, Stefanie Seibold and Bettina Federmann. Additionally, I am thankful for the help and Munich updates from the TCII group.

Finally, I would like to thank my family and friends for their enormous encouragement, love and always being there to help and to listen. I could not have gone through this without you.

Laura

May 2022

Abstract

Increasingly negative electric potential enhances the hydrogenation rates of aromatic carbonyl compounds on Pd. The interaction between the reactant and the metal is the main descriptor for different trends of hydrogenation and concurrent H_2 evolution. Identical increases in thermo- and electro-catalytic reduction rates with decreasing pH show that neutral and charged hydrogen addition steps may occur. Proton coupled electron addition, however, dominates under applied electric potential. The increase in rates with decreasing pH is caused by a weakening of the metal-H bond.

Kurzzusammenfassung

Ein zunehmend negatives elektrisches Potenzial erhöht die Hydrierungsraten von aromatischen Carbonylverbindungen an Pd. Die Wechselwirkung zwischen den Reaktanten und dem Metall ist der Hauptdeskriptor für die verschiedenen Trends der Hydrierung und der simultanen H_2-Entwicklung. Identische Erhöhungen der thermo- und elektrokatalytischen Reduktionsraten mit sinkendem pH-Wert zeigen, dass neutrale und geladene Wasserstoffadditionsschritte auftreten können. Bei angelegtem elektrischem Potenzial dominiert jedoch die protonengekoppelte Addition von Elektronen. Der Anstieg der Raten mit abnehmendem pH-Wert ist auf eine Schwächung der Metall-Wasserstoff Bindung zurückzuführen.

Symbols and Abbreviations

A	Surface area
a_i	Activity of species i
b	Tafel slope
BET	Brunauer-Emmet-Teller
BJH	Barrett-Joyner-Halenda
Btu	British thermal unit
BZH	Benzaldehyde
C_i	Concentration of species i
CV	Cyclic voltammetry
E	Electrode potential
E^o	Standard electrode potential
E_A	Activation energy
E_{eq}	Equilibrium potential
ECH	Electrocatalytic hydrogenation
Eq.	Equation
EXAFS	Extended x-ray absorption fine structure
f	Fugacity
f	F/RT
F	Faraday constant
FA	Furfuryl alcohol
FE	Faradaic efficiency
FID	Flame ionization detector
GC	Gas chromatography
GS	Ground state
HER	Hydrogen evolution reaction
H_{upd}	Hydrogen underpotential deposition
Hy	Heyrovsky reaction
i (I)	Faradaic current
ICP	Inductively coupled plasma

IHP	Inner Helmholtz plane
iR	Current-resistance
j	Current density
j_o	Exchange current density
j_{kin}	Kinetic current density
k	Rate constant
k^o	Intrinsic, potential independent, rate constant
K	Adsorption constant
K^o	Intrinsic, potential independent, equilibrium constant
KIE	Kinetic isotope effect
$\boldsymbol{l_0}$	Pd-Pd distance
L-H	Langmuir-Hinshelwood mechanism
LSV	Linear sweep voltammetry
μM	Micromolar concentration
mM	Millimolar concentration
MF	2-methyl furan
n	Number of electrons transferred
N	Amount of moles reacted
N_i	Particle number of species i
OCP	Open circuit potential
OCV	Open circuit voltage
OER	Oxygen evolution reaction
OHP	Outer Helmholtz plane
Ox	Oxidized species
p	pressure
PCET	Proton coupled electron transfer
PEIS	Potentiostatic electrochemical impedance spectroscopy
$Q_{H\text{-}UPD}$	Hydrogen underpotential deposition charge
r	Reaction rate
R	Ohmic resistance
R	Radius

R	Universal gas constant
RCHO	Carbonyl compound
RCHOH	Hydrogenated carbonyl intermediate
RCH_2OH	Hydrogenated carbonyl compound
RDE	Rotating disk electrode
Red	Reduced species
RHE	Reversible hydrogen electrode
rpm	Revolution per minute
RRDE	Rotating ring disk electrode
t	time
T	temperature
TCH	Thermal catalytic hydrogenation
TEM	Transmission electron microscopy
TOF	Turnover frequency
TS	Transition state
Vr	Volmer reaction
z_i	Valence of component i
α	Charge transfer coefficient
α-PdH_x	Palladium hydride ($x < 0.15$)
β-PdH_x	Palladium hydride ($x \geq 0.4$)
γ	Activity coefficient
ΔG	Gibbs free energy
ΔG^o	Standard Gibbs free energy
η	overpotential
θ_i	Coverage of species i
$\boldsymbol{\mu_i}$	Chemical potential of species i
$\boldsymbol{\bar{\mu}_i}$	Electrochemical potential of species i
$\boldsymbol{\mu_i^0}$	Standard chemical potential of species i
Φ	Inner (Galvani) potential
$\boldsymbol{\partial l}$	Expansion of Pd-Pd lattice
*	Active surface site

Table of Contents

Acknowledgments ..... **i**

Abstract ..... **iii**

Kurzzusammenfassung ..... **iii**

Symbols and Abbreviations ..... **iv**

Table of Contents ..... **vii**

1. Introduction **1**

1.1. General background 1

1.1.1. Lignocellulose feedstock 2

1.1.2. From biomass to bio-oil 3

1.2. Bio-oil upgrading 5

1.2.1. Importance of oxygen removal in biomass-derived compounds 5

1.2.2. Thermal upgrading of oxygenated compounds in aqueous phase 7

1.3. Theory background of electrocatalysis 9

1.4. Electrochemical hydrogenation of oxygenated compounds 14

1.4.1. Electrocatalytic reduction of model compounds in aqueous phase 14

1.4.2. Mechanistic studies of hydrogenation 20

1.5. Scope of this thesis 26

1.6. References 27

2. Influence of Molecular Structure on the Electrocatalytic Hydrogenation of Carbonyl Groups and H_2 Evolution on Pd **32**

2.1. Introduction 32

2.2. Results and discussion 33

2.2.1. Electrocatalytic hydrogenation of carbonyl compounds 33

2.2.2. Kinetics of electrocatalytic hydrogenation and competing H_2 evolution 36
2.2.3. Evaluating the interactions of organic compounds with Pd 39
2.2.4. Probing the state of Pd by EXAFS during electrocatalytic hydrogenation 41
2.3. Conclusion 42
2.4. Acknowledgements 43
2.5. Supporting information 44
2.5.1. Experimental methods 44
2.5.2. Characterization of the catalyst and quantification of the exposed Pd area .. 50
2.5.3. Complementary figures 52
2.5.4. Electrocatalytic hydrogenation of furfural 53
2.5.5. Kinetic models of electrocatalytic hydrogenation coupled with hydrogen evolution. 54
2.5.6. Determination of organic adsorption constants on Pd/C using a rotating disc electrode 65
2.5.7. X-ray Absorption Spectroscopy 67
2.6. References 68
3. Role of Hydronium ions for Controlling and Enhancing Catalytic Hydrogenation in Aqueous Phase 72
3.1. Introduction 72
3.2. Results and discussion 74
3.2.1. Electrocatalytic hydrogenation of benzaldehyde and acetophenone 74
3.2.2. Conversion of benzaldehyde and benzyl alcohol at varying pH 75
3.2.3. Effect of pH on hydrogen binding energy 76
3.2.4. Mechanisms for reduction in water 77
3.3. Conclusion 82

3.4. Acknowledgements 82
3.5. Supporting Information 83
3.5.1. Experimental methods 83
3.5.2. Influence of pH on benzaldehyde and acetophenone hydrogenation rates and pathways 86
3.5.3. Determination of the hydrogen binding energy on Pd at varying pH 91
3.5.4. Kinetic isotope effect in neutral and acidic pH 91
3.5.5. Kinetic derivation of hydrogenation mechanisms in water 92
3.6. References 94
4. Influence of Ionic Strength and Cation Type on Catalytic Hydrogenation 97
4.1. Results and discussion 97
4.2. References 103
5. Summary and Conclusion 104
List of Publications 106
List of Presentations 107

1. Introduction

1.1. General background

Nearly 100 million barrels of crude oil and other liquids were produced worldwide per day in 2021. As of today, more than 80% of the global energy consumption is based on fossil fuel resources i.e., primarily crude oil, natural gas, and coal. [1, 2] As economies and populations grow, the energy demand in the world will increase and due to the finite nature of fossil fuels alternative renewable energy resources must be developed. Figure 1.1 a) outlines the primary energy consumption in the US since 1950. Even so fossil fuels still prevail, the production and consumption of renewable energy has been increasing in the last few decades. [3]

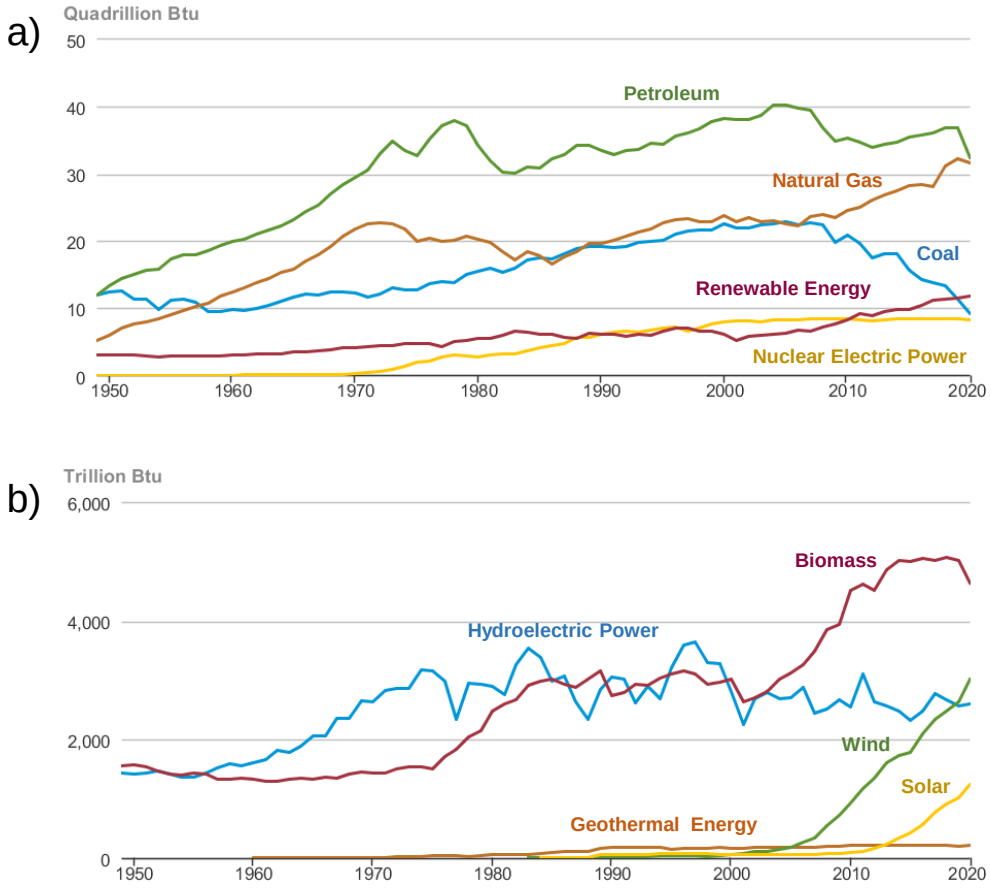

Figure 1.1. a) Primary energy consumption by source in the US since 1950. (Btu, British thermal unit); b) Renewable energy consumption by source in the US since 1950. Source: U.S. Energy Information Administration - Monthly Energy Review November 2021 [3]

The U.S. Energy Information Administration predicts an increase of renewable energy production to around 20 quadrillion Btu till 2050. [4] Out of the renewable energy sources like biomass, solar, wind, geothermal energy, and hydroelectric power, biomass particularly gained interest and a strong increase in consumption and is currently one of the main sources for renewable energy (Figure 1.1 b). [3] In addition, biomass is especially important as it is the only current renewable resource to produce liquid transportation fuels, chemicals, and carbon-based materials. [5, 6]

1.1.1. Lignocellulose feedstock

Biomass is a general term for all organic material that is derived from growing plants or from animal manure (processed version of plant matter). Typical feedstocks for the production of renewable energy include agricultural and forest residues, energy crops, and algae. Through photosynthesis plants store radiant energy from the sun as chemical energy in the form of carbohydrates. [7, 8] Lignocellulosic biomass constitutes the major components of plant cell walls and is therefore the most abundant plant material and an excellent renewable resource to produce sustainable transportation biofuels.

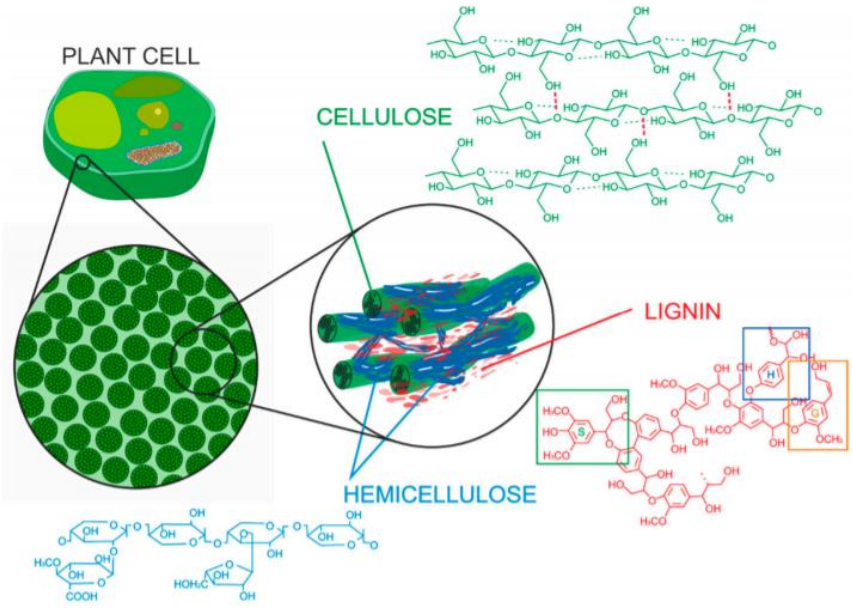

Figure 1.2. Structure of the different components of lignocellulosic biomass: cellulose, hemicellulose, and lignin. (Open access Ref. [9])

Lignocellulose consists of oxygen-containing organic polymers i.e., cellulose (28 - 55 wt.%), hemicellulose (17 - 35 wt.%) and lignin (17 – 35 wt.%). Hemicellulose and lignin form a cross-

linked matrix which encloses the cellulose fibers, where lignin provides the mechanical strength and hydrophobic character to plant cell walls. [9, 10] Cellulose is composed of linear polysaccharides with D-glucopyranose monomers connected through β-1,4 linkages. It is a high-molecular-weight polymer with a polymerization degree of around 10,000 glucopyranose monomer units in wood (green, Figure 1.2). Hemicellulose consists of shorter polymer chains with around 200 sugar units, partly branched, and features several sugars besides glucose (blue, Figure 1.2). Lignin is a highly branched and substituted aromatic polymer and consists of an irregular array of "hydroxyl"- and "methoxyl" substituted phenylpropane units. Three main types of phenylpropane monomers are p-coumaryl alcohol (H), coniferyl alcohol (G), and sinapyl alcohol (S) (red, Figure 1.2). [9-12]

1.1.2. From biomass to bio-oil

Current research focuses intensely on so called "drop-in" biofuels. These biomass-based hydrocarbon fuels are molecularly identical to petroleum-derived fuels which they are designed to replace and are fully compatible with existing refineries and end-use infrastructure. Fossil fuels are characterized by a high degree of hydrocarbon saturation and the near absence of oxygen. This applies for almost all kinds of transportation fuels like gasoline, diesel, and jet fuels. [13] Drop-in biofuels can be produced via several processes, the main of which are (i) hydroprocessing of oleochemical feedstocks from oil crops, algae or tallow; (ii) thermochemical conversion of lignocellulosic biomass to fluid intermediates (gas or oil) which are catalytically upgraded in a second step; and (iii) biochemical conversion of sugars or cellulosic material to longer chain alcohols and hydrocarbons. [14] Oleochemical processing only requires the catalytic removal of oxygen, by hydroprocessing, from the fatty acid chains present in the lipid material to produce diesel-like hydrocarbons i.e., renewable diesel. Lipid feedstocks are advantageous due to their lower oxygen content and therefore, lower amount of hydrogen is needed to produce petroleum-like fuel. However, the cultivation and use of lipid feedstocks for fuel generation are often limited due to the competition and demand with other industries i.e., food and cosmetics. Additionally, its production is land and resource intensive and thus more costly. [15] During biochemical conversion i.e., low-temperature deconstruction, the physical structure of the cell walls opens up in a first pretreatment step, followed by a breakdown of the accessible polysaccharides through enzymatic or chemical hydrolysis. Thus, only the cellulose and hemicellulose fraction of lignocellulosic biomass can be utilized in this process. [5, 6] Both procedures i.e., oleochemical processing and

biochemical conversion are promising but not the focus of this work and not further elaborated. Thermochemical conversion i.e., high-temperature deconstruction, utilizes whole lignocellulosic biomass. As lignocellulosic biomass is the most abundant source of plant biomass and most inexpensive, it is worthwhile to convert the whole material to liquid fuels. [10] To break down the tough rigid plant cell walls lignocellulosic biomass is converted into liquid or gaseous intermediates by extreme heat and pressure using one of these three primary processes: pyrolysis, hydrothermal liquefaction, and gasification. [14] Hydrothermal liquefaction of biomass occurs under moderate temperatures (200°C – 350°C) and elevated pressures in water. It is therefore favored for wet feedstocks and produces liquid bio-oil with high H/C ratios. During the process lignocellulosic carbon chains are thermally cracked and oxygen is removed as H_2O (dehydration) and CO_2 (decarboxylation). [14, 16] The gasification process consists of exposing the organic material to temperatures above 700°C with injections of controlled amounts of molecular oxygen and/or steam to produce synthesis gas (syngas). Syngas is a mixture primarily consisting of carbon monoxide and hydrogen. It can be used for electricity generation and can also be catalytically upgraded to synthetic fuel via the Fischer-Tropsch process. [14, 17] Pyrolysis is the simplest technology leading to the most cost-effective renewable biofuels. During this process, lignocellulosic material is thermally decomposed into short chain molecules by the rapid heating at temperatures between 400 and 600 °C, gas residence times below two seconds, and in the absence of molecular oxygen. These conditions result in several reactions occurring e.g., depolymerization, dehydration and C-C bond cleavage. After rapid cooling and quenching the pyrolysis vapor and aerosol condense into pyrolysis- or bio-oil, a complex mixture of hundreds of oxygenated compounds with additional moisture from the starting material. Thus, the thermally decomposed products of cellulose, hemicellulose and lignin retain a content of carbon, hydrogen, and oxygen like that of the initial bio-feedstock. [10, 18, 19]

1.2. Bio-oil upgrading

1.2.1. Importance of oxygen removal in biomass-derived compounds

Although bio-oil can be processed in a simple way, its properties result in multiple significant complications and upgrading is imperative. The direct utilization of raw bio-oil as transportation fuel in standard equipment like combustion boilers, engines, and turbines developed for petroleum-based fuels leads to serious challenges like ignition and combustion difficulties, coking, clogging and engine seizure. [10, 20] Bio-oil is neither suited as a single feedstock in crude oil refineries nor blended with conventional petroleum due to excessive coke deposition leading to lower gasoline yields. [19] In addition, raw bio-oil is not at thermodynamic equilibrium, thus its chemical composition is not stable and tends to change during storage. [18] When comparing bio-oil to conventional fuel oil the elemental composition is distinctly different, since bio-oil consists of variously sized oxygenated compounds derived from deconstructed lignocellulosic feedstocks. Table 1.1 represents an overview of various bio-oil and fuel oil characteristics [18, 19].

Table 1.1. Typical physical properties of pyrolysis bio-oil derived from biomass and petroleum-based fuel oil. (Reprinted with permission from Ref. [19]. Copyright © 2014 Royal Society of Chemistry)

Analysis	Pyrolysis oil	Fuel oil
C, dry (wt.%)	56	85
H, dry (wt.%)	6	11.1
O, dry (wt.%)	38	1
Water (wt.%)	20-30	0.025
Solids (wt.%)	0.01-0.1	0
Ash (wt.%)	0.01-0.2	0.01
Nitrogen (wt.%)	0-0.4	0
Sulfur (wt.%)	0-0.05	0.2
Stability	Unstable	Stable
Viscosity @40 °C	15-35	3.0-7.5
Density @15 °C	1.10-1.30	0.89
Flash point (°C)	40-110	60
Pour point (°C)	-9 to -36	-15
LHV (MJ kg-1)	13-18	40.3
pH	2-3	Neutral
Boiling range	Decomposes	160-400 °C

The high oxygen content of bio-oils, usually between 20 to 50 wt.% distributed in more than 200 compounds, creates compatibility issues between bio-oils and hydrocarbon fuels and its infrastructure. [21, 22] The high oxygen content also leads to lower energy density compared to conventional fuels by 50%. Major groups of compounds, apart from water, include simple

oxygenates (e.g., aldehydes, ketones, acids, alcohols, esters), furans (e.g., furfural, hydroxymethyl furfural), miscellaneous oxygenates, sugars, phenolics, and high-molecular weight compounds. Furans, miscellaneous oxygenates and sugars are mainly derived from cellulose and hemicellulose fractions of biomass, while phenolics come from the lignin part of biomass. Simple oxygenates like aldehydes and ketones are likely generated by decomposition of furans, miscellaneous oxygenates and sugars. [10, 18, 23-25] The strong acidity (pH of 2-3), caused by a substantial amount of carboxylic acids, makes bio-oil extremely corrosive and unstable. [18] Several of these oxygenated organics and oxygen functional groups, such as aldehydes, ketones, phenolics and the acids are reactive, undergoing intertwining interactions and complicating bio-oil storage as well as downstream processes. [26] Aldehydes require careful attention since they can react with phenolics and polymerize to higher molecular weight compounds via aldol condensation or even increase bio-oil viscosity by forming resins and cause solid formation.[27, 28] A water content of 20-30 wt.% of bio-oil based on the original moisture in the lignocellulosic feedstock and from dehydration during biomass deconstruction and storage causes the lower heating value and flame temperature during combustion when bio-oil is used directly in the engine. [18] Further, bio-oils show a wide range of boiling point temperatures due to the complex composition. This induces the polymerization of the reactive components during distillation leaving 35-50 wt.% solid residues. In conclusion, bio-oils are highly oxygenated and molecular complex mixtures making extensive oxygen removal a requirement for the upgrading of bio-oils to liquid transportation fuels. [10, 18, 19] Particularly the reduction of the carbonyl content, which distributes among aldehydes, ketones and sugars improves the bio-oil quality. There, abundant aromatic aldehydes exhibit a carbon yield of up to 18%. [29, 30] For a better understanding of bio-oil upgrading and due to the complexity and variability of bio-oil, fundamental studies on simple model compounds, representing the main functional groups of the oxygenates like carbonyls are crucial. Through this, analysis of reaction pathways and catalytic reactivity of single compound groups can be predicted and are simplified relative to the complicated original feedstock.

1.2.2. Thermal upgrading of oxygenated compounds in aqueous phase

The adverse properties of bio-oil necessitate the reduction of its oxygen content. In oil refineries, hydroprocessing i.e., hydrogen-consuming processes like hydrotreating and hydrocracking, are common procedures to upgrade low grade crude oil at elevated temperatures and pressures. Heteroatom impurities, like sulfur and nitrogen, are removed during hydrotreating (hydrodesulfurization and hydrodenitrogenation, respectively) and longer hydrocarbon chains are "cracked" into shorter ones and enriched with hydrogen during hydrocracking. The same principles can be applied in biofuel processing to upgrade oxygen-rich bio-oil after biomass deconstruction. Hydrodeoxygenation (HDO) i.e., oxygen removal, which is often accompanied by hydrogenation (saturation) of the lignocellulose derived feedstock, lead to hydrocarbons that are functionally equivalent to petroleum-based fuels. [14, 31] During HDO, the oxygen content is reduced by C=O bond hydrogenation, C-O bond cleavage, and C-H bond formation. In this way, oxygen can be expelled as H_2O (dehydration), CO_2 and CO (decarboxylation and decarbonylation, respectively). Oxygen removal as water is preferred as CO_2 and CO formation lead to lower carbon yields. [19, 32] Hydrogenation is important for the enhancement of H/C ratios in bio-oils by saturating e.g., olefins and aromatic rings. As most biomass feedstocks have a low H/C ratio compared to fossil derived feedstocks, high H/C ratio are required for the substitution of traditional fuels with bio-oil derived ones. Through this HDO increases the energy density and stability of bio-oil. Major HDO reactions occurring on bio-oil organics are shown in Figure 1.3. The HDO procedure occurs at high H_2 pressures (usually > 70 bar) and temperatures between 127 and 500 °C in the presence of supported transition metals (noble and base metals) or Mo-based sulfide catalysts. [10, 31, 33] Sulfide catalysts have been extensively used in petroleum hydrotreating processes. They are, however, disadvantageous for applications in bio-oil upgrading. In order to prevent catalyst deactivation, the sulfide form must be maintained by adding sulfur compounds to the feed increasing bio-oil's beneficial low sulfur concentration. [34, 35] Supported noble metals (e.g., Ru, Pd, Pt and Rh), on the other side, have aroused great attention as non-sulfide-based hydrotreating catalysts as they lead to higher hydrocarbon yields and deoxygenation levels. [36, 37]

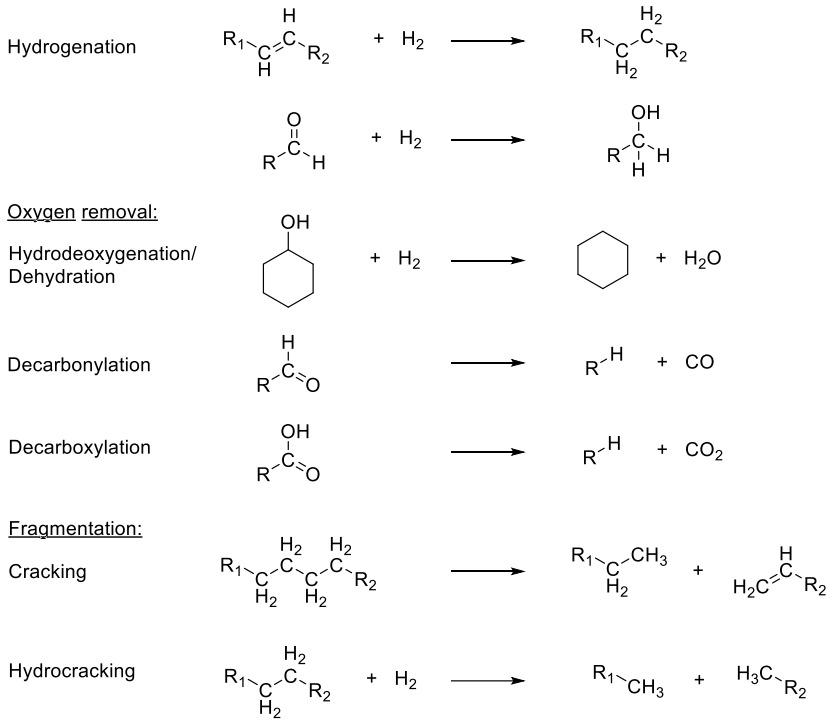

Figure 1.3. Main organic reactions i.e., hydrogenation, oxygen removal and fragmentation during HDO of bio-oil. (Adapted with permission from Ref. [19]. Copyright © 2014 Royal Society of Chemistry)

A main drawback of conventional hydrotreating treatment is the high temperature instability of bio-oil components, leading to a high propensity of coke formation and consequently deactivation of the catalyst and even plugging of the reactor during hydroprocessing. [10, 28, 38] Further, the high H_2 pressures require external H_2 supplies, which result in high operating costs and energy demands. [39, 40] However, since bio-oil exhibits a high-water content, the possibility for electrocatalytic hydrogenation and deoxygenation in aqueous phase opens up. Electrochemical upgrading poses an outstanding alternative to the traditional catalytic high-pressure/-temperature processing. Here, bio-oil stabilization can be realized under mild conditions i.e., low or ambient temperatures and pressures, and under exclusion of external hydrogen. Upon applying of a cathodic bias surface hydrogen is formed *in situ* on the cathode avoiding the need for additional molecular H_2. In the upgraded bio-oil, electrical energy is preserved in new formed chemical bonds, representing a time-insensitive method for connecting intermittent, renewable electricity with liquid fuels. [38, 39, 41] This is further elaborated in the next two chapters.

1.3. Theory background of electrocatalysis

General concepts

Electrocatalysis has received global attention in recent years as a sustainable and efficient way for energy supply and energy storage. The two basic classifications of electrochemical reactions are galvanic and electrolytic systems. In galvanic systems like fuel cells, reactions occur spontaneously. By combining hydrogen and oxygen in a controlled fashion, chemical energy is directly converted into electricity. In electrolytic processes i.e., non-spontaneous reactions, the reverse is employed. Here, a current or potential is applied to drive a chemical reaction storing electrical energy in chemical bonds. During the well-known electrolysis reaction, water is split on the anode site into oxygen and protons (oxygen evolution reaction - OER). The latter migrates to the cathode through the electrolyte and reduces to hydrogen on the surface (hydrogen evolution reaction – HER). Storing electrical energy in molecular oxygen and hydrogen. Therefore, electrochemistry depends on the processes of electron transfer occurring at the solution/electrode boundary making a detailed description of this interface essential. [42-44]

The hydrogen evolution/oxidation reactions are subject to numerous investigations and are one of the most intensely studied topics in electrochemistry. Focusing on the hydrogen evolution reaction in acidic media in this work, it is generally accepted that it can be categorized into three elementary steps. First, adsorbed hydrogen is generated by the reduction of hydronium ions in solution or water (Volmer step (i), (ii)). Followed by the actual HER, which can either proceed through the reaction of adsorbed hydrogen with hydronium ions/water and the additions of electrons (Heyrovsky step (iii), (iv)) or the combination of two adsorbed hydrogens (Tafel step (v)). [45-48] Here, the steps are reported for the reaction occurring in acidic media:

Volmer step (acidic):	$H_3O^+ + e^- + * \rightarrow H^* + H_2O$	(i)
Volmer step (basic):	$H_2O + e^- + * \rightarrow H^* + OH^-$	(ii)
Heyrovsky step (acidic):	$H^* + H_3O^+ + e^- \rightarrow H_2 + H_2O + *$	(iii)
Heyrovsky step (basic):	$H^* + H_2O + e^- \rightarrow H_2 + OH^- + *$	(iv)
Tafel step:	$2\ H^* \rightarrow H_2 + 2*$	(v)

* represents a free active surface site and H* an adsorbed hydrogen on the catalyst surface.

Electrode processes are a special kind of heterogenous surface reactions due to transfers of electrons on the surface. The boundary between a solid and aqueous phase can be described by the electric double layer i.e., the arrangement of charged species and oriented dipoles on the metal surface (Figure 1.4). Closest to the electrode, an inner Helmholtz plane (IHP) is formed by solvent molecules and non-solvated ions which adsorb strongly onto the electrode surface through chemical bonds. An outer Helmholtz plane (OHP) is formed through solvated ions of opposite charge to the electrode held away by the hydration shell in proximity to the electrode surface. The charge separation of the OHP and the electrode surface leads to a double-layer capacitance of the electrode-solution interface. To account for the thermal motion of ions in the electrolyte, which disperses the outer plane of charge, the range from the OHP to the bulk is defined as the diffuse layer in which ions are freely distributed. [49-51]

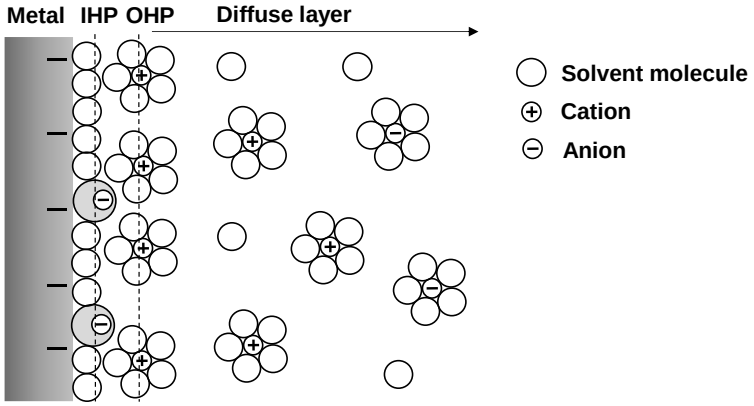

Figure 1.4. Model of the electric double layer of solvated anion and cations on a negatively charged metal surface. Arrangement of inner Helmholtz plane (IHP), outer Helmholtz plane and diffuse layer are defined. (Adapted from Ref. [51] and adapted with permission from Ref. [52]. Copyright © 2018 American Chemical Society)

Thermodynamics

The following equilibrated reduction reaction is a simple possible electrode process, wherein the oxidized species Ox and the reduced species Red engage in an electron transfer (n number of electrons involved) at the interface:

$$Ox + ne^- \rightleftharpoons Red \qquad \text{(vi)}$$

At equilibrium the activities of the oxidized and the reduced species can be related to the Gibbs free energy ΔG by:

$$\Delta G = \Delta G^0 + RT \ln\left(\frac{a_{Red}}{a_{Ox}}\right) \qquad (1.1)$$

where R is the gas constant (8.314 J mol^{-1} K^{-1}), T is the temperature, ΔG^0 is the standard Gibbs free energy and a_i is the activity of species i. The activity a_i is related to the concentration C_i and pressure p_i by $a_i = \gamma_i\, C_i$ for ions and liquids, $a_i = f_i\, p_i$ for gases and $a_i = 1$ for solids or dilute solutions. γ_i is the activity coefficient and f_i the fugacity, both account for deviations from ideal mixtures of chemical components. Commonly, ideal conditions are assumed and γ_i and f_i are taken to be 1. Following Eq. (1.1), the Gibbs free energy is further defined by the electrode or cell potential:

$$\Delta G = -nFE \qquad (1.2)$$

with the Faraday constant F (96485 C mol^{-1}), the stochiometric number n of electrons transferred during reaction and the maximum potential between two electrodes, the cell potential E. When all substances are at unit activity, the standard Gibbs free energy can be expressed as follows:

$$\Delta G^0 = -nFE^0 \qquad (1.3)$$

where E^0 is the standard electrode potential. In case of an electrolytic process the overall reaction is endergonic ($\Delta G^0 > 0$) and for galvanic reactions it is exergonic ($\Delta G^0 < 0$). Note that the standard electrode potential is negative for electrolytic and positive for galvanic processes. Substituting Eq. (1.2) and (1.3) into (1.1), relate the reduction potential of a reaction to the activities of the chemical species undergoing reduction and oxidation, a central correlation in electrochemistry. This mathematical expression is known as the Nernst equation and is only valid at equilibrium:

$$E = E^0 + \frac{RT}{nF} \ln\left(\frac{a_{Ox}}{a_{Red}}\right) \qquad (1.4)$$

The Nernst equation can be used to determine the reduction potential of a half-cell reaction or the total voltage of a cell reaction. [51, 53, 54] When a redox couple is present at each electrode in a cell with no liquid junctions arising and the system contains a cathodic current balanced by an equal and opposite anodic current, the Nernst equation can be applied to calculate the open circuit potential (OCP). In this case it also represents the equilibrium potential. In general, the OCP is defined as the resting potential between two terminals in an electrochemical system when no current is transferred in the cell. Thus, to measure the OCP, the chemical system does not have to be at equilibrium. [51]

The driving force of any chemical or physical system is important to describe its energetic state i.e., the direction in which the system can spontaneously move and its position of equilibrium (driving force of zero). In chemistry, the driving force is defined as the gradient of the partial molar Gibbs energy i.e., chemical potential μ_i:

$$\mu_i = \left(\frac{\partial G}{\partial N_i}\right)_{p,T,N_{j\neq i}} \tag{1.5}$$

where, ∂G is the infinitesimal change of Gibbs free energy, ∂N_i is the infinitesimal change of particle number N_i of a species i and p the pressure. [49] According to Eq. (1.1) the chemical potential relates to the activity of a species under ideal conditions through:

$$\mu_i = \mu_i^0 + RT \ln(a_i) \tag{1.6}$$

where μ_i^0 is the standard chemical potential and the activity a_i is linked with the concentration by the activity coefficient ($a_i = \gamma_i\, C_i$) as mentioned previously. To account for the effect of electric field during electrochemical reactions, a new thermodynamic function, the electrochemical potential $\bar{\mu}_i$, is defined by:

$$\bar{\mu}_i = \mu_i + z_i F\Phi = \mu_i^0 + RT \ln(a_i) + z_i F\Phi \tag{1.7}$$

$z_i F\Phi$ represents the work done by the electric potential. Here, z_i is the valence of component i and Φ depicts the inner (Galvani) potential on the electrode. [51, 55]

Electrode kinetics

The overpotential, a primary parameter in this work, is defined as the deviation of the electrode or cell potential from its thermodynamic equilibrium potential upon the passage of faradaic current and occurrence of redox events. This implies that in galvanic cells less energy is obtained than thermodynamically expected. Whereas in electrolytic cells, more energy is necessary than thermodynamics anticipate to drive a reaction. In both systems the lost energy (galvanic cell) or additionally needed energy (electrolytic cell) is wasted in heat. Therefore, for a non-spontaneous (electrolytic) reaction to occur, the overpotential η must be applied:

$$\eta = E - E_{eq} \tag{1.8}$$

where E is the electrode potential and E_{eq} the equilibrium potential. [53, 56]

Electrode processes are heterogenous reactions which occur at the electrode-solution interface. As any heterogeneous reaction they rely on mass transfer of the electroactive species from the bulk to the electrode and microkinetic surface effects. When charge, i.e., electrons, is transferred across the catalyst-electrolyte boundary due to an applied bias, oxidation or reduction reactions arise. Following Faraday's law, the rate of electrochemical reaction is direct proportional to the faradaic current (density). These reactions are called faradaic or charge-transfer processes.

$$Rate\ \left(\frac{mol}{s}\right) = \frac{dN}{dt} = \frac{i}{nF} \tag{1.9}$$

$$Rate\ \left(\frac{mol}{cm^2 s}\right) = \frac{i}{nFA} = \frac{j}{nF} \tag{1.10}$$

N is the amount of moles reacted and i the faradaic current. Since, the total current depends on the electrode size, it must be normalized to the electrode surface area A, yielding the current density j.[51, 53]

The correlation between the applied potential and the resulting kinetic current for a reversable process is described by the Butler-Volmer equation. A derivation is beyond the scope of this study and not outlined.

$$j_{kin} = j_0 \left[exp\left(-\frac{\alpha nF}{RT}\eta\right) - exp\left(\frac{(1-\alpha)nF}{RT}\eta\right)\right] \tag{1.11}$$

j_{kin} stands for the kinetic current density and j_0 represents the exchange current density, which is defined as the current density obtained at zero overpotential during the electrochemical reaction. j_0 determines the charge transfer rate at equilibrium and indicates the ability for the electrode reaction to proceed. α is the charge the transfer coefficient, a dimensionless parameter which indicates the symmetry of the reaction energy barrier between the anode and cathode. α is the proportion of the activation energy E_A for the oxidation. Thus, (1-α) depicts the part of E_A necessary for the reduction on the cathode. Its value is within the interval 0 to 1, while a symmetric reaction has α = 0.5. Note, Eq. (1.11) is only valid when mass-transfer limitation can be neglected i.e., when the electroactive species concentration at the surface is equal to the bulk electrolyte. Thus, during charge transfer processes, it is characteristic for Butler-Volmer kinetics to demonstrate an exponential increase of current density with applied overpotential. [57, 58]

For large overpotential values (> 50 or 100 mV) the Butler-Volmer equation can be simplified to the Tafel equation. Specifically, the term corresponding to the opposite reaction (compared to the reaction of interest) is negligible and an irreversible reaction is established. [57]

$$\eta = \frac{RT}{\alpha F}\ln j_o - \frac{RT}{\alpha F}\ln j \tag{1.12}$$

$$\eta = a + b\log(j) \tag{1.13}$$

Where $a = \frac{2.3RT}{\alpha nF}\log j_o$, $b = -\frac{2.3RT}{\alpha nF}$, which is the Tafel slope (mV dec^{-1}), and j is the current density. From a the exchange current density j_0 can be directly measured. The Tafel analysis explores the sensitivity response of electric current upon applied potential for a reaction, leading to insights about the electric rate determining step. [42, 53]

1.4. Electrochemical hydrogenation of oxygenated compounds

1.4.1. Electrocatalytic reduction of model compounds in aqueous phase

Electrocatalytic hydrogenation (ECH) integrates electrolysis i.e., the splitting of water into molecular hydrogen and oxygen, and the reduction of organic compounds. Through this, electrical energy is stored in the form of chemical bonds in upgraded bio-oil compounds, increasing the energy density and providing the opportunity of linking renewable electricity with biofuels. ECH is analogous to conventional thermocatalytic hydrogenation (TCH) or open circuit voltage hydrogenation (OCV), where thermal and external H_2 inputs are replaced by applied cathodic potentials. In this way, adsorbed hydrogen is electrochemically generated in situ on the electrode surface by hydronium ion/protons or water reduction (Volmer step (i), (ii)), bypassing the kinetic barrier of thermal dissociation of molecular H_2 during TCH and enabling the reduction of biogenic compounds at mild conditions in ECH. A second advantage of ECH over TCH is the avoidance of the mass transport limitations of the poorly soluble molecular H_2. [59-61] Thus, externally applied potentials offer another parameter for which hydrogenation reactivity on the catalyst can be controlled. However, ECH is often in competition with the prevalent side reaction i.e., hydrogen evolution reaction (HER), for reduction equivalents. The adsorbed hydrogen can react towards hydrogenation of the adsorbed organic substrate via addition of neutral adsorbed hydrogen or towards HER through Tafel or Heyrovsky steps (see chapter 1.3) lowering the faradaic efficiency (FE), which is defined as the selectivity of electrons reducing the organic compared to the overall

current passed. An electrochemical hydrogenation step is also possible in which the adsorbed organic reacts via a proton coupled electron transfer (PCET) step (Figure 1.5). [29, 41, 62]

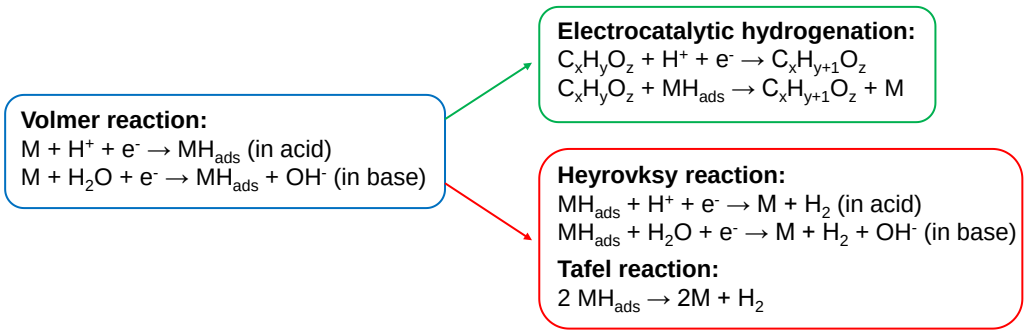

Figure 1.5. Processes during electrocatalytic hydrogenation: Adsorbed hydrogen generation (Volmer step), followed by organic hydrogenation or side reaction hydrogen evolution reaction. (Adapted with permission from Ref. [41]. Copyright © 2018 American Chemical Society)

In this chapter an overview of the hydrogenation of typical biomass-derived carbonyl model compounds present in bio-oil feedstocks is given. This includes aromatic, heterocyclic, and aliphatic aldehydes and ketones like benzaldehyde, acetophenone, furanic compounds and cyclohexanone.

Generally, the reactivity of aromatic rings strongly depends on the substituting functional groups on the ring. Benzene, the simplest molecule, is known to bind to the metal surface through the interaction of its π-electrons with the metal surface and is readily hydrogenated to cyclohexane. The presence of e.g., methyl-substituents decreases the hydrogenation rate during ECH as well as the efficiency towards hydrogenation. [63, 64] This can be assigned to the organic-metal interaction strength, which reduces with higher steric hindrance of the substituents. Carbonyl groups can even fully suppress ring hydrogenation, while the carbonyl groups themselves undergo reduction to hydroxyl groups. [11, 29] Aromatic aldehydes and ketones are readily hydrogenated to hydrocarbons unless the molecules are sterically hindered. The hydrogenation can proceed in two paths: hydrogenation of only the carbonyl functional group forming the corresponding alcohol, which is more commonly observed and typically under electrochemical conditions, and hydrogenation of the aromatic ring, resulting in saturated alcohols or carbonyls. In contrast, aliphatic carbonyls are harder to reduce and preferentially lead to the formation of the alcohol species. [61, 65, 66] Noble metals are particularly active for the electrocatalytic hydrogenation of organic bio-oil based compounds. For example, palladium is inefficient for hydrogenation of saturated aliphatic ketones

but exceptional for the reduction of aromatic ketones. Pd is widely used for the hydrogenolysis of aromatic ketones as it exhibits good activity for hydrogenation and hydrogenolysis of the carbonyl group with low activity for the aromatic ring saturation. [29, 65] Overall, the hydrogenation of an organic strongly depends on the functional group, the nature of the catalyst, and the surrounding chemical environment like pH and electrolyte composition. [28]

Benzaldehyde:

Benzaldehyde, the simplest aromatic aldehyde, shows high reactivity towards hydrogenation under applied potential on noble metals in aqueous electrolyte. Pd supported on C is the most active metal, followed by Rh/C and Pt/C. The same trend is observed under thermocatalytic hydrogenation conditions at 1 bar H_2, but with comparatively lower rates. Remarkably, on Pd HER is nearly suppressed, leading to Faradaic efficiencies of ~100% with minimal changes when varying the reduction potential. Further, the ECH rates increased as a function of the cathodic potential on all metals. The reaction kinetics is zero order in benzaldehyde on Pd, while it is first order on Pt and Rh. Ni/C was also investigated and reactive for benzaldehyde ECH, however at higher negative potentials compared to noble metals (passivating hydroxide layer form at less negative potentials) and lower FE. Under TCH conditions, no conversion was observed. On all metals under ECH and TCH conditions, benzaldehyde was exclusively reduced to benzyl alcohol, while the aromatic ring was unreactive. This product selectivity is explained by the impact of substituting groups leading to a decrease in organic adsorption strength. [29] Several groups investigated the influence of alcohols addition and acids to the electrolyte altering FE and hydrogenation rates. Polcaro's study showed that an ethanol containing electrolyte led to FE below 10% for the ECH of benzaldehyde to benzyl alcohol on Pd. [67] Lopez-Ruiz et al. performed ECH reactions of benzaldehyde to benzyl alcohol in a flow fixed-bed reactor studying the impact of methanol, ethanol, or isopropanol added to the aqueous electrolyte. They report a decrease in hydrogenation rates and FE with increasing alcohol concentration, while HER stayed constant. The negative impact on the ECH activity increased with longer hydrocarbon chain of the alcohol. Lastly, an increase of benzaldehyde reaction orders from around zero to nearly 1 were observed with increasing negative applied potential. Using kinetic analysis, it was interpretated as a change in organic and hydrogen coverage in dependence of the reduction potential. [68] A change in pH from basic to acidic conditions for the ECH of benzaldehyde in a hydroalcoholic solution resulted in the formation of the hydrogenolysis product, toluene, on Pt and Pd (Figure 1.6). [69] Reduction

experiments on several metals i.e., Pt, Pd, Au and Cu revealed the unique ability of Cu to perform C-C coupling of benzaldehyde to the dimer product, hydrobenzoin, apart from the typical product benzyl alcohol. [70]

Vannice et al. showed how the support for different Pt catalysts for the thermocatalytic hydrogenation of benzaldehyde influence conversion and product selectivity. Pt/TiO_2 was the most active with 4-10 times higher TOFs than on Pt/SiO_2 and Pt/Al_2O_3 and a nearly 100% selectivity towards benzyl alcohol, while the latter two catalysts began to form toluene and benzene at conversions above 20%. They showed that benzene is only produced by the hydrogenolysis of benzaldehyde while toluene is generated from the hydrogenolysis of benzyl alcohol. [71]

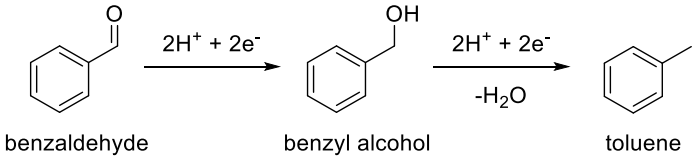

Figure 1.6. Reaction scheme of benzaldehyde hydrogenation and hydrogenolysis to benzyl alcohol and toluene, respectively.

Furanic compounds:

Furfural, a hydrolysis and dehydration product of hemicellulose in biomass, hydrogenates commonly to furfuryl alcohol (FA) and 2-methyl furan (MF), the hydrogenolysis product (Figure 1.7). Apart from the use in biofuels, FA and MF can also be utilized in the production of e.g., polymers and fine chemicals. [62, 72] Initially, during ECH of furfural the primary product was reported as furfuryl alcohol. The Belgsir group studied furfural reduction on Cu deposited graphite felt cathodes in neutral phosphate buffer leading to the sole formation of FA. [73] Zhao et al. reported 99% selectivity of furfural to FA on activated carbon fibers supported Pt compared to Ni, Cu and Pb in aqueous solution. [74] When changing the pH to higher acidic conditions during ECH, several studies showed the generation of MF. Using a sacrificial Ni or Ni-Fe alloy anode with various metals as cathode material in an undivided cell, Saffron et al. reported FA and MF formation in acidic electrolytes. Under mild pH values FA was favored, while MF generation dominated at pH 1. [75] Also, Nilges et al. obtained high selectivity towards MF on Cu in acidic media i.e., 0.5M H_2SO_4. [76] Based on these results, the Biddinger group systematically investigated ECH of furfural on a Cu electrode in various acidic electrolytes and confirmed the main generation of FA under mildly acidic conditions, while strongly acidic electrolytes produce both FA and MF (Figure 1.7).[72]

They further reported a double increase in reduction rates of FA + MF on nanocrystalline Cu compared to bare one at negative potentials beyond the onset potential. [77] Under similar reaction conditions, Li and group also observed, in addition to FA and MF, the formation of the dimerization product hydrofuroin on Cu. [62] In addition to FA and MF, tetrahydrofurfuryl alcohol, 2-methyl tetrahydrofuran and other minor products such as furan and tetrahydrofuran can form during thermocatalytic hydrogenation of furfural in liquid- or gas-phase depending on the reaction conditions and catalyst nature. [78]

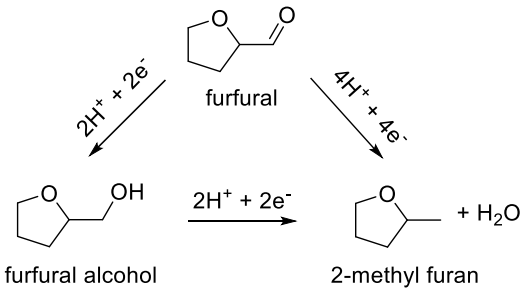

Figure 1.7. Reaction scheme of furfural hydrogenation and hydrogenolysis yielding furfuryl alcohol and 2-methyl furan, respectively. (Adapted with permission from Ref. [77]. Copyright © 2018 Elsevier Inc.)

Acetophenone:

On platinized platinum electrodes Pletcher showed that electrocatalytic reduction of acetophenone to its alcohol species, 1-phenylethanol, occurs in neutral and alkaline media while the hydrogenolysis product, ethylbenzene, is observed under acidic conditions (Figure 1.8). [79, 80]

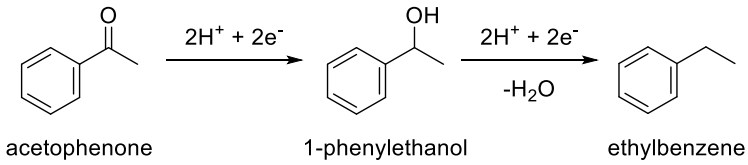

Figure 1.8. Reaction scheme for the hydrogenation of acetophenone to 1-phenylethanol and its hydrogenolysis to ethylbenzene.

Following approaches in the fuel cell field, Sáez et al explored the synthesis of 1-phenylethanol through ECH of acetophenone on Pd/C in an ethanol/water and 0.1M H_2SO_4 electrolyte using a Nafion membrane to separate both compartments, cathode and anode, in a polymer electrolyte membrane electrochemical reactor. [81] They obtained a selectivity of 90% for 1-phenylethanol, with ethylbenzene and hydrogen as side products. [82] Using a sacrificial nickel anode in an undivided cell with water/methanol solvent, Vilar et al. investigated the ECH reactions of acetophenones and

benzaldehydes. As cathode, several materials like Cu, Ni and Fe were utilized. During the ECH process, nickel deposited and the Ni deposit/Ni cathode matrix showed the highest catalytic activities. In agreement with literature, benzaldehydes were more reactive than acetophenones mainly due to steric reasons. [83] In another study the group showed further activity increments in the same order for both reactants by addition of β-cyclodextrin, an inverse phase transfer catalyst.[84] On Pd in 0.5M H_2SO_4, Villalba compared ECH of acetophenone and benzophenone on via their corresponding alcohols. They showed that the ECH efficiency depends on the adsorption strength of the organic substrates, particularly the number of phenyl rings controlling hydrogenation rates. This led to higher activities of acetophenone, as lower numbers of phenyl rings adsorb less strong and lead to higher molecule mobility on the surface. [85]

Cyclohexanone:

It is known from literature, that thermocatalytic and electrocatalytic hydrogenation of cyclohexanone, a product of phenol reduction, on Pd is difficult to conduct. [86] However, Cirtiu and coworkers demonstrated that cyclohexanone is very efficiently converted through EC on Pd/alumina in slightly acidic acetic acid (pH 5 and 6), compared to phosphoric acid as supporting electrolyte. This is explained by in situ alumina surface modification through acetic acid adsorption, which is pH dependent, influencing organic adsorption and the hydrogenation process. Cyclohexanone is thereby reduced in a two-proton and two-electron process to its corresponding hydroxyl form (Figure 1.9). [65]

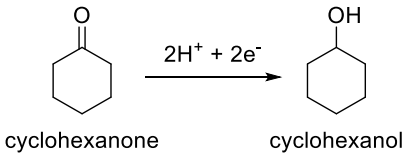

Figure 1.9. Reaction scheme for the hydrogenation of cyclohexanone to cyclohexanol.

In line with Breitner et al. [86] results, TCH reaction conditions using Pd/alumina and same electrolytes let to neglectable hydrogenation yields. [65] The same applied for ECH and TCH reactions on finely divided, non-supported Pd. Further, Dube et al. showed in their study that the cyclohexanone ECH activity of metals dispersed on alumina matrix increases in the following Ru < Pd = Pt < Rh. On a strong adsorbent matrix like activated carbon, ECH even improved and followed the order Pd < Ru < Pt < Rh. [87] Similar substrate functionalization behavior in acetic acid

with strong pH dependency were obtained on Pd supported on fluorine-doped tin dioxide (Pd/SnO_2:F), however, favoring cyclohexanone hydrogenation in a basic medium. [88] Furthermore, electrodes modified with a film of poly-[allyl ether p-(2-aminoethyl)phenol] and incorporated Pt particles also exhibited significant hydrogenation rates of several carbonylic compounds, such as cyclohexanone, acetophenone and benzaldehyde. [89]

1.4.2. Mechanistic studies of hydrogenation

It is well established that gas phase hydrogenation proceeds through the dissociative adsorption of molecular hydrogen, subsequently reacting with the adsorbed organic on the catalyst surface trough a neutral hydrogen addition mechanism i.e., Langmuir-Hinshelwood formalism (reaction (vii)). The same pathway is generally accepted for hydrogenation in aprotic solvents. For the thermocatalytic hydrogenation (TCH) in aqueous phase, several studies emphasized that after dissociatively adsorption of hydrogen the organic hydrogenation also follows a Langmuir-Hinshelwood formalism. [90-92]

Neutral H-addition: $C_xH_yO_z* + H* \rightarrow C_xH_{y+1}O_z* + *$ (vii)

Merenkov and others postulated that in general gas-phase catalysis, just as in the case of corrosion, an electrochemical mechanism cannot be ruled out on metallic catalysts. [66] In aqueous solvents, which are commonly used in electrochemical hydrogenation (ECH), the possibility of an alternative electrochemical reduction mechanism, i.e., proton coupled, or stepwise electron transfer step (PCET) also opens up. Here, the adsorbed organic reacts with protons or water from the electric double layer combined with an electron addition from the charged surface (reaction (viii), (ix)). [28, 29]

PCET (acidic): $C_xH_yO_z* + H^+ + e^- \rightarrow C_xH_{y+1}O_z*$ (viii)

PCET (basic): $C_xH_yO_z* + H_2O + e^- \rightarrow C_xH_{y+1}O_z* + OH^-$ (ix)

Nevertheless, Langmuir-Hinshelwood formalism is still feasible in aqueous solvent and externally applied potential. Adsorbed hydrogen can be formed electrochemically via the Volmer step (i) or (ii) and react through neutral hydrogen addition with the adsorbed organic. [93]

From literature, a coexistence of electrocatalytic hydrogenation (ECH) and direct electroreduction mechanism, where radical organic intermediates are formed (reaction (x) and (xi)), is known

during electrochemical reduction of organics. The preference between the two mechanisms is mainly dependent on the hydrogen evolution activity of the catalyst metal. ECH is favored on low hydrogen overpotential electrodes such as platinum-group metals while direct electroreduction is dominant on high hydrogen overpotential materials (like Pb and graphite). Thus, the latter pathway usually occurs at much more negative potential than ECH. [61, 94] Direct electroreduction is an outer-sphere process where strong interaction between reactant and surface are not required as the electron addition proceeds via electron tunneling (reaction (x)), followed by protonation in solution (reaction (xi)). This yields a radical intermediate ($C_xH_{y+1}O_z^{\bullet}$), which can be further hydrogenated or dimerize through C-C coupling with a second radical species (reaction (xii), (xiii)). [51, 94, 95]

Direct electroreduction is an outer-sphere reaction, which does not require strong interaction between reactant and surface as

Direct electroreduction:	$C_xH_yO_z + e^- \rightarrow C_xH_yO_z^{\bullet -}$	(x)
(acidic/basic)	$C_xH_yO_z^{\bullet -} + H^+(H_2O) \rightarrow C_xH_{y+1}O_z^{\bullet} (+ OH^-)$	(xi)
	$C_xH_{y+1}O_z^{\bullet} + e^- + H^+(H_2O) \rightarrow C_xH_{y+2}O_z (+ OH^-)$	(xii)
Dimerization:	$2\ C_xH_{y+1}O_z^{\bullet} \rightarrow C_xH_{y+1}O_z{-}C_xH_{y+1}O_z$	(xiii)

Song et. al proposed in their work different reaction pathways for the organic hydrogenation, particularly benzaldehyde to benzyl alcohol, in aqueous phase in absence and presence of an external cathodic potential. In absence of a reduction potential i.e., open circuit potential (OCP) or thermal catalytic hydrogenation (TCH) measurements, and instead at 1 bar H_2 they highlight that the reduction indeed proceeds via a Langmuir-Hinshelwood formalism (Figure 1.10 left side). First, hydrogen adsorbs dissociatively on the catalyst surface, followed by the addition of the hydrogen adatom to the adsorbed organic on the catalyst surface. Reaction orders in hydrogen of 1 and zero in benzaldehyde lead to the conclusion that the second hydrogen addition or product desorption is rate determining. [29] During ECH reactions, a general increase of hydrogenation rates with increasing cathodic potential, following Butler-Volmer kinetics, is observed. This could be related to the known increase of H coverage or increase of electrical reduction equivalents (driving force) on the surface upon higher applied negative potential. Thus, a decrease in Faradaic efficiency is often observed as HER increases faster than organic ECH with higher negative potential. [11, 29, 93] TCH measurements of benzaldehyde featured activation energies of 32 kJ mol^{-1},

27 kJ mol^{-1} and 21 kJ mol^{-1} for hydrogenation on Pt/C, Rh/C and Pd/C, respectively. In comparison, ECH showed slightly lower values of 25 kJ mol^{-1}, 21 kJ mol^{-1} and 14 kJ mol^{-1} on the same catalysts. Reaction orders of benzaldehyde in ECH were zero on Pd/C and 1 on Pt/C and Rh/C. [29] From Ref. [68] it is known that the reaction order of benzaldehyde ECH on Pd increases with higher cathodic potential. Increase in reaction orders are attributed to a decrease in coverages. Thus, if the change in coverages in ECH and TCH would account for the various reduction activities, hydrogenation rates would have decreased at unchanging activation barriers on Pd/C, Pt/C and Rh/C. Therefore, the various hydrogenation rates in TCH and ECH were interpretated in Song et al. study as a change in reaction mechanism upon applying a reduction potential. [29]

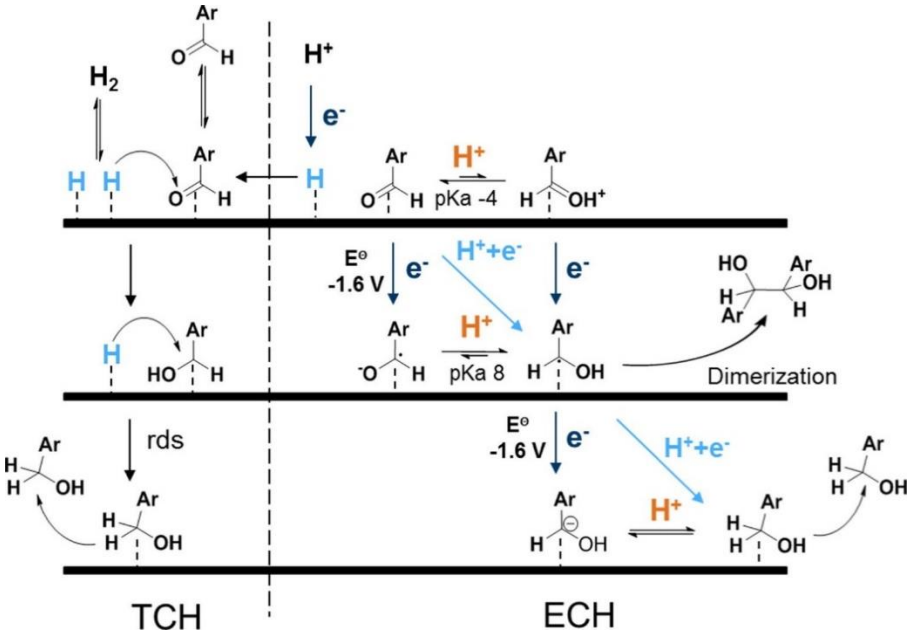

Figure 1.10. Proposed hydrogenation mechanisms of benzaldehyde under open circuit potential conditions (TCH) and for electrocatalytic hydrogenation (ECH). (Reprinted with permission from Ref [29]. Copyright © 2018 Elsevier Inc.)

As shown on the right side of Figure 1.10, it was proposed that electrochemical hydrogenation can proceed either through a stepwise (horizontal and vertical lines) or coupled (diagonal lines) addition of protons and electrons. According to polarization curves from ref [96], the most likely orders of stepwise addition in protic media are H^+-e^--e^--H^+ and e^--H^+-e^--H^+, portrayed in Figure 1.10. However, too acidic pKa values of conjugated acids compared to the mild media conditions used (pH 5) and required direct reduction potentials, which are above the experimentally applied potentials, oppose stepwise reaction mechanisms. [97] Thus, electrocatalytic hydrogenation of benzaldehyde is postulated to proceed via a coupled pathway of proton and electron addition

(diagonal lines). This results in same intermediates as during TCH reaction while high-energy charged intermediates are avoided. Finally, it is concluded that benzaldehyde hydrogenation proceeds through an inner-sphere reaction since the reaction is interfering with HER, which is known to go through inner-sphere processes. [29, 95, 98]

Bondue and Koper also concluded in their work that the electrocatalytic hydrogenation of aliphatic ketones proceeds through a proton-coupled electron transfer as limiting step. However, with the difference that protonated acetone is forming in solution as active species followed by adsorption and electrochemical reduction. Specifically, the mechanism of electrocatalytic hydrogenation of acetone and higher aliphatic ketones and role of adsorbed hydrogen were examined on Pt. [40]

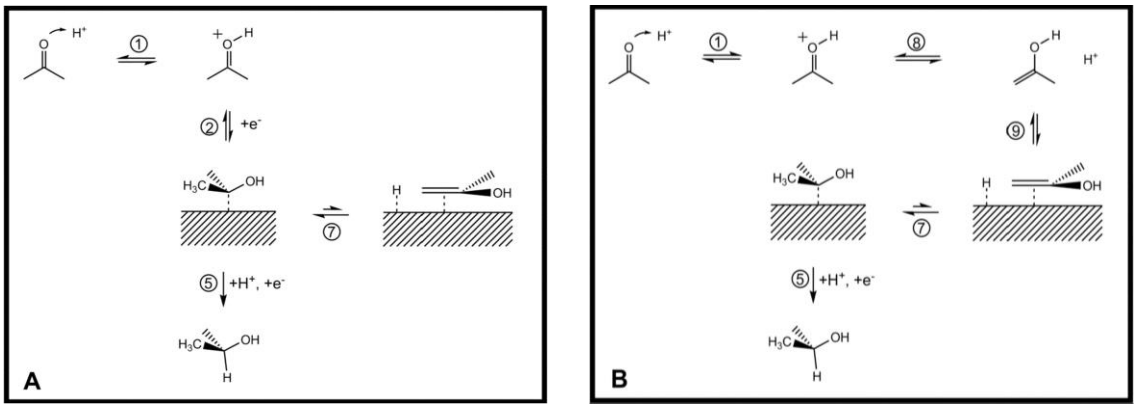

Figure 1.11. Proposed reaction mechanisms of acetone reduction at low overpotential (A) i.e., through direct adsorption of protonated ketone species and high overpotential (B) i.e., via enol-tautomer adsorption of protonated ketone. (Adapted with permission from Ref. [40]. Copyright © 2019 Elsevier Inc.)

The analogue dependence of proton and ketone reaction orders with potential as well as kinetic considerations, point to a competitive adsorption of hydrogen and ketones on the catalyst surface. Further, the effect of proton concentration on acetone reduction rates, emphasized that acetone hydrogenation proceeds through the formation of protonated acetone as the reactive species in equilibrium in solution (equilibrium 1, Figure 1.11). Calculated Tafel slopes and reaction orders indicate that the rate determining reduction after adsorption of the reaction species follows a proton-coupled electron transfer (reaction 5). Using Surface-Enhanced Raman spectroscopy, a surface equilibrium between the enol-tautomer of acetone reacting with adsorbed hydrogen and the protonated acetone species was determined (equilibrium 7, Figure 1.11). Adsorbed hydrogen is therefore necessary to shift the equilibrium to the active ketone species. From the proton concentration effect and the not exact matching reaction orders for acetone and hydrogen, let

conclude that the reduction proceeds through the enol-based pathways at low overpotentials (Figure 1.11 B) and changes to the immediate adsorption of protonated acetone at higher cathodic potentials (Figure 1.11 A). Finally, higher aliphatic ketones exhibited an insensitivity on variations in proton concentration, pointing out the route of enol-tautomer adsorption (Figure 1.11 B).

The prevalence of a proton-electron transfer mechanism in water was also proposed by Shangguan et al. during the thermocatalytic reduction of aliphatic carbonyls (C3-C6) at protic solvents and transition-metal catalysts, particularly Ru. [99] Kinetic and isotopic H-D measurements showed that the carbonyl hydrogenation occurs through the initial ionization of a hydrogen adatom forming a proton and electron pair. The proton transfers onto the carbonyl oxygen atom in a quasi-equilibrated step leading to the generation of a charged hydroxy intermediate, followed by the kinetically relevant neutral hydrogen addition to the carbonyl carbon. This forms a charged alcohol, which recombines with the electron from the surface and the alcohol product desorbs (Figure 1.12).

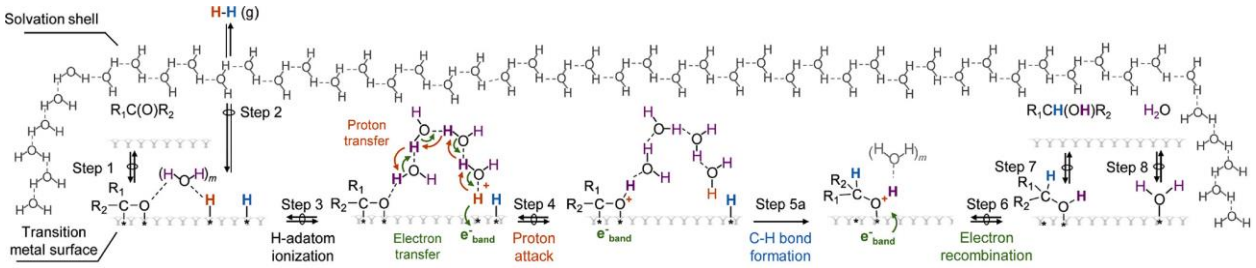

Figure 1.12. Reaction sequence for thermocatalytic carbonyl hydrogenation on transition metals and in protic solvents following a proton-electron transfer step. (Adapted with permission from Ref. [99]. Copyright © 2019 American Chemical Society)

On intermediate hydrogen overpotential metals, like Ni, Co, Cu and Au, a distinction between ECH and direct electroreduction mechanism is less clear due to potential competition between these two reaction pathways. Chadderdon et al. showed that both mechanisms proceed on Cu in acidic electrolyte during electrochemical hydrogenation of furfural (Figure 1.13). Using electrodes modified with organothiol self-assembled monolayers it was possible to investigate the direct interaction between reactant and the catalyst surface and define the nature of the electron transfer. Hydrogenation and hydrogenolysis products i.e., furfuryl alcohol and 2-methylfuran, respectively, were strongly suppressed on the surface modified electrodes, indicating the requirement for direct interaction, and pointing to an inner-sphere electron transfer mechanism. This is supported by HER

being an inner-sphere reaction occurring right on the electrode surface and highly sensitive to the state of the catalyst surface. [95, 98] However, the simultaneous formation of the hydrodimerization product (hydrofuroin) was unchanged on the surface modified electrodes, emphasizing an outer-sphere process of the first electron transfer in the electroreduction pathway (blue marking, Figure 1.13). Kinetic isotope effect and rotating disk electrode (RDE) measurements further highlighted that hydrogen adatoms (formed through electrochemical Volmer step (i)) are required for ECH reactions under the investigated conditions. Emphasizing a Langmuir-Hinshelwood formalism for the electrochemical reduction of furfural on Cu in acidic electrolyte. [62] Lastly, the study verified parallel routes of the hydrogenation and hydrogenolysis reactions during ECH reactions (red marking, Figure 1.13). [62]

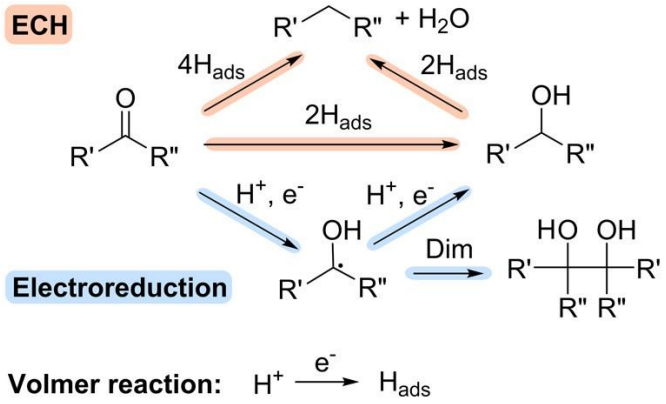

Figure 1.13. Reaction pathways of electrocatalytic hydrogenation and direct electroreduction of carbonyls in acidic solution. Through generation of adsorbed hydrogen (Volmer reaction), the carbonyl can undergo hydrogenation to the alcohol species or hydrogenolysis to its alkane species. Further, the carbonyl molecule can also undergo direct electroreduction, which either results in alcohol formation or dimerization. (Reprinted with permission from Ref. [62]. Copyright © 2019 American Chemical Society)

1.5. Scope of this thesis

The primary goal of this work is to elucidate the mechanisms underlying electrocatalytic hydrogenation of bio-oil derived carbonyl model compounds and to compare them with thermocatalytic hydrogenation processes. Benzaldehyde is chosen as the main carbonyl example and Pd as the metal of choice as a particular interaction between benzaldehyde and Pd has been observed, which suppresses HER during ECH leading to high hydrogenation activities. In chapter 2, the hydrogenation of a series of aromatic and aliphatic carbonyl compounds i.e., benzaldehyde, furfural, acetophenone, cyclohexanone and butyraldehyde on Pd is investigated to quantitatively determine the influence of molecular structure and cathodic potential on ECH rates and selectivity. To study the Pd bulk composition during ECH conditions in presence and absence of the organic compounds, extended X-ray absorption fine structure experiments were implemented. Linear sweep voltammetry on a rotating disk electrode were used to monitor the impact of the carbonyls on the current response when scanning the potential range used during the hydrogenation reactions. Leading to insights of the different interactions of the organics with the metal. Lastly, reaction kinetic analysis was applied to develop a rate model that captures the different trends of the organic hydrogenation and the concurrent HER. In chapter 3, we found that Brønsted acid sites had a key impact on hydrogenation. We probed the effect of increasing hydronium ion concentration on the reductive conversion of benzaldehyde, its hydrogenation product i.e., benzyl alcohol and acetophenone under ECH and TCH conditions. To gain insights into the reaction mechanism under electric and thermal conditions and differentiate between PCET and neutral H addition, activation energies of benzaldehyde hydrogenation in different solvents during ECH and TCH were determined. Considering this, isotope-labeled and high-pressure experiments were additionally performed. As there are reported effects of cations during electrochemical CO_2 reduction and an enhancement of reaction rates with high ionic strength during the dehydration of cyclohexanol on zeolites in water, the influence of the electrolyte ionic strength and changes in cation size on the electro- and thermocatalytic hydrogenation of benzaldehyde are examined in chapter 4. In chapter 5, the summary and conclusion of this work are given.

1.6. References

1. Short-Term Energy Outlook, US Energy Information Administration, 2021, https://www.eia.gov/outlooks/steo/report/global_oil.php.
2. bp's Statistical Review of World Energy 2021, 2021, https://www.bp.com/en/global/corporate/energy-economics/statistical-review-of-world-energy.html.
3. Monthly Energy Review November 2021, US Energy Information Administration, 2021, https://www.eia.gov/totalenergy/data/monthly/.
4. Annual Energy Outlook 2021, US Energy Information Administration, 2021, https://www.eia.gov/outlooks/aeo/.
5. Serrano-Ruiz, J. C.; Dumesic, J. A., Catalytic routes for the conversion of biomass into liquid hydrocarbon transportation fuels. *Energy & Environmental Science* **2011,** *4* (1), 83-99.
6. Huber, G. W.; Iborra, S.; Corma, A., Synthesis of Transportation Fuels from Biomass: Chemistry, Catalysts, and Engineering. *Chemical Reviews* **2006,** *106* (9), 4044-4098.
7. Biomass explained, U.S. Energy Information Administration, 2021, https://www.eia.gov/energyexplained/biomass/.
8. Vassilev, S. V.; Baxter, D.; Andersen, L. K.; Vassileva, C. G., An overview of the chemical composition of biomass. *Fuel* **2010,** *89* (5), 913-933.
9. Hasanov, I.; Raud, M.; Kikas, T., The Role of Ionic Liquids in the Lignin Separation from Lignocellulosic Biomass. *Energies* **2020,** *13* (18), 4864.
10. Wang, H.; Male, J.; Wang, Y., Recent Advances in Hydrotreating of Pyrolysis Bio-Oil and Its Oxygen-Containing Model Compounds. *ACS Catalysis* **2013,** *3* (5), 1047-1070.
11. Akhade, S. A.; Singh, N.; Gutiérrez, O. Y.; Lopez-Ruiz, J.; Wang, H.; Holladay, J. D.; Liu, Y.; Karkamkar, A.; Weber, R. S.; Padmaperuma, A. B.; Lee, M.-S.; Whyatt, G. A.; Elliott, M.; Holladay, J. E.; Male, J. L.; Lercher, J. A.; Rousseau, R.; Glezakou, V.-A., Electrocatalytic Hydrogenation of Biomass-Derived Organics: A Review. *Chemical Reviews* **2020,** *120* (20), 11370-11419.
12. Zoghlami, A.; Paës, G., Lignocellulosic Biomass: Understanding Recalcitrance and Predicting Hydrolysis. *Frontiers in Chemistry* **2019,** *7* (874).
13. Vennestrøm, P. N. R.; Osmundsen, C. M.; Christensen, C. H.; Taarning, E., Beyond Petrochemicals: The Renewable Chemicals Industry. *Angewandte Chemie International Edition* **2011,** *50* (45), 10502-10509.
14. Karatzos, S.; McMillan, J. D.; Saddler, J. N., The potential and challenges of drop-in biofuels. *Report for IEA Bioenergy Task* **2014,** *39*.
15. Wagenhofer, M. F. Unsupported transition metal sulfides for hydrotreating of conventional and renewable feedstock, Dissertation. Technische Universität München, 2020.
16. Biller, P.; Ross, A. B., 17 - Production of biofuels via hydrothermal conversion. In *Handbook of Biofuels Production (Second Edition)*, Luque, R.; Lin, C. S. K.; Wilson, K.; Clark, J., Eds. Woodhead Publishing: 2016; pp 509-547.
17. Du, C.; Zhao, X.; Liu, D.; Lin, C. S. K.; Wilson, K.; Luque, R.; Clark, J., 1 - Introduction: An overview of biofuels and production technologies. In *Handbook of Biofuels Production (Second Edition)*, Luque, R.; Lin, C. S. K.; Wilson, K.; Clark, J., Eds. Woodhead Publishing: 2016; pp 3-12.
18. Zhang, Q.; Chang, J.; Wang, T.; Xu, Y., Review of biomass pyrolysis oil properties and upgrading research. *Energy Conversion and Management* **2007,** *48* (1), 87-92.
19. Zacher, A. H.; Olarte, M. V.; Santosa, D. M.; Elliott, D. C.; Jones, S. B., A review and perspective of recent bio-oil hydrotreating research. *Green Chemistry* **2014,** *16* (2), 491-515.
20. Czernik, S.; Bridgwater, A. V., Overview of Applications of Biomass Fast Pyrolysis Oil. *Energy & Fuels* **2004,** *18* (2), 590-598.
21. Mohan, D.; Pittman, C. U.; Steele, P. H., Pyrolysis of Wood/Biomass for Bio-oil: A Critical Review. *Energy & Fuels* **2006,** *20* (3), 848-889.

22. Oasmaa, A.; Czernik, S., Fuel Oil Quality of Biomass Pyrolysis OilsState of the Art for the End Users. *Energy & Fuels* **1999,** *13* (4), 914-921.
23. Hao, N.; Ben, H.; Yoo, C. G.; Adhikari, S.; Ragauskas, A. J., Review of NMR Characterization of Pyrolysis Oils. *Energy & Fuels* **2016,** *30* (9), 6863-6880.
24. Mullen, C. A.; Strahan, G. D.; Boateng, A. A., Characterization of Various Fast-Pyrolysis Bio-Oils by NMR Spectroscopy. *Energy & Fuels* **2009,** *23* (5), 2707-2718.
25. Negahdar, L.; Gonzalez-Quiroga, A.; Otyuskaya, D.; Toraman, H. E.; Liu, L.; Jastrzebski, J. T. B. H.; Van Geem, K. M.; Marin, G. B.; Thybaut, J. W.; Weckhuysen, B. M., Characterization and Comparison of Fast Pyrolysis Bio-oils from Pinewood, Rapeseed Cake, and Wheat Straw Using 13C NMR and Comprehensive GC × GC. *ACS Sustainable Chemistry & Engineering* **2016,** *4* (9), 4974-4985.
26. Diebold, J. P. *A review of the chemical and physical mechanisms of the storage stability of fast pyrolysis bio-oils*; 1999.
27. Hu, X.; Wang, Y.; Mourant, D.; Gunawan, R.; Lievens, C.; Chaiwat, W.; Gholizadeh, M.; Wu, L.; Li, X.; Li, C.-Z., Polymerization on heating up of bio-oil: A model compound study. *AIChE Journal* **2013,** *59* (3), 888-900.
28. Cantu, D. C.; Padmaperuma, A. B.; Nguyen, M.-T.; Akhade, S. A.; Yoon, Y.; Wang, Y.-G.; Lee, M.-S.; Glezakou, V.-A.; Rousseau, R.; Lilga, M. A., A Combined Experimental and Theoretical Study on the Activity and Selectivity of the Electrocatalytic Hydrogenation of Aldehydes. *ACS Catalysis* **2018,** *8* (8), 7645-7658.
29. Song, Y.; Sanyal, U.; Pangotra, D.; Holladay, J. D.; Camaioni, D. M.; Gutiérrez, O. Y.; Lercher, J. A., Hydrogenation of benzaldehyde via electrocatalysis and thermal catalysis on carbon-supported metals. *Journal of Catalysis* **2018,** *359*, 68-75.
30. Chumpoo, J.; Prasassarakich, P., Bio-Oil from Hydro-Liquefaction of Bagasse in Supercritical Ethanol. *Energy & Fuels* **2010,** *24* (3), 2071-2077.
31. Furimsky, E., Catalytic hydrodeoxygenation. *Applied Catalysis A: General* **2000,** *199* (2), 147-190.
32. Bridgwater, A. V., Review of fast pyrolysis of biomass and product upgrading. *Biomass and Bioenergy* **2012,** *38*, 68-94.
33. Elliott, D. C., Historical Developments in Hydroprocessing Bio-oils. *Energy & Fuels* **2007,** *21* (3), 1792-1815.
34. Kubička, D.; Horáček, J., Deactivation of HDS catalysts in deoxygenation of vegetable oils. *Applied Catalysis A: General* **2011,** *394* (1), 9-17.
35. Laurent, E.; Delmon, B., Influence of water in the deactivation of a sulfided NiMoγ-Al2O3 catalyst during hydrodeoxygenation. *Journal of Catalysis* **1994,** *146* (1), 281-291.
36. Elliott, D. C.; Hart, T. R.; Neuenschwander, G. G.; Rotness, L. J.; Zacher, A. H., Catalytic hydroprocessing of biomass fast pyrolysis bio-oil to produce hydrocarbon products. *Environmental Progress & Sustainable Energy* **2009,** *28* (3), 441-449.
37. Wildschut, J.; Mahfud, F. H.; Venderbosch, R. H.; Heeres, H. J., Hydrotreatment of Fast Pyrolysis Oil Using Heterogeneous Noble-Metal Catalysts. *Industrial & Engineering Chemistry Research* **2009,** *48* (23), 10324-10334.
38. Garedew, M.; Young-Farhat, D.; Jackson, J. E.; Saffron, C. M., Electrocatalytic Upgrading of Phenolic Compounds Observed after Lignin Pyrolysis. *ACS Sustainable Chemistry & Engineering* **2019,** *7* (9), 8375-8386.
39. Lam, C. H.; Das, S.; Erickson, N. C.; Hyzer, C. D.; Garedew, M.; Anderson, J. E.; Wallington, T. J.; Tamor, M. A.; Jackson, J. E.; Saffron, C. M., Towards sustainable hydrocarbon fuels with biomass fast pyrolysis oil and electrocatalytic upgrading. *Sustainable Energy & Fuels* **2017,** *1* (2), 258-266.
40. Bondue, C. J.; Koper, M. T. M., A mechanistic investigation on the electrocatalytic reduction of aliphatic ketones at platinum. *Journal of Catalysis* **2019,** *369*, 302-311.
41. Sanyal, U.; Lopez-Ruiz, J.; Padmaperuma, A. B.; Holladay, J.; Gutiérrez, O. Y., Electrocatalytic Hydrogenation of Oxygenated Compounds in Aqueous Phase. *Organic Process Research & Development* **2018,** *22* (12), 1590-1598.

42. Shinagawa, T.; Garcia-Esparza, A. T.; Takanabe, K., Insight on Tafel slopes from a microkinetic analysis of aqueous electrocatalysis for energy conversion. *Scientific Reports* **2015,** *5*, 13801.
43. Newman, J.; Thomas-Alyea, K. E., *Electrochemical systems*. John Wiley & Sons: 2012.
44. O'Hayre, R.; Cha, S.-W.; Colella, W.; Prinz, F. B., *Fuel Cell Fundamentals*. Wiley: 2009.
45. Durst, J.; Simon, C.; Hasché, F.; Gasteiger, H. A., Hydrogen Oxidation and Evolution Reaction Kinetics on Carbon Supported Pt, Ir, Rh, and Pd Electrocatalysts in Acidic Media. *Journal of The Electrochemical Society* **2015,** *162* (1), F190-F203.
46. Conway, B. E.; Bai, L., Determination of adsorption of OPD H species in the cathodic hydrogen evolution reaction at Pt in relation to electrocatalysis. *Journal of Electroanalytical Chemistry and Interfacial Electrochemistry* **1986,** *198* (1), 149-175.
47. Gennero de Chialvo, M. R.; Chialvo, A. C., Existence of Two Sets of Kinetic Parameters in the Correlation of the Hydrogen Electrode Reaction. *Journal of The Electrochemical Society* **2000,** *147* (5), 1619.
48. Zheng, Y.; Jiao, Y.; Jaroniec, M.; Qiao, S. Z., Advancing the Electrochemistry of the Hydrogen-Evolution Reaction through Combining Experiment and Theory. *Angewandte Chemie International Edition* **2015,** *54* (1), 52-65.
49. Atkins, P. W.; de Paula, J., *Atkins' Physical Chemistry*. OUP Oxford: 2014.
50. Burt, R.; Birkett, G.; Zhao, X. S., A review of molecular modelling of electric double layer capacitors. *Physical Chemistry Chemical Physics* **2014,** *16* (14), 6519-6538.
51. Bard, A. J.; Faulkner, L. R., *Electrochemical Methods: Fundamentals and Applications, 2nd Edition*. John Wiley & Sons, Incorporated: 2000.
52. Wang, H.; Pilon, L., Accurate Simulations of Electric Double Layer Capacitance of Ultramicroelectrodes. *The Journal of Physical Chemistry C* **2011,** *115* (33), 16711-16719.
53. Zoski, C. G., *Handbook of electrochemistry*. Elsevier Science: 2007.
54. Hamann, C. H.; Hamnett, A.; Vielstich, W., *Electrochemistry*. 1998.
55. Gileadi, E., *Electrode Kinetics for Chemists, Chemical Engineers, and Materials Scientists*. Wiley-VCH: 1993.
56. Appel, A. M.; Helm, M. L., Determining the Overpotential for a Molecular Electrocatalyst. *ACS Catalysis* **2014,** *4* (2), 630-633.
57. Abderezzak, B., *Introduction to transfer phenomena in PEM fuel cells*. Elsevier: 2018.
58. Ghassemi, M.; Kamvar, M.; Steinberger-Wilckens, R., Chapter 4 - Fundamentals of electrochemistry. In *Fundamentals of Heat and Fluid Flow in High Temperature Fuel Cells*, Ghassemi, M.; Kamvar, M.; Steinberger-Wilckens, R., Eds. Academic Press: 2020; pp 75-99.
59. Lessard, J., *Electrocatalytic Hydrogenation. In Organic Electrochemistry, 5th ed.; Hammerich, O., Speiser, B., Eds.;*. CRC Press: Boca Raton, FL, 2015; p 1658 - 1664.
60. Chapuzet, J. M.; Lasia, A.; Lessard, J., Electrocatalytic hydrogenation of organic compounds. Wiley-VCH: New York: 1998; pp 155-159.
61. Lessard, J., Chapter 44 Electrocatalytic Hydrogenation. In *Organic electrochemistry*, CRC Press Boca Raton, FL: 2016.
62. Chadderdon, X. H.; Chadderdon, D. J.; Matthiesen, J. E.; Qiu, Y.; Carraher, J. M.; Tessonnier, J.-P.; Li, W., Mechanisms of Furfural Reduction on Metal Electrodes: Distinguishing Pathways for Selective Hydrogenation of Bioderived Oxygenates. *Journal of the American Chemical Society* **2017,** *139* (40), 14120-14128.
63. Huang, H.; Yu, Y.; Chung, K. H., Performance of Au/Nafion/Pt electrodes in benzene–water electrochemical hydrogenation. *International Journal of Hydrogen Energy* **2014,** *39* (25), 13832-13837.
64. Baltruschat, H.; Ernst, S., Molecular Adsorbates at Single-Crystal Platinum-Group Metals and Bimetallic Surfaces. *ChemPhysChem* **2011,** *12* (1), 56-69.
65. Cirtiu, C. M.; Brisach-Wittmeyer, A.; Ménard, H., Electrocatalysis over Pd catalysts: A very efficient alternative to catalytic hydrogenation of cyclohexanone. *Journal of Catalysis* **2007,** *245* (1), 191-197.

66. Birkett, M. D.; Kuhn, A. T.; Bond, G. C., The catalytic hydrogenation of organic compounds–a comparison between the gas–phase, liquid–phase, and electrochemical routes. In *Catalysis: Volume 6*, Bond, G. C.; Webb, G., Eds. The Royal Society of Chemistry: 1983; Vol. 6, pp 61-89.
67. Polcaro, A. M.; Palmas, S.; Dernini, S., Role of catalyst characteristics in electrocatalytic hydrogenation: reduction of benzaldehyde and acetophenone on carbon felt/palladium electrodes. *Industrial & engineering chemistry research* **1993,** *32* (7), 1315-1322.
68. Lopez-Ruiz, J. A.; Sanyal, U.; Egbert, J.; Gutiérrez, O. Y.; Holladay, J., Kinetic Investigation of the Sustainable Electrocatalytic Hydrogenation of Benzaldehyde on Pd/C: Effect of Electrolyte Composition and Half-Cell Potentials. *ACS Sustainable Chemistry & Engineering* **2018,** *6* (12), 16073-16085.
69. Polcaro, A. M.; Palmas, S.; Dernini, S., Electrochemical reduction of carbonyl compounds at modified carbon felt electrodes. *Electrochimica Acta* **1993,** *38* (2), 199-203.
70. Anibal, J.; Malkani, A.; Xu, B., Stability of the Ketyl Radical as a Descriptor in the Electrochemical Coupling of Benzaldehyde. *Catalysis Science & Technology* **2020**.
71. Vannice, M. A.; Poondi, D., The Effect of Metal-Support Interactions on the Hydrogenation of Benzaldehyde and Benzyl Alcohol. *Journal of Catalysis* **1997,** *169* (1), 166-175.
72. Jung, S.; Biddinger, E. J., Electrocatalytic Hydrogenation and Hydrogenolysis of Furfural and the Impact of Homogeneous Side Reactions of Furanic Compounds in Acidic Electrolytes. *ACS Sustainable Chemistry & Engineering* **2016,** *4* (12), 6500-6508.
73. Chamoulaud, G.; Floner, D.; Moinet, C.; Lamy, C.; Belgsir, E. M., Biomass conversion II: simultaneous electrosyntheses of furoic acid and furfuryl alcohol on modified graphite felt electrodes. *Electrochimica Acta* **2001,** *46* (18), 2757-2760.
74. zhao, B.; Chen, M.; Guo, Q.; Fu, Y., Electrocatalytic hydrogenation of furfural to furfuryl alcohol using platinum supported on activated carbon fibers. *Electrochimica Acta* **2014,** *135*, 139-146.
75. Li, Z.; Kelkar, S.; Lam, C. H.; Luczek, K.; Jackson, J. E.; Miller, D. J.; Saffron, C. M., Aqueous electrocatalytic hydrogenation of furfural using a sacrificial anode. *Electrochimica Acta* **2012,** *64*, 87-93.
76. Nilges, P.; Schröder, U., Electrochemistry for biofuel generation: production of furans by electrocatalytic hydrogenation of furfurals. *Energy & Environmental Science* **2013,** *6* (10), 2925-2931.
77. Jung, S.; Karaiskakis, A. N.; Biddinger, E. J., Enhanced activity for electrochemical hydrogenation and hydrogenolysis of furfural to biofuel using electrodeposited Cu catalysts. *Catalysis Today* **2018**.
78. Mariscal, R.; Maireles-Torres, P.; Ojeda, M.; Sadaba, I.; Lopez Granados, M., Furfural: a renewable and versatile platform molecule for the synthesis of chemicals and fuels. *Energy & Environmental Science* **2016,** *9* (4), 1144-1189.
79. Antonietta Casadei, M.; Pletcher, D., The influence of conditions on the electrocatalytic hydrogenation of organic molecules. *Electrochimica Acta* **1988,** *33* (1), 117-120.
80. Pletcher, D.; Razaq, M., The reduction of acetophenone to ethylbenzene at a platinised platinum electrode. *Electrochimica Acta* **1981,** *26* (7), 819-824.
81. Sáez, A.; García-García, V.; Solla-Gullón, J.; Aldaz, A.; Montiel, V., Electrochemical synthesis at pre-pilot scale of 1-phenylethanol by cathodic reduction of acetophenone using a solid polymer electrolyte. *Electrochemistry Communications* **2013,** *34*, 316-319.
82. Sáez, A.; García-García, V.; Solla-Gullón, J.; Aldaz, A.; Montiel, V., Electrocatalytic hydrogenation of acetophenone using a Polymer Electrolyte Membrane Electrochemical Reactor. *Electrochimica Acta* **2013,** *91*, 69-74.
83. Vilar, M.; Oliveira, J. L.; Navarro, M., Investigation of the hydrogenation reactivity of some organic substrates using an electrocatalytic method. *Applied Catalysis A: General* **2010,** *372* (1), 1-7.
84. Vilar, M.; Navarro, M., β-cyclodextrin as inverse phase transfer catalyst on the electrocatalytic hydrogenation of organic compounds in water. *Electrochimica Acta* **2012,** *59*, 270-278.
85. Villalba, M.; del Pozo, M.; Calvo, E. J., Electrocatalytic hydrogenation of acetophenone and benzophenone using palladium electrodes. *Electrochimica Acta* **2015,** *164*, 125-131.
86. Breitner, E.; Roginski, E.; Rylander, P. N., Low Pressure Hydrogenation of Ketones with Platinum Metal Catalysts. *The Journal of Organic Chemistry* **1959,** *24* (12), 1855-1857.

87. Dubé, P.; Kerdouss, F.; Laplante, F.; Proulx, P.; Brossard, L.; Ménard, H., Electrocatalytic hydrogenation of cyclohexanone: Simple dynamic cell design. *Journal of Applied Electrochemistry* **2003,** *33* (6), 541-547.
88. Tountian, D.; Brisach-Wittmeyer, A.; Nkeng, P.; Poillerat, G.; Ménard, H., On the efficiency of phenol and cyclohexanone electrocatalytic hydrogenation—Effect of conditioning and working pH in acetic acid solution on palladium/fluorine-doped tin dioxide supported catalyst. *Canadian Journal of Chemistry* **2010,** *88* (5), 463-471.
89. Lofrano, R. C. Z.; Madurro, J. M.; Abrantes, L. M.; Romero, J. R., Electrocatalytic hydrogenation of carbonylic compounds using an electrode with platinum particles dispersed in films of poly-[allyl ether p-(2-aminoethyl) phenol] co-polymerized with allyl phenyl ether. *Journal of Molecular Catalysis A: Chemical* **2004,** *218* (1), 73-79.
90. Yoon, Y.; Rousseau, R.; Weber, R. S.; Mei, D.; Lercher, J. A., First-Principles Study of Phenol Hydrogenation on Pt and Ni Catalysts in Aqueous Phase. *Journal of the American Chemical Society* **2014,** *136* (29), 10287-10298.
91. Wagner, C., Considerations on the mechanism of the hydrogenation of organic compounds in aqueous solutions on noble metal catalysts. *Electrochimica Acta* **1970,** *15* (6), 987-997.
92. Takehara, Z., Hydrogenation of some organic compounds in acidic aqueous solutions on noble metal catalysts. *Electrochimica Acta* **1970,** *15* (6), 999-1012.
93. Singh, N.; Sanyal, U.; Ruehl, G.; Stoerzinger, K. A.; Gutiérrez, O. Y.; Camaioni, D. M.; Fulton, J. L.; Lercher, J. A.; Campbell, C. T., Aqueous phase catalytic and electrocatalytic hydrogenation of phenol and benzaldehyde over platinum group metals. *Journal of Catalysis* **2020,** *382*, 372-384.
94. Speiser, B.; Hammerich, O., *Organic Electrochemistry*. CRC Press: 2015.
95. Schmickler, W.; Santos, E., Theoretical considerations of electron-transfer reactions. In *Interfacial Electrochemistry*, Springer Berlin Heidelberg: Berlin, Heidelberg, 2010; pp 99-115.
96. Carlá, M.; Aloisi, G.; Foresti, M. L.; Guidelli, R., Adsorption behaviour of n-hexylamine at the Hg/water interphase and its comparison with a molecular model accounting for local order. *Journal of Electroanalytical Chemistry and Interfacial Electrochemistry* **1986,** *197* (1), 123-141.
97. Zuman, P., Aspects of Electrochemical Behavior of Aldehydes and Ketones in Protic Media. *Electroanalysis* **2006,** *18* (2), 131-140.
98. Schmickler, W.; Santos, E., Hydrogen reaction and electrocatalysis. In *Interfacial Electrochemistry*, Springer Berlin Heidelberg: Berlin, Heidelberg, 2010; pp 163-175.
99. Shangguan, J.; Chin, Y.-H. C., Kinetic Significance of Proton–Electron Transfer during Condensed Phase Reduction of Carbonyls on Transition Metal Clusters. *ACS Catalysis* **2019,** *9* (3), 1763-1778.

2. Influence of Molecular Structure on the Electrocatalytic Hydrogenation of Carbonyl Groups and H_2 Evolution on Pd

Abstract

The hydrogenation rates of aldehydes and ketones over Pd in aqueous phase follow disparate trends with varying applied electric potential and nature of the organic substrate. Hydrogenation and H_2 evolution depend on the sorption of the reacting substrate with Pd. Strong interactions, associated with fast hydrogenation kinetics, hinder the evolution of H_2 and the formation of H-rich bulk Pd hydride. Hydrogenation dominates at low overpotential but is surpassed in rate by H_2 evolution with increasingly negative potential, as the coverage of organic substrate decreases. The mechanism of hydrogenation, which includes proton coupled electron transfer steps and sorption on the metal surface determines the range of electric potential favoring hydrogenation. Thus, the standard free energy of adsorption is the key factor enabling charge transfer, concurrent hydrogenation and H_2 evolution and even the bulk state of Pd.

2.1. Introduction

Conversion of organic intermediates derived from biogenic sources to energy carriers and chemicals could significantly contribute to a carbon balanced future.[1-3] These transformations require the reduction of functional oxygen containing groups on the path to produce stable energy carriers.[4, 5] Electrocatalysis is particularly attractive because of the complex logistic questions with respect to provide H_2 for decentralized hydrodefunctionalization of bioderived molecules. Compounds with carbonyl groups like aldehydes and ketones are fairly reactive and, thus, particularly susceptible to be selectively reduced at low temperature.[6, 7] However, a general fundamental understanding of these processes is currently still not achieved, because the information of how active metal catalysts interact with the reacting molecules during electrocatalysis is limited at best. Studies exist, aiming at describing electrocatalytic hydrogenation (ECH) and how reaction rates change by varying the external electric potential (i.e., the electrochemical potential of the hydrogen).[8-13] However, the lack of studies decoupling kinetic and thermodynamic parameters makes it challenging to derive precise reaction mechanisms.

Hydrogenation on supported metal catalysts tends to require that the organic reactants adsorb on the metal, particularly under relatively low overpotentials that make electron tunneling unfavorable. The organic molecule is hydrogenated via addition of H atoms absorbed on the active metal or via the quasi-simultaneous proton and electron transfer (proton-coupled electron transfers, PCET), using protons of hydronium ions in the double layer. Contributions to these pathways are challenging to attribute, as they depend on the overpotential, the proton affinities of the organic compound, and solvent as well as on the activity of hydronium ions.[14, 15]

The H_2 evolution reaction (HER) is frequently observed to surpass ECH with increasing negative electric potentials, as the higher rate of reduction of hydronium ions tends to favor the reaction of adsorbed hydrogen atoms with each other or with protons coupled to the electron transfer over the hydrogenation of the organic substrate. Thus, the relative rates of HER and ECH pathways will markedly depend on the relative surface concentrations of H atoms and organic substrates. To probe the validity of such a hypothesis, we report here the hydrogenation of a series of carbonyl compounds using Pd as catalyst to quantitatively determine the influence of molecular structure and cathodic potential on ECH rates and selectivity. We combine spectroscopy, electrochemical characterization, and reaction kinetics to show that increasing cathodic potential has two major effects on hydrogenation, i.e., (i) increasing the rates of charge transfer in PCET mechanisms, i.e., directly influencing the reaction rates at the level of rate constant rather than controlling the coverage of hydrogen; and (ii) decreasing the surface coverage of the organic compound when increasing the applied potential.

2.2. Results and discussion

2.2.1. Electrocatalytic hydrogenation of carbonyl compounds

Carbon supported Pd was used, because it has been identified as an excellent catalyst to hydrogenate carbonyl compounds.[9, 10, 16, 17] Reaction rates are analyzed and discussed upon normalization to the concentration of exposed metal, i.e., turnover frequencies (TOFs). We determined the concentration of exposed Pd by using a combination of techniques, i.e., H_2 and CO chemisorption, in situ titration with butanethiol, and transmission electron microscopy (Supporting information 2.5.2).

Benzaldehyde, acetophenone, furfural, cyclohexanone, and butyraldehyde were selected as model compounds. The reactive carbonyl groups were converted to hydroxyl groups, yielding the corresponding alcohols without parallel or secondary reactions (Figure S2.4), in agreement with other studies in mildly acidic electrolytes.[9, 12, 18-22] Hydrogenolysis of the alcohol to the hydrocarbon may occur with increasing electrolyte acidity.[23, 24]

When applying an external electric potential, HER competed with ECH. The total current recorded during the experiments (i.e., the sum of HER and ECH) increased with increasingly negative potential without signs of mass transfer limitations (Figure S2.6). Figure S2.5 shows that the faradaic efficiency, i.e., the fraction of the current utilized to reduce the organic compound, decreased with increasing overpotential as consequence.

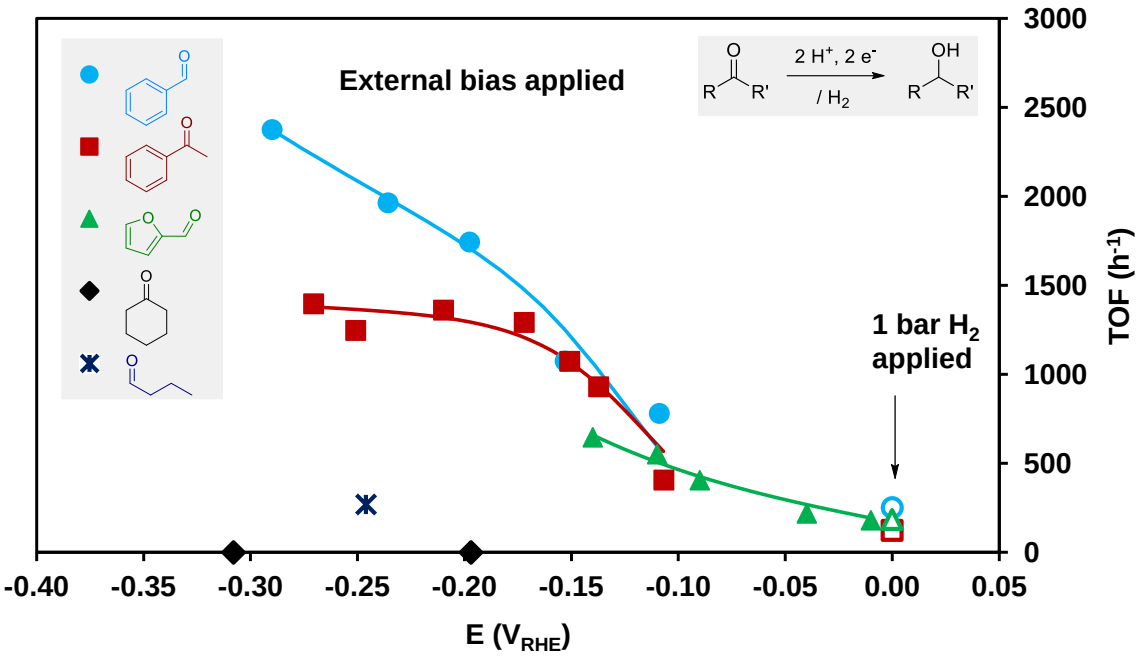

Figure 2.1. Hydrogenation rates of benzaldehyde, acetophenone, furfural, butyraldehyde, and cyclohexanone during the application of an external bias (close symbols) and under open circuit voltage conditions with 1 bar H_2 (open symbols). All reactions were performed in an acetate buffer (pH 5.2) at room temperature. The lines correspond to rates predicted by the kinetic model described in the text.

Figure 2.1 shows benzaldehyde to be the most reactive molecule, followed by furfural and acetophenone, while the aliphatic compounds showed negligible reactivity. The hydrogenation rates of the three aldehydes responded differently to changes of electric potential. The reduction rate for benzaldehyde increased almost linearly with cathodic potential (from 782 h^{-1} at -0.1 V_{RHE} to 2376 h^{-1} at -0.3 V_{RHE}), and less so for furfural (from 194 h^{-1} at -0.01 V_{RHE} to 659 h^{-1}

at -0.14 V_{RHE}). For acetophenone, the rate also increased linearly at low overpotential (from 407 h^{-1} at -0.1 V_{RHE} to 1363 h^{-1} at -0.2 V_{RHE}) but remained constant at potentials more negative than -0.2 V_{RHE}. It should be noted in passing that the high reactivity of furfural required using a rotating ring disk electrode (RRDE) instead of the two-compartment batch electrolysis cell (Supporting information 2.5.4), limiting the overpotentials to be applied.

The key factor for hydrogenation of organic compounds appears to be the reactivity of the hydrogen for a particular substrate across different reactive substrates or solvents.[25] We hypothesize that the observed rate differences between the reacting organic substrates correlate with their relative surface abundance. Thus, the interaction strengths of the organic compounds with Pd would be the cause for the variations and rates observed. The importance of the adsorbed organic substrates for the hydrogen addition reactions is good agreement with studies on different metal catalysts[19, 26] and with model surfaces of Pt.[27]

Figure 2.1 also shows that the rates of hydrogenation with 1 bar H_2, at the corresponding open circuit voltage (OCV). These rates are significantly lower than those in ECH at applied potentials. Namely, OCV hydrogenation proceeded with a TOF of 252 h^{-1} for benzaldehyde, 185 h^{-1} for furfural and 123 h^{-1} for acetophenone. Cyclohexanone and butyraldehyde did not react under these conditions. The low rates under OCV are attributed to the relatively low chemical potential of hydrogen under these conditions compared to its chemical potential under electrocatalytic conditions. Extrapolating results from phenol hydrogenation,[17, 28, 29] this indicates relatively low coverages of adsorbed hydrogen on the metal surface equilibrated with 1 bar H_2 (compared to the charged surface). However, in contrast to the well-studied reduction of phenol on Pt, the availability of adsorbed hydrogen on Pd differs in ECH and OCV operations, i.e., there is much more hydrogen available when the catalyst is equilibrated with 1 bar H_2 than under ECH conditions (vide supra). Because of this difference, for Pd, the higher electrochemical potential of hydrogen upon the application of the external potential does not appear to increase hydrogen coverage. This points to the fact that the overpotential directly influences the rate of the reaction at the level of a rate constant instead of indirectly via coverages of reactants. In the following, we discuss the implications of this hypothesis for the molecular-level mechanisms of ECH, explaining the varying kinetics compiled in Figure 2.1 and the conversion of selected molecules.

2.2.2. Kinetics of electrocatalytic hydrogenation and competing H_2 evolution

As HER competes with ECH for hydrogen, hydronium ions and electrons, the rates of both reactions are influenced by the applied potential. Thus, let us first start with considering the mechanisms of HER during the reported experiments. HER proceeds through a series of consecutive reactions, which start with the reduction of hydronium ions to produce adsorbed H (Volmer step, reaction (i)). H_2 evolves either through reaction of adsorbed H with protons and electrons (Heyrovsky step, reaction (ii)) or by combination of adsorbed H (Tafel step, reaction (iii)).[30, 31] Any of these steps can be rate determining and depends on the metal and the reaction conditions,[32] which is relevant for the possibility of building up a hydrogen coverage on the surface.

$$H_3O^+ + e^- + * \rightleftarrows H^* + H_2O \qquad \text{(i)}$$

$$H^* + H_3O^+ + e^- \rightleftarrows H_2 + H_2O + * \qquad \text{(ii)}$$

$$2H^* \rightleftarrows H_2 + 2* \qquad \text{(iii)}$$

To describe the mechanism of ECH, we consider first that the adsorption of the organic substrate is quasi-equilibrated (reaction (iv)). In presence of an external potential, we surmise that the first and second hydrogen addition proceed as PCET (reaction (v) and (vi)), where the second hydrogen addition is rate determining. Indirect previous experience supports this hypothesis, i.e., (a) acidic groups at the carbon support on ECH have a strong positive effect on the rate of hydrogenation (but not on HER or on OCV hydrogenation);[18] (b) theoretical calculations of aldehyde ECH show PCET mechanism energetically favored under the experimental conditions employed;[15, 18, 33] and (c) phenol or more acidic molecules enhance the ECH of benzaldehyde (but not on OCV hydrogenation).[34] Our own kinetic analysis (below) shows that a PCET mechanisms fits the experimental data significantly better than mechanisms requiring the formation of adsorbed H prior to hydrogenation.

$$RCHO + * \rightleftarrows RCHO^* \qquad \text{(iv)}$$

$$RCHO^* + e^- + H_3O^+ \rightleftarrows RCHOH^* + H_2O \qquad \text{(v)}$$

$$RCHOH^* + e^- + H_3O^+ \rightarrow RCH_2OH^* + H_2O \qquad \text{(vi)}$$

The rate equation (2.1) corresponds to hydrogenation proceeding as described in reactions (iv) – (vi), while HER occurs through a quasi-equilibrated Volmer step (reaction (i)), and a rate determining Heyrovsky step (reaction (ii)). In Eq. (2.1), k_{ECH}^{o} is the rate constant for the rate determining step; f is F/RT (F: Faraday's constant, R: universal gas constant, T: absolute temperature); η is the applied overpotential; α_{ECH} is the charge transfer coefficient for ECH; K_{RCHO} is the adsorption equilibrium constant of the carbonyl compound and K_{RCHOH}^{o} is the equilibrium constant for the hydrogenated carbonyl intermediate RCHOH; a_{RCHO}, a_{H_2O}, and $a_{H_3O^+}$ are the activities of the organic compound, water, and hydronium ions, respectively; and K_{Vr}^{o} is the equilibrium constant for the Volmer step. The rate equation for HER occurring in the presence of the organic compound is depicted in Eq. (2.2), where r_{HER} is the rate of HER, k_{Hy}^{o} is the standard rate constant of the Heyrovsky step, and α_{HER} is the charge transfer coefficient for HER. The derivations of Eq. (2.1) and Eq. (2.2) are detailed in Supporting Information 2.5.5.

$$r_{ECH} = \frac{k_{ECH}^{o}\, e^{-f\eta(\alpha_{ECH}+1)}\, K_{RCHOH}^{o}\, K_{RCHO}\, a_{RCHO}\, a_{H_3O^+}^{2}}{a_{H_2O}\left(1+K_{RCHO}a_{RCHO}+\frac{K_{Vr}^{o}\, e^{-f\eta}\, a_{H_3O^+}}{a_{H_2O}}+\frac{K_{RCHOH}^{o}\, e^{-f\eta}\, K_{RCHO}\, a_{RCHO}\, a_{H_3O^+}}{a_{H_2O}}\right)} \tag{2.1}$$

$$r_{HER} = \frac{k_{Hy}^{o}\, e^{-f\eta(\alpha_{HER}+1)}\, K_{Vr}^{o}\, a_{H_3O^+}^{2}}{a_{H_2O}\left(1+K_{RCHO}a_{RCHO}+\frac{K_{Vr}^{o}\, e^{-f\eta}\, a_{H_3O^+}}{a_{H_2O}}+\frac{K_{RCHOH}^{o}\, e^{-f\eta}\, K_{RCHO}\, a_{RCHO}\, a_{H_3O^+}}{a_{H_2O}}\right)} \tag{2.2}$$

Eq. (2.1) and Eq. (2.2) show that the ECH and HER rates both increase with overpotential because the rate constants are modified by the exponential terms containing the overpotential following Butler-Volmer-type kinetics. The product $K_{RCHOH}^{o}\, K_{RCHO}\, a_{RCHO}$ in the ECH numerator describes the coverage of the organic and its partially hydrogenated species and the term associated with K_{Vr}^{o} in the denominator describes the changes in coverage of hydrogen with applied potential. The equation suggests that the hydrogenation rates increase with negative potential until the potential-dependent coverage of adsorbed H hinders the adsorption of organic reactants. Thus, ECH rates will peak or plateau with increasing cathodic potential as we have observed for the ECH of acetophenone. The denominator in Eq. (2.2), on the other hand, shows that adsorbed organic compounds hinder the rates of HER.

We derived rate equations for several reaction mechanisms involving both neutral H additions and PCET steps. Overall, only mechanisms containing PCET steps led to a very good description of

the ECH rates, while also capturing the increase of HER rates as the electric potential increased. The model presented in Reactions (i) – (vi) fits our experimental data, including the onsets of ECH and HER rates with overpotential.

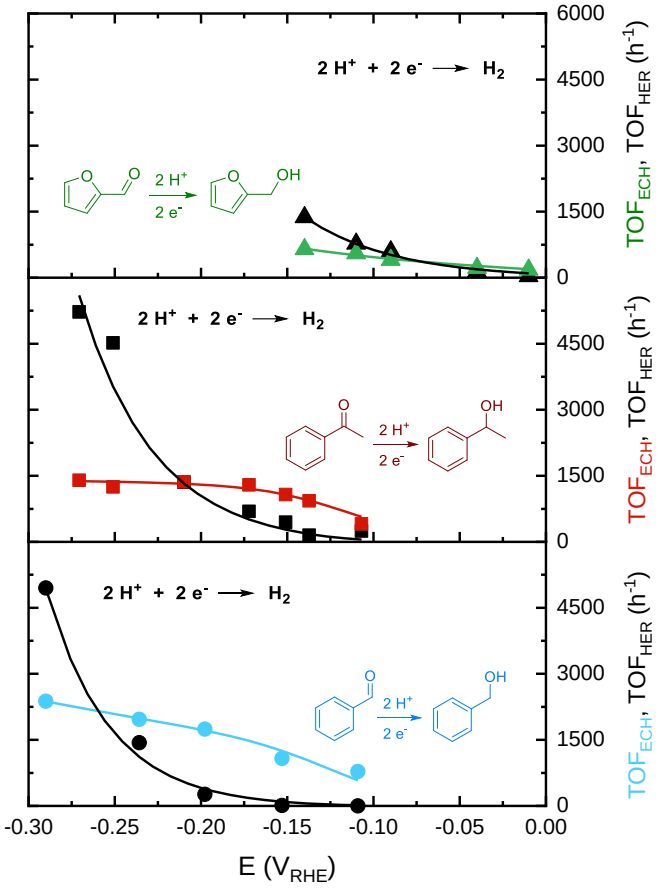

Figure 2.2. Rates of electrocatalytic hydrogenation (ECH) and H_2 evolution (HER - black) observed during the conversion of benzaldehyde (blue), acetophenone (red) and furfural (green) at varying potentials. All reactions were performed in an acetate buffer (pH 5.2) at room temperature in a divided electrolysis batch reactor. The lines correspond to rates fitted as described in the text.

However, at present we do not exclude rigorously other mechanisms that include PCET steps for ECH and competition between adsorbed H and organic compounds (such models are commented in the Supporting Information 2.5.5). The resulting fits of benzaldehyde, acetophenone, and furfural ECH rates, as well as the simultaneous HER are shown in Figure 2.1 and Figure 2.2. Note that the adsorption equilibrium constants of the organic compounds on Pd were determined experimentally (Table S2.4) in the underpotential deposition region and only the rate constants were fitted with equations (2.1) and (2.2). We also note that this mechanistic interpretation does not consider repulsive forces between negatively charged metal and the organic compounds, which

would also decrease its coverage. However, the charge at the metal is considered not to be sufficiently negative at the used overpotential to show significant repulsion effects that could affect the coverage of organic compounds.[15] Figure 2.2 shows organic compounds suppressing HER to varying extents. However, HER rates always increase exponentially and surpass ECH rates at sufficiently negative potentials. As a result, the FE decreases with increasing overpotential (Figure S2.5). Furthermore, the onset of HER and the potential at which HER becomes faster than ECH together depend on the nature of the reacting substrates.

Of course, the electric current I reflects the sum of ECH and HER and can be described as accordingly (Eq. (2.3)):

$$I = nFAr_i = nFA(r_{ECH} + r_{HER}) \tag{2.3}$$

where n is the number of electrons involved in the overall reaction (2 for both ECH and HER) and A is the surface area of the electrocatalyst. Eq. (2.3) and the kinetic fitting are in excellent agreement with the experimental currents (Figure S2.6). The exponential increase in total currents with overpotential indicate the linear increase in ECH rates and the rate plateau for acetophenone versus potential do not arise from diffusion limitations of hydrated hydronium ions (Figure 2.1 and Figure 2.2).

2.2.3. Evaluating the interactions of organic compounds with Pd

Let us address in the next step the adsorption of the organic substrates and their equilibrium constants via the concentration-dependent influence on the underpotentially deposited hydrogen (H_{UPD}) current during cyclic voltammograms (CVs) in the presence of varying concentrations of organics (Figure S2.7 and Supporting Information 2.5.6).[17, 34-37] The corresponding Gibb's free energies of adsorption on Pd were -42 kJ mol^{-1}, -39 kJ mol^{-1}, -37 kJ mol^{-1} and -35 kJ mol^{-1} for benzaldehyde, furfural, acetophenone, and cyclohexanone, respectively. This trend is in line with Gibbs free energies reported for adsorption on Pt in water (i.e., -31 kJ mol^{-1}, -26 kJ mol^{-1}, and -17 kJ mol^{-1} for benzaldehyde, furfural, and cyclohexanone),[17, 38] although the interactions are stronger with Pd than with Pt. The differences in the interaction strengths of benzaldehyde and acetophenone agree also well with theory.[39]

We also explored charge transfer in the presence of the organic compounds by linear sweep voltammetry (LSV) on a rotating polycrystalline Pd disc electrode. Figure 2.3 a) shows that the

onset potential with a Pd disc is about 0 V_{RHE} whether in pure electrolyte (HER only) or with any dissolved organic compound. There is, however, suppression of cathodic current by the organic compounds, which indicates that organics inhibit access to surface Pd sites. The extent of current suppression was proportional to the adsorption equilibrium constants determined by the CV analysis, i.e., cyclohexanone < acetophenone < furfural < benzaldehyde.

The adsorption equilibrium constants that we calculated indicate that at potentials close to 0 V_{RHE}, the Pd surface is saturated with organic compounds. This is in line with the reaction order of zero in benzaldehyde measured during hydrogenation on Pd at OCV or at low overpotentials.[9] However, the activity results and kinetic analysis indicate that hydrogen and hydronium ions decrease the coverages of organic compounds with increasing electrochemical potential of hydrogen at more negative potentials. This is reflected in the change of reaction order in, e.g., benzaldehyde, from zero to positive with cathodic potential during ECH.[10]

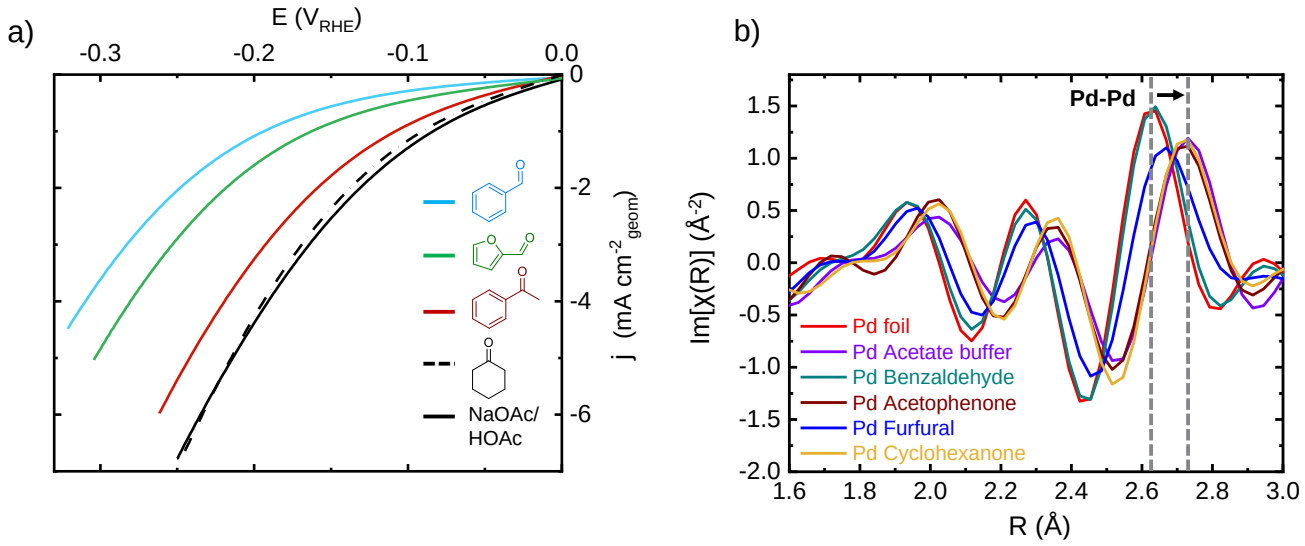

Figure 2.3. (a) Linear sweep voltammograms on polycrystalline Pd rotating disc electrode in the absence and the presence of organic compounds (20 mM): pure electrolyte – dashed black; benzaldehyde – blue; furfural – green; acetophenone – red; cyclohexanone – black. The experiments were performed in 3 M sodium acetate buffer (pH 5) at 0.05 V s^{-1}. (b) Pd K edge EXAFS Im[χ(R)] plot of 5 wt.% Pd/C held at -0.1 V_{RHE} in pure buffer (sodium acetate 0.1 M, pH 5) and in presence of benzaldehyde, acetophenone, furfural or cyclohexanone (20 mM). Pd foil was used as reference.

2.2.4. Probing the state of Pd by EXAFS during electrocatalytic hydrogenation

Palladium reversibly incorporates hydrogen into its lattice to form Pd hydrides (PdH_x), i.e., α-PdH_x with $x < 0.15$ and β-PdH_x with $x \geq 0.4$. Both phases co-exist at intermediate concentrations of interstitial hydrogen,[28, 40, 41] and the lattice parameters of Pd increase as a function of the amount of H incorporated.[41, 42] Interestingly, the concentration of H in the bulk of Pd correlates linearly with the steady state coverage of hydrogen at the surface.[28, 43, 44] Thus, we employed in situ extended fine structure X-ray absorption spectroscopy (EXAFS) to monitor the hydrogen content of the Pd catalyst during ECH.[28]

We calculated the Pd-Pd distance (l_0) of a (hydride-free) reference Pd foil as 2.63 Å from the EXAFS spectra at the Pd K-edge (Figure 2.3 b). Indeed, the Pd-Pd distance increased, e.g., to 2.73 Å at -0.1 V_{RHE}, for Pd/C under cathodic potential in acetate buffer due to the hydrogen incorporation. The molar ratios of hydrogen incorporated into the Pd bulk ([H]/[Pd]) obtained from the lattice expansions increased from 0.04 at 0.15 V_{RHE} (α-PdH_x) to 0.57 at -0.1 V_{RHE}. The latter is close to the nominal β-PdH_x ([H]/[Pd] = 0.67).[45] Interestingly, the presence of the organic compounds hindered further expansion of the Pd-Pd lattice. In presence of acetophenone, cyclohexanone, and furfural, the expansions (∂l) were 0.084 Å, 0.09 Å, and 0.032 Å, respectively. The addition of benzaldehyde resulted in an expansion of only 0.004 Å. These values translate to a phase transition to β-PdH_x with [H]/[Pd] ratios of 0.51 and 0.55 in the presence of acetophenone and cyclohexanone, respectively. In contrast, the [H]/[Pd] ratios were 0.02 and 0.18, in the presence of benzaldehyde and furfural respectively, i.e., in the α-PdH_x ratio range. The trend in bulk H concentration is consistent with the decrease of charge transfer and of the surface availability of hydrogen (from LSV and CV, respectively), which were affected the most by benzaldehyde, followed by furfural, acetophenone, and cyclohexanone. A summary of the [H]/[Pd] ratios is shown in Figure S2.8 and the details of the calculations are described in the Supporting Information 2.5.7. As H atoms are present at the surface under all reaction conditions the rate of H addition is concluded to be significantly slower than the PCET. The presence of the organic compounds, i.e., benzaldehyde and furfural, decreases the coverage of hydrogen by up to two orders of magnitude under OCV and low overpotential ECH conditions. This rapidly changes with increasingly negative potential as the coverage of hydrogen is an exponential function of the overpotential.

The correlation between the bulk [H]/[Pd] ratios and the hydrogenation rates of different molecules (Figure 2.4) indicates that the rate of hydrogenation influences the steady state concentration of surface H available to form hydrogen. Higher hydrogenation rates are coupled to less surface H being present at the surface, and, therefore, less interstitial H in the bulk Pd. Thus, the coverage of the organic compound and the intrinsic reactivity of the relevant surface intermediates determine the availability of hydrogen which impacts the phase composition of Pd.

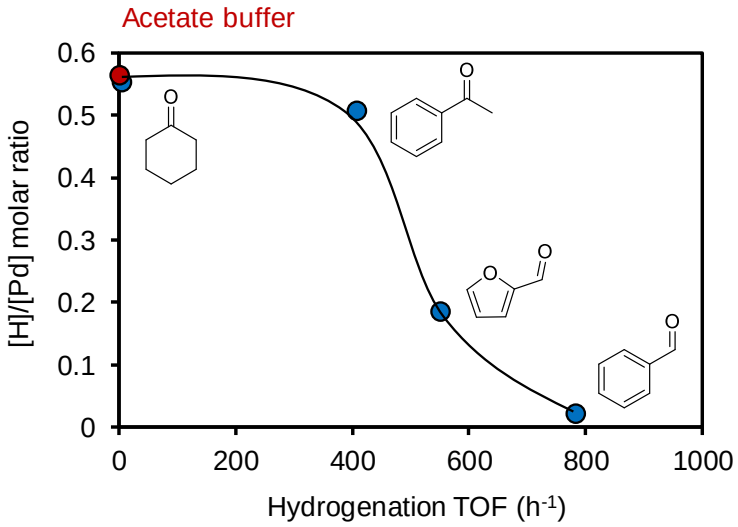

Figure 2.4. Content of absorbed hydrogen (expressed as [H]/[Pd] molar ratio) as a function of the rate of electrocatalytic hydrogenation of different molecules at -0.1 V_{RHE}. The red symbol represents the [H]/[Pd] ratio in the absence of organic compounds.

2.3. Conclusion

We investigated the effect of electric potential and molecular structure of aldehydes and ketones on the state of Pd and its ability to hydrogenate the carbonyl group and to evolve H_2. The rates of electrocatalytic hydrogenation (ECH) of the carbonyl group correlate with their interaction strength with the Pd electrocatalyst (e.g., cyclohexanone < acetophenone < furfural < benzaldehyde). These interactions influence the rates of the competitive H_2 evolution and the cumulative rates of charge transfer at the metal. We hypothesize this is due to the high coverage and reactivity of the organic compounds for hydrogen addition, which decreases the availability of hydrogen directly affecting the rates of H_2 evolution and the phase composition of Pd (PdH_x during reaction).

More negative potentials increase the rates of both hydrogenation and the hydrogen evolution reaction (HER). However, as the electrochemical potential of hydrogen increases with the external bias, competition for active sites limits the concentration of adsorbed organics and decreases hydrogenation rates. The potential at which the HER exceeds the ECH in rate correlates with the adsorption strength of the organic compound. The quantitative description of how the adsorption strength (of the organic substrates) affects the ability of the catalyst to transfer charge to protons, to hydrogenate, and to produce adsorbed H, helps interpreting numerous, so far empiric, observations in the field.

One of the most consequential findings is that the PCET must be significantly more favored than hydrogen addition for these functionalized molecules. The proton coupled electron transfer in the rate determining step capture different trends in ECH rates with applied potential for a range of aldehydes and ketones on Pd. This provides new evidence how electrocatalysis offers a path for the polar groups of organic compounds which is different from the reactions in the absence of an external electric potential and for the hydrogenation of arenes via electrocatalysis.

2.4. Acknowledgements

The research described in this paper is part of the Chemical Transformation Initiative at Pacific Northwest National Laboratory (PNNL), conducted under the Laboratory Directed Research and Development Program at PNNL, a multiprogram national laboratory operated by Battelle for the U.S. Department of Energy under Contract No. DE-AC05-76RL01830. L.C.M., O.Y.G., and J.A. L. would like to acknowledge support by the US DOE, Office of Science, Office of Basic Energy Sciences, Division of Chemical Sciences, Geosciences, and Biosciences. This research used resources of the Advanced Photon Source, an Office of Science User Facility operated for the U.S. Department of Energy (DOE) Office of Science by Argonne National Laboratory and was supported by the U.S. DOE (under Contract No. DE-AC02-06CH11357) and the Canadian Light Source and its funding partners. We acknowledge help from Dr. Mahalingam Balasubramanian and Dr. Nirala Singh.

2.5. Supporting information

2.5.1. Experimental methods

Reagents and materials

All chemicals and reagents were obtained from Sigma-Aldrich and used without further purification: benzaldehyde (≥99.0%), benzyl alcohol (≥99.0%), toluene (≥99.0%), acetophenone (≥99.0%), 1-phenylethanol (≥99.0%), styrene (≥99.0%), ethylbenzene (≥99.0%), furfural (≥99.0%), furfuryl alcohol (≥99.0%), cyclohexanone (≥99.0%), cyclohexanol (≥99.0%), butyraldehyde (≥99.0%), 1-butanol (≥99.0%), vanillin (≥99.0%), vanillyl alcohol (≥99.0%), sodium acetate buffer solution (pH 5.2, 3 M), dichloromethane, isopropanol, NaCl (≥99.0%), KCl (≥99.0%), sodium acetate and acetic acid. $Pd(NO_3)_2$, which was purchased from VWR, and Vulcan® XC-72 carbon were used as received to prepare the 5 wt.% Pd/C electrocatalyst. Carbon felts (> 99.0%) were purchased from Alfa Aesar and graphite rods (99.99%) from Sigma Aldrich. High purity water was obtained from a Milli-Q water purification system with a resistivity of 18 MΩ cm. N_2 (Air Liquide) was utilized as protection gas to remove O_2 from the electrolyte before and during electrocatalytic hydrogenation (ECH) measurements. H_2 (Air Liquide) was used for open circuit voltage measurements.

Catalyst preparation

The carbon supported 5 wt.% Pd catalyst was prepared by the wet impregnation method. To prepare 1g of Pd/C, 0.11 g of $Pd(NO_3)_2$ was dissolved in 3 mL Millipore water and added dropwise to Vulcan® XC-72 carbon and water mixture under continuous stirring. The resulting slurry was stirred for 6 h and then dried overnight at 393 K. The black powder was then heated at 453 K for 3 h under N_2 and subsequently under H_2 at 523 K for 3 h. The heating rate for both thermal steps was 2 K min^{-1} wherein the flow rate of the corresponding gas was 100 mL min^{-1}.

Catalyst characterization: metal content and textural properties

The Pd content of the catalyst was 5 wt. % as determined by ICP measurements. Therefore, the catalyst was digested in concentrated nitric acid in a sealed microwave vessel. After dissolution of all solids, the solution was analyzed on a Perkin Elmer Optima 7300DV ICP-OES instrument.

The specific surface area and pore diameter of the Pd/C electrocatalyst was determined by N_2 physisorption conducted on a Micromeritics ASAP 2020 at liquid nitrogen temperature (77 K). The sample was outgassed at 573 K for 2 h prior to the measurements. The textural properties, as derived from the BET and BJH models applied to the N_2 sorption data showed a surface area of 242 $m^2 g^{-1}$, pore volume of 0.15 $cm^3 g^{-1}$ and average pore width of 4.4 nm (pore volume and width were obtained from BJH adsorption branch)

Catalyst characterization: dispersion of supported Pd

Gas-phase H_2 chemisorption was utilized to determine the Pd dispersion. Before the measurement, the catalyst was outgassed at 543 K for 1 h, followed by activation under H_2. First adsorption isotherms were recorded from 1.3 mbar to 600 mbar at 393 K. After evacuation at 393 K for 1 h, a second isotherm set was measured corresponding to physisorbed H_2 under the same conditions as the first isotherm. The concentration of chemisorbed H_2 was calculated by subtracting the two isotherms and extrapolating to zero H_2 pressure. A stoichiometry of 1:1 for metal to hydrogen was assumed to derive the dispersion from the concentration of chemisorbed hydrogen. The measurements were carried out at high temperatures (393 K) to avoid the formation of bulk Pd hydride.

Transmission electron microscopy (TEM) was performed, as an additional analysis of metal dispersion, on a FEI Tecnai F20 electron microscope. Few catalyst particles were ground and ultrasonically dispersed in ethanol. Drops of the suspension were applied on a copper grid coated with a carbon film and measurements were carried out with an electron detector acceleration voltage of 200 keV. Statistical analysis of the Pd particle size was realized by counting at least 300 particles in several places of the mesh.

In-situ titration of metal sites was performed as described in Ref.[46] We took the TOF of benzaldehyde reduction under open circuit voltage conditions (1 bar H_2) at pH5 as reference (described below), wherein the TOF was calculated using the Pd dispersion determined by hydrogen chemisorption. Then, we measured the TOFs in the presence of increasing amounts of butanethiol.

Electrochemical CO stripping was determined as described in Ref.[47] A 1 M $HClO_4$ solution was saturated with CO in a rotating disc electrode (RDE) setup. We used a Pd/C catalyst ink coated on

glassy carbon as working electrode, a carbon rod as counter electrode and an $Ag/AgCl_2$ electrode as reference. The working electrode was held at 0.4 V_{RHE} for 30 min under bubbling CO, which was followed by removal of CO in the solution by purging Ar for 20 min. The CO stripping voltammograms were finally conducted at a 20 mV s^{-1} scan rate.

Electrocatalytic hydrogenation measurements

Electrocatalytic hydrogenation (ECH) reactions were carried out in a two-compartment well-mixed batch electrolysis cell as described previously.[9] A Nafion 117 proton exchange membrane (Ion Power Inc) was used for separation of cathode and anode compartments. A piece of carbon felt (Alfa Aesar >99.0%, 3 cm x 1.5 cm and 3.2 mm thickness), connected to a graphite rod (Sigma Aldrich, 99.99%), was used as working electrode in the cathode compartment. 10 mg of 5 wt% Pd/C catalyst was dispersed in 1 mL of Millipore water and 1.5 mL of isopropanol, followed by ultrasonication for 10 minutes. The catalyst suspension was then dropped on the carbon felt and dried. An Ag/AgCl electrode (saturated KCl) from Ametek with a double junction protection was used as reference electrode in the cathode chamber and a platinum mesh (Alfa Aesar, 99.9 %) was used as counter electrode in the anodic compartment. A schematic view of the experimental setup is shown in Figure S2.1.

The reference electrode was calibrated against a reversible hydrogen electrode (RHE) in sodium acetate buffer and all potentials throughout this work are reported on the RHE reference scale. 60 mL sodium acetate buffer (3 M) with a pH of 5.2 was used as both catholyte and anolyte for all electrocatalytic hydrogenation reactions. The measurements were conducted at atmospheric pressure and at room temperature (298 K). During the experiments, the catholyte was sparged with N_2. All electrocatalytic experiments were performed using a BioLogic SP-150 potentiostat. Prior to the measurement, polarization of the catalyst was conducted under a constant current of -40 mA for 15 minutes. For all reactions the organic compound was added to the cathode compartment to adjust the initial concentration of 20 mmol L^{-1}. Previous control experiments showed an increasing ECH rate with increasing stirring speed until 400 rpm and hence all of the experiments were carried out at 500 rpm. The cell resistance was determined by potentiostatic electrochemical impedance spectroscopy (PEIS), followed by an 85 % iR compensation and correction of the applied potentials during all measurements.

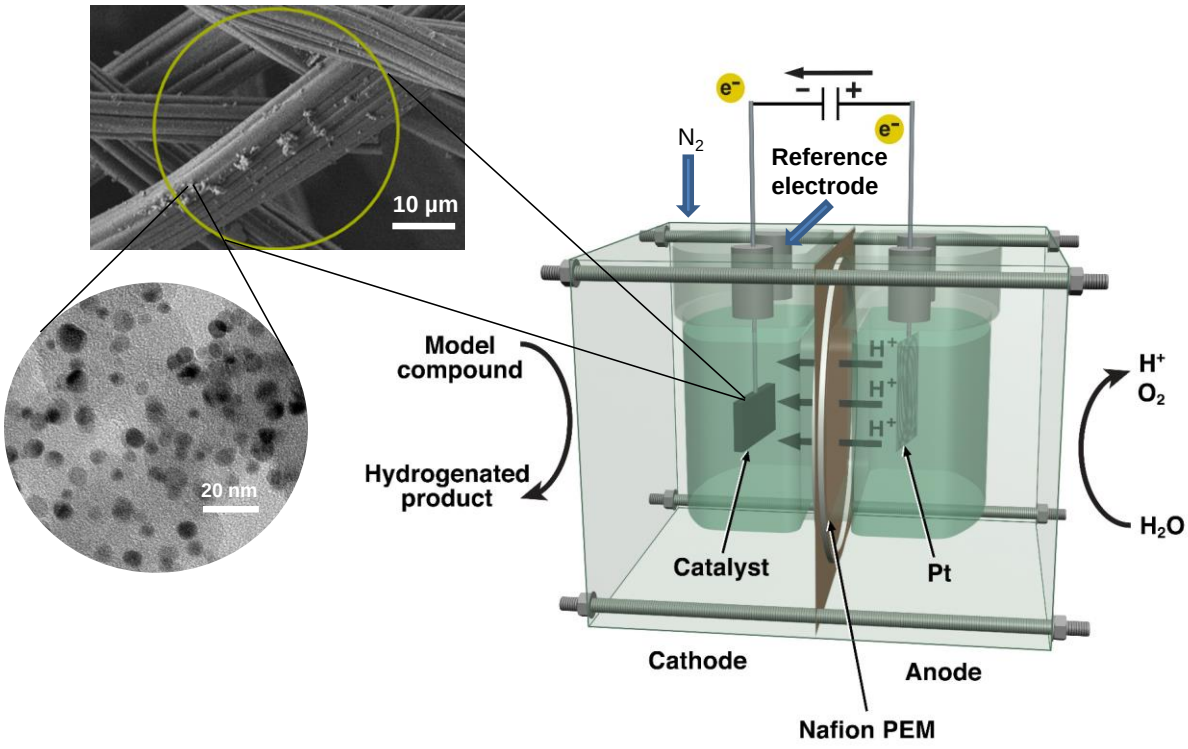

Figure S2.1. Scheme of the batch cell for electrochemical hydrogenation with the catalyst loaded into the carbon felt working electrode. Adapted from Refs.[9, 29]

Catalytic hydrogenation under open circuit voltage conditions and open circuit voltage measurements

Hydrogenation under open circuit voltage conditions (OCV) (previously referred to as thermo-catalytic hydrogenation - TCH) were performed in a glass beaker using 60 mL acetate buffer (pH 5.2) as electrolyte. 10 mg of Pd/C were added to the electrolyte and stirred at 500 rpm for 20 minutes with 1 bar of H_2 saturating the solution. All measurements were conducted at room temperature (298 K) and atmospheric pressure while the electrolyte was sparged continuously with H_2 throughout the experiments. The concentration of the organics was 20 mmol L^{-1}.

Determination of the actual open circuit voltage (OCV) in presence of organics were conducted using the same cell set-up as for ECH experiments. The catalyst was reduced under a constant current of -40 mA for 15 min prior to each measurement while passing a N_2 flow. Afterwards, the gas was switched to H_2 and after 20 minutes the first OCV was measured in the absence of reactive organic compounds. Then, the organic compound was added to obtain a concentration of 20 mmol L^{-1} and the change in the OCV was monitored.

Product analysis of batch reactions

The progress of the reaction was monitored by sampling aliquots of 1 mL from the cathode compartment of the electrocatalytic cell or thermal reactor. The organic compounds were extracted by using 3 mL of dichloromethane. NaCl was used to enhance the extraction efficiency and cyclohexanone was chosen as the external standard. In case of cyclohexanone hydrogenation, acetophenone was used as the external standard. The quantitative analysis of the extracted organic compounds was conducted by gas chromatography (GC 2010 Plus, Shimadzu) equipped with a Rtx®-5MS column (30 m x 250 µm) and a flame ionization detector.

Calculations

Conversion, reaction rate of ECH, OCV/TCH and HER, turnover frequency (TOF), and Faradaic efficiency (FE) were calculated as follows.

$$\text{Conversion} = \frac{\text{moles of reactant consumed}}{\text{initial moles of reactant}} \text{ x } 100 \qquad [\%]$$

$$\text{ECH reaction rate} = \frac{\text{moles of reactant consumed by ECH}}{\text{time x mass of metal}} \qquad [\text{mol s}^{-1}\ \text{g}_{\text{metal}}^{-1}]$$

$$\text{TCH reaction rate} = \frac{\text{moles of reactant consumed by TCH}}{\text{time x mass of metal}} \qquad [\text{mol s}^{-1}\ \text{g}_{\text{metal}}^{-1}]$$

$$\text{HER reaction rate} = \frac{\text{moles of hydrogen gas produced by HER}}{\text{time x mass of metal}} \qquad [\text{mol s}^{-1}\ \text{g}_{\text{metal}}^{-1}]$$

$$\text{TOF} = \frac{\text{moles of reactant consumed}}{\text{time x moles of exposed metal}} \qquad [\text{h}^{-1}]$$

$$\text{FE} = \frac{\text{electrons consumed by ECH}}{\text{total electrons passed}} \text{ x } 100 \qquad [\%]$$

Rotating ring disk electrode measurements

Additional electrocatalytic measurements of furfural hydrogenation were carried out on a rotating ring disk electrode (RRDE) setup from Pine Research with a Bio-Logic VSP-300 as potentiostat at room temperature. A glassy carbon disk drop-casted with 5 wt. % Pd/C with a Pd loading of 19 µg cm^{-2} and a polycrystalline Pt ring were used as working electrodes. The rotation speed was set to 1600 rpm. The counter electrode was a Pt-wire separated from the working electrode chamber by a porous glass frit. An Ag/AgCl (saturated KCl) reference electrode with a double

junction protection (Ametek) was utilized as reference electrode. Prior to the experiments, the glassy carbon disk was polished with 0.05 µm alumina suspension on a microcloth polishing pad (Buehler) and cleaned by ultrasonication in Millipore water. Sodium acetate buffer (3 M, pH 5.2) was used as electrolyte and was purged with Ar throughout the experiments. To prepare the thin film Pd/C electrode, 4 mg of 5 wt.% Pd/C were dispersed in 1.4 ml isopropanol, 0.6 ml water and 10 µL of 5 wt. % Nafion solution (Ion Power) by sonication. The ink was drop-casted onto the glassy carbon disk in order to result in a Pd loading of 19 µg cm^{-2}. To determine the collection efficiency N of hydrogen formed on the disk and detected at the ring, simultaneous chronoamperometry measurements were performed in the pure electrolyte. An oxidizing potential of 0.5 V_{RHE} was constantly applied on the ring electrode, while the disk was held at reduction potentials, starting from 0 V_{RHE} to -0.14 V_{RHE} until constant currents were obtained. To deconvolute organic hydrogenation current and hydrogen evolution current, the same experiments were performed in presence of 20 mM organic. Using Eq. (S2.1) from reference [14], the hydrogenation current can be calculated by utilizing the collection efficiencies corresponding to the applied potential.

$$I_{hydrogenation} = I_{disk} - \frac{I_{ring}}{N} \qquad (S2.1)$$

Where $I_{hydrogenation}$ describes the current due to organic hydrogenation, I_{disk} is the overall current on the disk (current of organic hydrogenation and hydrogen evolution combined) and I_{ring} is the current detected from oxidizing hydrogen on the ring electrode. The collection efficiencies obtained from the chronoamperometry measurements were 13% at low potential and decreased to 6% at more negative -0.14 V_{RHE} potential.

Linear sweep voltammetry using a rotating disc electrode

Linear sweep voltammograms (LSV) were performed on a rotating disc electrode (RDE) setup with a Pd disc (Pine Research) as working electrode. The same setup as in the RRDE experiments was used with 0.1 M sodium acetate buffer (pH 4.7) as electrolyte purged with N_2. The LSV measurements were carried out in blank electrolyte or 20 mM organic concentration and were recorded at 0.05 V s^{-1} scan rate.

2.5.2. Characterization of the catalyst and quantification of the exposed Pd area

We have used a Pd/C catalyst (5 wt. % Pd) as a benchmark material to compare different techniques to determine the dispersion of the supported metal. As we reported before for C-supported Pt,[46] the determination of exposed metal surface by gas-phase hydrogen titration and aqueous phase titration with a thiol were in excellent agreement for our Pd catalyst. We determined a value of 94 m^2 of exposed Pd per gram of catalyst, i.e., a metal dispersion of 21 %. This value was further confirmed by electrochemical CO stripping and the corresponding Pd particle size, 4.7 nm, was in excellent agreement with statistical analysis of TEM images. Representative TEM micrographs and the corresponding particle size distribution is shown in Figure S2.2.

In the in-situ titration of metal sites with butanethiol, the reactivity decreased as a linear function of the molar ratio of thiol and Pd with an intercept close to one (Figure S2.3). This validates the H_2 chemisorption measurements and the H:Pd stoichiometry of one assumed in such technique.

The outcome of all techniques is summarized in Table S2.1. The excellent agreement shows that –at least for the particle size range of our Pd benchmark catalyst– metal dispersion determined by TEM and H_2 chemisorption (common techniques for characterization of heterogeneous catalysts) are valid for electrochemical reactions occurring in aqueous phases.

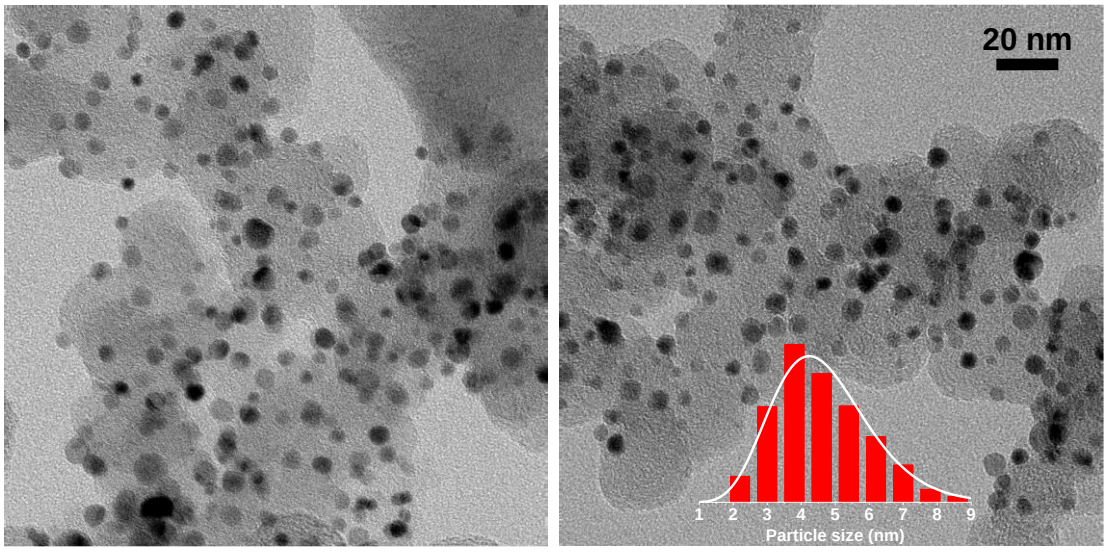

Figure S2.2. Representative TEM image and the corresponding particle size distribution histogram of the 5 wt. % Pd/C catalyst.

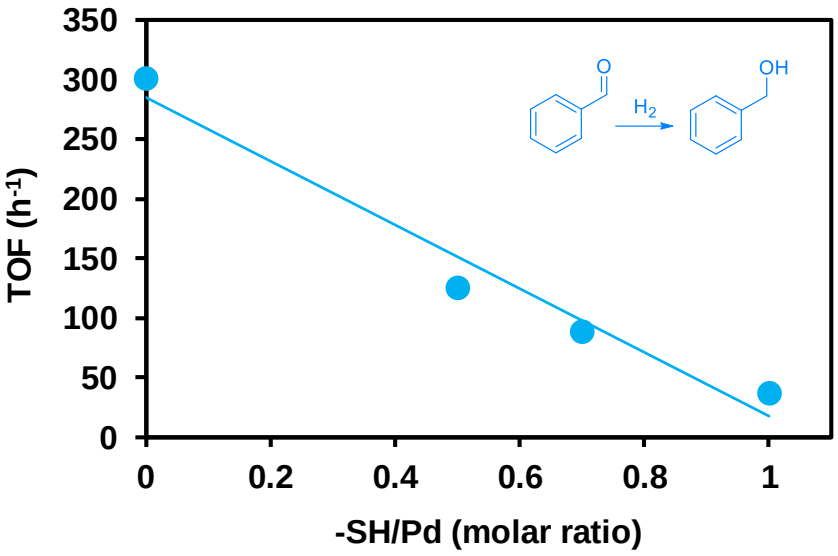

Figure S2.3. Turnover frequencies (TOF) of open circuit benzaldehyde hydrogenation on Pd/C catalyst in the presence of varying butanethiol concentration. –SH/Pd indicates the molar ratio of added thiol to exposed Pd.

Table S2.1. Summary of exposed metal, metal dispersion, and particle size as determined by several physicochemical characterization techniques.

		Gas Phase	**Liquid-phase**	
	TEM	H_2	Thiol titration	CO stripping
Exposed metal (μmol g^{-1})	99	99	94	89
Exposed metal (m^2 g^{-1})	94	94	90	86
Dispersion (%)	21	21	20	19
Particle size (nm)	4.7	4.7	5	5.2

2.5.3. Complementary figures

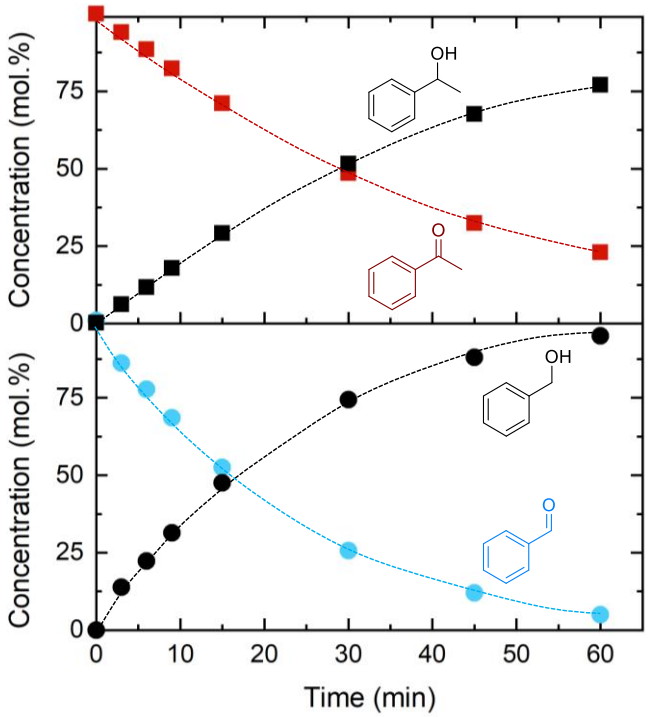

Figure S2.4. Concentration profiles along time for the electrocatalytic hydrogenation of benzaldehyde and acetophenone. Dashed lines are to guide the eye. The reactions were performed in an acetate buffer (pH 5.2) at room temperature in a divided electrolysis batch reactor applying a potential of -0.28 V vs RHE.

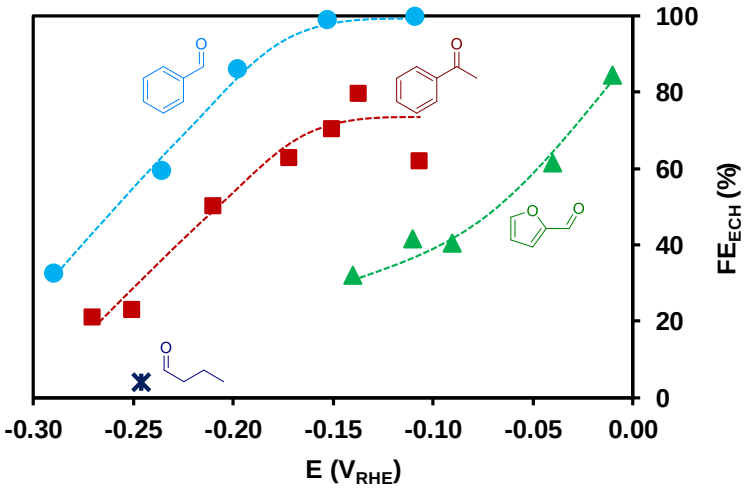

Figure S2.5. Faradaic efficiencies observed during the electrocatalytic hydrogenation of benzaldehyde, acetophenone and butyraldehyde in the electrochemical batch cell and of furfural under RRDE conditions at varying potentials. All reactions were performed in an acetate buffer (pH 5.2) at room temperature in a divided electrolysis batch reactor. Dashed lines are to guide the eye.

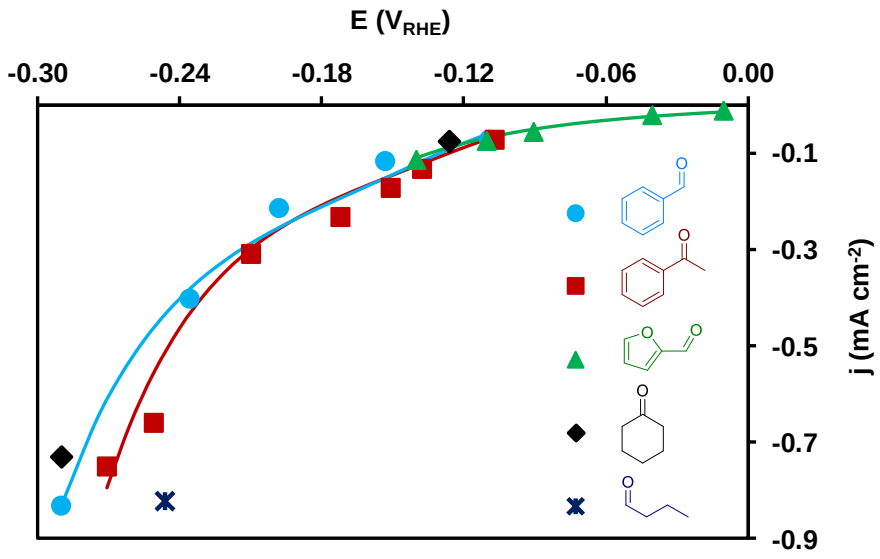

Figure S2.6. Current densities measured during the conversion of organic molecules - benzaldehyde–blue; acetophenone–red; furfural–green (from RRDE experiments); cyclohexanone-black; butyraldehyde-purple - at varying potential. The lines correspond to fitted rates calculated with Butler-Volmer kinetics as described in the main text.

2.5.4. Electrocatalytic hydrogenation of furfural

The experiment of furfural hydrogenation in batch mode exhibited carbon balances (quantifying furfuryl alcohol and unreacted furfural in solution and evaporated during the experiment) from 60 % to 80 %, which suggested the presence of parasitic polymerization reactions. In line with this proposal, several studies have shown that furanic compounds like furfural and furfuryl alcohol are prone to degrade and polymerize, particularly under electrocatalytic conditions. Carbon balances below 70 % are common[21, 22, 48] and long-chain molecules such as humins have been found to form on the electrodes and in solution as a function of the pH and potential.[22, 48-52]

Interestingly, polymerization seems to be slower under gas phase H_2. For instance, Jung et al showed that in mildly acidic electrolytes (under nonelectrochemical conditions) the carbon balance decreased with time at constant applied cathodic potentials but at slow rate.[22] Other studies have reported that, under thermal hydrogenation, no polymerization on Pd/C has not been observed in water.[51]

Other operation parameters seem to influence the side reactions of furfural. For instance, in previous reports, furfural polymerization was negligible under flow conditions (carbon balances around 100 %).[19, 20] In retrospective, this may have been due to shorter residence times of the

organics on the catalyst surface. Thus, to minimize the possibility of polymerization affecting the kinetic data, we performed the hydrogenation of furfural on a rotating ring disk electrode (RRDE). Here, a laminar flow of solution towards and across the electrode is maintained by the electrode rotation, which results in a continuous replacement of solution and electrode reaction products. The experimental protocols to deconvolute the currents from furfural reduction and from H_2 evolution were taken from literature.[14] Unfortunately, the collection efficiency of H_2 generated on the disk and detected on the ring decreased with negative potential. Hence, only electrode potentials more positive than -0.14 V_{RHE} were utilized for the analysis of furfural ECH.

2.5.5. Kinetic models of electrocatalytic hydrogenation coupled with hydrogen evolution.

First hydrogenation (proton couple electron transfer) being rate limiting

In this kinetic model, we assumed that the hydrogen evolution reaction as well as the electrocatalytic hydrogenation (ECH) proceed through reduction of hydronium ions. For the ECH we proposed a proton coupled electron transfer (PCET) mechanism. The adsorption of the organic molecule is fast and equilibrated (Si) and the rate determining step is the first hydrogen addition to the adsorbed compound. This, in turn, proceeds as a proton coupled electron transfer (PCET) (Sii). Therefore, the second hydrogenation and the product desorption are kinetically irrelevant, (Siii) and (Siv).

Organic adsorption:	$RCHO + * \rightleftarrows RCHO*$	(Si)
1.H addition :	$RCHO* + H_3O^+ + e^- \rightarrow RCHOH* + H_2O$	(Sii)
2.H addition:	$RCHOH* + H_3O^+ + e^- \rightleftarrows RCH_2OH* + H_2O$	(Siii)
Organic desorption:	$RCH_2OH* \rightleftarrows RCH_2OH + *$	(Siv)

We consider the aldehyde “RCHO” as the organic species which undergoes reduction to the intermediate “RCHOH” and further to the alcohol “RCH_2OH”. “*” denotes the active empty sites or compounds adsorbed on active sites.

The H_2 evolution reaction (HER) occurs through Volmer step, followed by either Heyrovsky or Tafel step. For this kinetic model we assume that the Volmer step (Sv), the reduction of hydronium

ions, is equilibrated and the electrochemical hydrogen generation (Heyrovsky step (Svi)) is rate limiting.

Volmer step: $H_3O^+ + e^- + * \rightleftarrows H^* + H_2O$ (Sv)

Heyrovsky step: $H^* + H_3O^+ + e^- \rightarrow H_2 + H_2O + *$ (Svi)

Since the adsorption of the organic reactant is equilibrated, its equilibrium constant K_{RCHO} can be described as follows (Eq. (S2.2)) and further rearranged to the organic coverage θ_{RCHO} (Eq.(S2.3)).

$$K_{RCHO} = \frac{\theta_{RCHO}}{a_{RCHO}\theta_*} \quad (S2.2)$$

$$\theta_{RCHO} = K_{RCHO}\, a_{RCHO}\, \theta_* \quad (S2.3)$$

K_{RCHO} is the equilibrium constant of the organic reactant, θ_{RCHO} and θ_* are the organic and empty site coverages, respectively, and a_{RCHO} denotes the organic compounds activity.

For the hydrogen evolution reaction, we assumed a fast Volmer reaction. The forward r_{Vr} and backward reaction r_{-Vr} are:

$$r_{Vr} = k_{Vr}\, a_{H_3O^+}\theta_* = k^o_{Vr}\, e^{-\alpha f \eta}\, a_{H_3O^+}\, \theta_* \quad (S2.4)$$

$$r_{-Vr} = k_{-Vr}\, \theta_H\, a_{H_2O} = k^o_{-Vr}\, e^{(1-\alpha) f \eta}\, \theta_H\, a_{H_2O} \quad (S2.5)$$

The potential dependent rate constants are defined as $k = k^0\, e^{-\alpha f \eta}$ for the forward reaction and as $k_- = k^o_-\, e^{(1-\alpha) f \eta}$ for the backward reaction.[32] k^0 is the intrinsic, potential independent, rate constant, η is the applied overpotential, α is the electron transfer coefficient, and f is F/RT with F: Faraday's constant, R: universal gas constant and T: absolute temperature. θ_H is the hydrogen coverage, $a_{H_3O^+}$ and a_{H_2O} are the hydronium ion and water activities, respectively. Equalizing the two equation (S2.4) and (S2.5) due to the equilibrated Volmer step and rearranging to the intrinsic equilibrium constant K^o_{Vr}:

$$r_{Vr} = r_{-Vr} \quad (S2.6)$$

$$k^o_{Vr}\, e^{-\alpha f \eta}\, a_{H_3O^+}\, \theta_* = k^o_{-Vr}\, e^{(1-\alpha) f \eta}\, \theta_H\, a_{H_2O} \quad (S2.7)$$

$$\frac{k^o_{Vr}\, e^{-\alpha f \eta}}{k^o_{-Vr}\, e^{(1-\alpha) f \eta}} = K^o_{Vr}\, e^{-f\eta} = K_{Vr} = \frac{\theta_H\, a_{H_2O}}{a_{H_3O^+}\, \theta_*} \quad (S2.8)$$

where, K_{Vr} is the potential dependent Volmer equilibrium constant. Solving Eq. (S2.8) for the hydrogen coverage θ_H gives Eq. (S2.9).

$$\theta_H = \frac{K_{Vr}\, a_{H_3O^+}\, \theta_*}{a_{H_2O}} = \frac{K_{Vr}^o\, e^{-f\eta}\, a_{H_3O^+}\, \theta_*}{a_{H_2O}} \qquad (S2.9)$$

In the site balance, we include adsorbed hydrogen and the reactant as we infer these are the dominant species under our conditions.

$$1 = \theta_* + \theta_{RCHO} + \theta_H \qquad (S2.10)$$

Substituting the hydrogen coverage θ_H (Eq. (S2.9)) and the organic coverage θ_{RCHO} (Eq. (S2.3)) leads to the expression of free site coverage θ_*.

$$1 = \theta_* + K_{RCHO} a_{RCHO} \theta_* + \frac{K_{Vr}^o\, e^{-f\eta}\, a_{H_3O^+}\, \theta_*}{a_{H_2O}} \qquad (S2.11)$$

$$\theta_* = \frac{1}{1 + K_{RCHO}\, a_{RCHO} + \frac{K_{Vr}^o\, e^{-f\eta}\, a_{H_3O^+}}{a_{H_2O}}} \qquad (S2.12)$$

Assuming the first hydrogen addition of the adsorbed organic is rate limiting and proceeds via a PCET mechanism (ii), the ECH rate is as follows:

$$r_{ECH_1} = k_{ECH_1}\, \theta_{RCHO}\, a_{H_3O^+} \qquad (S2.13)$$

where, k_{ECH_1} is the potential dependent rate constant of the first hydrogen addition step. Substitution with its intrinsic rate constant $k_{ECH_1}^o$, organic coverage θ_{RCHO} (Eq. (S2.3)), and the empty site coverage θ_* (Eq. (S2.12)), gives the final hydrogenation rate expression (Eq. (S2.15)) with α_{ECH} as the ECH charge transfer coefficient:

$$r_{ECH_1} = k_{ECH_1}^o\, e^{-\alpha_{ECH} f\eta}\, K_{RCHO}\, a_{RCHO}\, \theta_*\, a_{H_3O^+} \qquad (S2.14)$$

$$r_{ECH_1} = \frac{k_{ECH_1}^o\, e^{-\alpha_{ECH} f\eta}\, K_{RCHO}\, a_{RCHO}\, a_{H_3O^+}}{1 + K_{RCHO}\, a_{RCHO} + \frac{K_{Vr}^o\, e^{-f\eta}\, a_{H_3O^+}}{a_{H_2O}}} \qquad (S2.15)$$

When the Volmer step (v) is very fast and the electrochemical hydrogen evolution (vi) is determining, the HER rate equation is given by:

$$r_{HER} = k_{Hy}\, \theta_H\, a_{H_3O^+} \qquad (S2.16)$$

Where, k_{Hy} is the potential dependent Heyrovsky rate constant. Insertion of hydrogen θ_H and active site coverage θ_* (Eq. (S2.9) and (S2.12)) and rearrangement, leads to Eq. (S2.18), where α_{HER} is the hydrogen evolution charge transfer coefficient.

$$r_{HER} = k_{Hy}^{o}\, e^{-\alpha_{HER} f\eta}\, \frac{K_{Vr}^{o}\, e^{-f\eta}\, \theta_* a_{H_3O^+}}{a_{H_2O}}\, a_{H_3O^+} \qquad (S2.17)$$

$$r_{HER} = \frac{k_{Hy}^{o}\, e^{-f\eta(\alpha_{HER}+1)}\, K_{Vr}^{o}\, a_{H_3O^+}^{2}}{a_{H2O}\left(1 + K_{RCHO}\, a_{RCHO} + \frac{K_{Vr}^{\circ}\, e^{-f\eta}\, a_{H_3O^+}}{a_{H2O}}\right)} \qquad (S1.18)$$

Eq. (S2.19) describes the current, where *n* is the number of electrons involved in the overall reaction and *A* is the surface area of the catalyst.

$$I = nFAr_i = nFA(r_{ECH} + r_{HER}) \qquad (S2.19)$$

$$I = nFA\left(\frac{k_{ECH_1}^{o}\, e^{-\alpha_{ECH} f\eta}\, K_{RCHO}\, a_{RCHO}\, a_{H_3O^+}}{1 + K_{RCHO}\, a_{RCHO} + \frac{K_{Vr}^{o}\, e^{-f\eta}\, a_{H_3O^+}}{a_{H_2O}}} + \frac{k_{Hy}^{o}\, e^{-f\eta(\alpha_{HER}+1)}\, K_{Vr}^{o}\, a_{H_3O^+}^{2}}{a_{H2O}\left(1 + K_{RCHO}\, a_{RCHO} + \frac{K_{Vr}^{\circ}\, e^{-f\eta}\, a_{H_3O^+}}{a_{H2O}}\right)}\right) \qquad (S2.20)$$

Kinetic fittings for benzaldehyde, acetophenone and furfural hydrogenation with the concurrent hydrogen evolution reactions were performed by using Eq. (S2.15) and (S2.18). The fitted rates are displayed in Figure 2.1 and Figure 2.2 in the main manuscript. Following Eq. (S2.20), the fitted current densities are portrayed in Figure S2.6. The associated fitting parameters are summarized in Table S2.2. For K_{RCHO}, we utilized the adsorption constants determined by RDE (Table S2.4).

Table S2.2. Kinetic fitting parameters for hydrogen evolution and benzaldehyde, acetophenone and furfural hydrogenation with a proton coupled electron transfer as first, rate determining hydrogenation step.

	K_{Vr}^{o}	$k_{ECH_1}^{o}$	k_{Hy}^{o}	α_{ECH}	α_{HER}
Benzaldehyde	58.17	0.11	1.81	0.18	0.1
Acetophenone	1153	0.015	0.58	0.47	0.1
Furfural	69600	0.034	0.31	0.5	0.1

Second hydrogenation (proton couple electron transfer) being rate limiting

In this kinetic model, we assumed that ECH proceeds with a proton coupled electron transfer (PCET) mechanism. The adsorption of the organic molecule (Si) as well as the first hydrogen addition step are fast (Svii), followed by the rate determining second hydrogen addition to the adsorbed intermediate, which also proceeds through a PCET mechanism (Sviii). Finally, the desorption of the organic is equilibrated (Siv).

1.H addition: $RCHO^* + H_3O^+ + e^- \rightleftarrows RCHOH^* + H_2O$ (Svii)

2.H addition: $RCHOH^* + H_3O^+ + e^- \rightarrow RCH_2OH^* + H_2O$ (Sviii)

Analogue to the previous HER kinetics, we propose an equilibrated Volmer step (Sv), the reduction of hydronium ions, followed by the rate limiting electrochemical hydrogen generation (Heyrovsky step (Svi)).

Considering the equilibrated organic adsorption, its coverage θ_{RCHO} is expressed as follows:

$$\theta_{RCHO} = K_{RCHO}\, a_{RCHO}\, \theta_* \qquad (S2.21)$$

where K_{RCHO} is the equilibrium constant of the organic reactant, θ_{RCHO} and θ_* are the organic and empty site coverages, respectively, and a_{RCHO} denotes the organic compound activity.

Following the previous derivations for the equilibrated Volmer step (Sv), the potential dependent coverage of hydrogen θ_H (Eq. (S2.22)) is given by:

$$\theta_H = \frac{K_{Vr}\, a_{H_3O^+}\, \theta_*}{a_{H_2O}} = \frac{K_{Vr}^o\, e^{-f\eta}\, a_{H_3O^+}\, \theta_*}{a_{H_2O}} \qquad (S2.22)$$

where, K_{Vr} and K_{Vr}^o are the potential dependent and intrinsic Volmer equilibrium constant, respectively. f is F/RT with F: Faraday's constant, R: universal gas constant and T: absolute temperature. η is the applied overpotential, $a_{H_3O^+}$ and a_{H_2O} are the hydronium ion and water activities.

The hydrogenated intermediate RCHOH* can be described through its potential dependent equilibrium constant K_{RCHOH} (Eq. (S2.23)), following the mechanism (Svii), and solved for its coverage θ_{RCHOH} (Eq. (S2.24)). The same potential dependencies are valid for K_{RCHOH} as derived previously for the Volmer equilibrium constant.

$$K_{RCHOH} = K^{o}_{RCHOH}\, e^{-f\eta} = \frac{\theta_{RCHOH}\, a_{H_2O}}{\theta_{RCHO}\, a_{H_3O^+}} \qquad (S2.23)$$

$$\theta_{RCHOH} = \frac{K^{o}_{RCHOH}\, e^{-f\eta}\, \theta_{RCHO}\, a_{H_3O^+}}{a_{H_2O}} \qquad (S2.24)$$

The site balance comprises of adsorbed hydrogen, the reactant and its intermediate. These are the main adsorbed compounds under our conditions.

$$1 = \theta_* + \theta_H + \theta_{RCHO} + \theta_{RCHOH} \qquad (S2.25)$$

Substituting the hydrogen coverage θ_H (Eq. (S2.22)), the organic coverages θ_{RCHO} (Eq. (S2.21)) and θ_{RCHOH} (Eq. (S2.24)) lead to the expression of active site coverage θ_* (Eq. (S2.27)).

$$1 = \theta_* + \frac{K^{o}_{Vr}\, e^{-f\eta}\, a_{H_3O^+}\, \theta_*}{a_{H_2O}} + K_{RCHO}\, a_{RCHO}\, \theta_* + \frac{K^{o}_{RCHOH}\, e^{-f\eta}\, K_{RCHO}\, a_{RCHO}\, \theta_*\, a_{H_3O^+}}{a_{H_2O}} \qquad (S2.26)$$

$$\theta_* = \frac{1}{1 + K_{RCHO} a_{RCHO} + \frac{K^{o}_{Vr}\, e^{-f\eta}\, a_{H_3O^+}}{a_{H_2O}} + \frac{K^{o}_{RCHOH}\, e^{-f\eta}\, K_{RCHO}\, a_{RCHO}\, a_{H_3O^+}}{a_{H_2O}}} \qquad (S2.27)$$

Assuming the second hydrogen addition of the organic intermediate is rate limiting and proceeds via a PCET mechanism (Sviii), the ECH rate is as follows:

$$r_{ECH_2} = k_{ECH_2}\, \theta_{RCHOH}\, a_{H_3O^+} \qquad (S2.28)$$

where, k_{ECH_2} is the potential dependent rate constant of the second hydrogen addition step. Substitution with its intrinsic rate constant $k^{o}_{ECH_2}$, organic intermediate coverage θ_{RCHOH} (Eq. (S2.24)) and this with the initial organic coverage θ_{RCHO} (Eq. (S2.21)), followed by θ_* (Eq. (S2.27)), gives the final hydrogenation rate expression (Eq. (S2.30)). Here, α_{ECH} is the charge transfer coefficient of ECH.

$$r_{ECH_2} = k^{o}_{ECH_2}\, e^{-\alpha_{ECH} f\eta}\, \frac{K^{o}_{RCHOH}\, e^{-f\eta}\, K_{RCHO}\, a_{RCHO}\, \theta_*\, a_{H_3O^+}}{a_{H_2O}}\, a_{H_3O^+} \qquad (S2.29)$$

$$r_{ECH_2} = \frac{k^{o}_{ECH_2}\, e^{-f\eta(\alpha_{ECH}+1)}\, K^{o}_{RCHOH}\, K_{RCHO}\, a_{RCHO}\, a^{2}_{H_3O^+}}{a_{H_2O}\left(1 + K_{RCHO} a_{RCHO} + \frac{K^{o}_{Vr}\, e^{-f\eta}\, a_{H_3O^+}}{a_{H_2O}} + \frac{K^{o}_{RCHOH}\, e^{-f\eta}\, K_{RCHO}\, a_{RCHO}\, a_{H_3O^+}}{a_{H_2O}}\right)} \qquad (S2.30)$$

Assuming mechanism (v) and (vi), the HER rate equation is expressed in Eq. (S2.31).

$$r_{HER} = k_{Hy}\,\theta_H\,a_{H_3O^+} \qquad (S2.31)$$

where, k_{Hy} is the potential dependent Heyrovsky rate constant. Insertion of the coverages θ_H and θ_* (Eq. (S2.21) and (S2.27)) and rearrangement, leads to the final Eq. (S2.33), where α_{HER} is the hydrogen evolution-based charge transfer coefficient.

$$r_{HER} = k_{Hy}^{o}\,e^{-\alpha_{HER} f\eta}\,\frac{K_{Vr}^{o}\,e^{-f\eta}\,a_{H_3O^+}\,\theta_*}{a_{H_2O}}\,a_{H_3O^+} \qquad (S2.32)$$

$$r_{HER} = \frac{k_{Hy}^{o}\,e^{-f\eta(\alpha_{HER}+1)}\,K_{Vr}^{o}\,a_{H_3O^+}^{2}}{a_{H_2O}\left(1+K_{RCHO}a_{RCHO}+\frac{K_{Vr}^{o}\,e^{-f\eta}\,a_{H_3O^+}}{a_{H_2O}}+\frac{K_{RCHOH}^{o}\,e^{-f\eta}\,K_{RCHO}\,a_{RCHO}\,a_{H_3O^+}}{a_{H_2O}}\right)} \qquad (S2.33)$$

As previously mentioned, the overall current is defined as follows (Eq. (S2.34)), where *n* it the number of electrons involved in the overall reaction and *A* is the surface area of the catalyst.

$$I = nFAr_i = nFA(r_{ECH} + r_{HER}) \qquad (S2.34)$$

$$\Rightarrow I = nFA\left(\frac{k_{ECH_2}^{o}\,e^{-f\eta(\alpha_{ECH}+1)}\,K_{RCHOH}^{o}\,K_{RCHO}\,a_{RCHO}\,a_{H_3O^+}^{2}}{a_{H_2O}\left(1+K_{RCHO}a_{RCHO}+\frac{K_{Vr}^{o}\,e^{-f\eta}\,a_{H_3O^+}}{a_{H_2O}}+\frac{K_{RCHOH}^{o}\,e^{-f\eta}\,K_{RCHO}\,a_{RCHO}\,a_{H_3O^+}}{a_{H_2O}}\right)}+\right.$$

$$\left.\frac{k_{Hy}^{o}\,e^{-f\eta(\alpha_{HER}+1)}\,K_{Vr}^{o}\,a_{H_3O^+}^{2}}{a_{H_2O}\left(1+K_{RCHO}a_{RCHO}+\frac{K_{Vr}^{o}\,e^{-f\eta}\,a_{H_3O^+}}{a_{H_2O}}+\frac{K_{RCHOH}^{o}\,e^{-f\eta}\,K_{RCHO}\,a_{RCHO}\,a_{H_3O^+}}{a_{H_2O}}\right)}\right) \qquad (S2.35)$$

Kinetic fittings for benzaldehyde, acetophenone and furfural hydrogenation with the concurrent hydrogen evolution reactions were performed by using Eq. (S2.30) and (S2.33). The fitting parameters are listed in Table S2.3. For K_{RCHO}, we utilized the adsorption constants determined by RDE (Table S2.4).

Table S2.3. Kinetic fitting parameters for hydrogen evolution and benzaldehyde, acetophenone and furfural hydrogenation with a proton coupled electron transfer as second, rate determining hydrogenation step.

	K_{RCHOH}^{o}	K_{Vr}^{o}	$k_{ECH_2}^{o}$	k_{Hy}^{o}	α_{ECH}	α_{HER}
Benzaldehyde	0.6	13.4	0.27	5.87	0.08	0.7
Acetophenone	0.7	1.8	0.35	111	0.01	0.6
Furfural	343	84	0.05	11345	0.22	0.5

Combined reversible electrochemical adsorption with first hydrogen addition

Implementing a steady state approximation, we consider the electrocatalytic hydrogenation occurring through a reversible step of combined reactant adsorption and first hydrogen addition by PCET (Six) and the second step proceeding through a reversible and neutral hydrogen addition (Sx). The product desorption is assumed to be equilibrated (iv).

Organic adsorption + 1.H addition: $RCHO + H_3O^+ + e^- + * \rightleftarrows RCHOH* + H_2O$ (Six)

2.H addition: $RCHOH* + H* \rightleftarrows RCH_2OH* + *$ (Sx)

For HER, an equilibrated generation of adsorbed hydrogen (Sv) and a limiting reduction of hydronium ions to molecular hydrogen (Svi) were assumed as for the previous models.

The former kinetic derivations of the equilibrated Volmer step (Sv) are used to yield Eq. (S2.36) for the hydrogen coverage θ_H.

$$\theta_H = \frac{K_{Vr}\, a_{H_3O^+}\, \theta_*}{a_{H_2O}} = \frac{K_{Vr}^o\, e^{-f\eta}\, a_{H_3O^+}\, \theta_*}{a_{H_2O}} \qquad (S2.36)$$

where, K_{Vr} and K_{Vr}^o are the potential dependent and independent Volmer equilibrium constants, respectively. f is F/RT with F: Faraday's constant, R: universal gas constant and T: absolute temperature. η is the applied overpotential, θ_* is the active site coverage, $a_{H_3O^+}$ and a_{H_2O} are the hydronium ion and water activity, respectively.

The coverage of the hydrogenated organic species θ_{RCHOH} can be expressed as follows:

$$\frac{\partial \theta_{RCHOH}}{\partial t} = k_1 e^{-\alpha f \eta} a_{RCHO} a_{H_3O^+} \theta_* - k_{-1} \theta_{RCHOH} a_{H_2O} - k_2 \theta_{RCHOH} \theta_H + k_{-2} \theta_{RCH_2OH} \theta_* = 0 \; (S2.37)$$

where, k_1 and k_{-1} are the forward and backward rate constants for reaction (Six), respectively, and k_2 and k_{-2} are the rate constants for reaction (Sx). a_{RCHO} denotes the organic activity, θ_{RCH_2OH} is the hydrogenated product coverage and α marks the charge transfer coefficient. Assuming the backward reaction of organic adsorption and hydrogenation (Six) and the backward reaction of the second hydrogen addition (Sx) are negligible, $r_{ECH_{-1}}$ and $r_{ECH_{-2}}$ go to zero. Thus, the organic coverage simplifies to:

$$\frac{\partial \theta_{RCHOH}}{\partial t} = k_1\, e^{-\alpha f \eta}\, a_{RCHO}\, a_{H_3O^+}\, \theta_* - k_2\, \theta_{RCHOH}\, \theta_H = 0 \qquad (S2.38)$$

$$k_1\, e^{-\alpha f \eta}\, a_{RCHO}\, a_{H_3O^+}\, \theta_* = k_2\, \theta_{RCHOH}\, \theta_H \qquad (S2.39)$$

Solving Eq. (S2.39) for the partly hydrogenated organic coverage θ_{RCHOH} and substituting θ_H (Eq. S2.36), gives Eq. (S2.41):

$$\theta_{RCHOH} = \frac{k_1\, e^{-\alpha f \eta}\, a_{RCHO}\, a_{H_3O^+}\, \theta_*}{k_2\, \theta_H} \qquad (S2.40)$$

$$\theta_{RCHOH} = \frac{k_1\, e^{-\alpha f \eta}\, a_{RCHO}\, a_{H_2O}}{k_2\, K_{Vr}^{o}\, e^{-f\eta}} \qquad (S2.41)$$

We expect adsorbed hydrogen and partly hydrogenated reactants are the prevalent species on the catalyst surface under our conditions, thus, the site balance is:

$$1 = \theta_* + \theta_H + \theta_{RCHOH} \qquad (S2.42)$$

Rearrangement and substitution of θ_H (Eq. (S2.36)) and θ_{RCHOH} (Eq. (S2.41)) lead to the empty site coverage expression (Eq. (S2.44)).

$$\theta_* = \frac{1 - \frac{k_1\, e^{-\alpha f \eta}\, a_{RCHO}\, a_{H_2O}}{k_2\, K_{Vr}^{o}\, e^{-f\eta}}}{1 + \frac{K_{Vr}^{o}\, e^{-f\eta}\, a_{H_3O^+}}{a_{H_2O}}} \qquad (S2.43)$$

$$\theta_* = \frac{\left(k_2\, K_{Vr}^{o}\, e^{-f\eta} - k_1\, e^{-\alpha f \eta}\, a_{RCHO}\, a_{H_2O}\right) a_{H_2O}}{\left(a_{H_2O} + K_{Vr}^{o}\, e^{-f\eta}\, a_{H_3O^+}\right) k_2\, K_{Vr}^{o}\, e^{-f\eta}} \qquad (S2.44)$$

Assuming the backward reaction $r_{ECH_{-1}}$ is zero, the rate expression for the simultaneous reactant adsorption and first hydrogen addition is described in Eq. (S2.45).

$$r_{ECH_1} = k_1\, e^{-\alpha f \eta}\, a_{RCHO}\, a_{H_3O^+}\, \theta_* \qquad (S2.45)$$

Substitution of θ_* (Eq. (S2.44)) and rearrangement gives the definitive ECH rate equation:

$$r_{ECH_1} = \frac{k_1\, e^{-\alpha f \eta}\, a_{RCHO}\, a_{H_3O^+} \left(k_2\, K_{Vr}^{o}\, e^{-f\eta} - k_1\, e^{-\alpha f \eta}\, a_{RCHO}\, a_{H_2O}\right) a_{H_2O}}{\left(a_{H_2O} + K_{Vr}^{o}\, e^{-f\eta}\, a_{H_3O^+}\right) k_2\, K_{Vr}^{o}\, e^{-f\eta}} \qquad (S2.46)$$

The HER rate, limited by the Heyrovsky step, is expressed in Eq. S2.47. Substitution of θ_H (Eq. (S2.36)), θ_* (Eq. (S2.44)) and rearrangement, yields the final HER rate expression (Eq. (S2.48)).

$$r_{HER} = k_{Hy}\, \theta_H\, a_{H_3O^+} \qquad (S2.47)$$

$$r_{HER} = \frac{k_{Hy}^{o}\, e^{-\alpha f\eta} K_{Vr}^{o}\, e^{-f\eta}\, a_{H_3O^+}{}^2 \left(k_2\, K_{Vr}^{o}\, e^{-f\eta} - k_1\, e^{-\alpha f\eta}\, a_{RCHO}\, a_{H_2O}\right) a_{H_2O}}{a_{H_2O}\left(a_{H_2O} + K_{Vr}^{o}\, e^{-f\eta}\, a_{H_3O^+}\right) k_2\, K_{Vr}^{o}\, e^{-f\eta}} \qquad (S2.48)$$

where, k_{Hy} is the potential dependent Heyrovsky rate constant.

This steady state approximation led to poor kinetic fittings of the experimental rates and was therefore discarded for further discussion.

Neutral addition of adsorbed hydrogen

In this model, we propose a classic Langmuir-Hinshelwood mechanism. The first hydrogenation step proceeds through a neutral, rate limiting addition of adsorbed hydrogen (Sxi) after an equilibrated organic adsorption (Si). The following second hydrogen addition step and product desorption (Siv) are equilibrated and kinetically irrelevant.

1.H addition: RCHO* + H* → RCHOH* + * (Sxi)

For the HER, we assume a fast Volmer step (Sv), followed by a rate determining electrochemical hydrogen generation (Heyrovsky step (Svi)) following the former derivations.

Since, the organic adsorption is equilibrated, the organic coverage is described in Eq. (S2.49).

$$\theta_{RCHO} = K_{RCHO}\, a_{RCHO}\, \theta_* \qquad (S2.49)$$

where K_{RCHO} is the equilibrium constant of the organic reactant, θ_{RCHO} and θ_* are the organic and empty site coverages, respectively, and a_{RCHO} denotes the organic compound activity.

The potential dependent hydrogen coverage θ_H is based on the previous kinetic derivations and depicted in Eq. (S2.50).

$$\theta_H = \frac{K_{Vr}\, a_{H_3O^+}\, \theta_*}{a_{H_2O}} = \frac{K_{Vr}^{o}\, e^{-f\eta}\, a_{H_3O^+}\, \theta_*}{a_{H_2O}} \qquad (S2.50)$$

where, K_{Vr} and K_{Vr}^{o} are the potential dependent and independent Volmer equilibrium constants, respectively. f is F/RT with F: Faraday's constant, R: universal gas constant and T: absolute temperature. η is the applied overpotential, θ_* is the active site coverage, $a_{H_3O^+}$ and a_{H_2O} are the hydronium ion and water activities.

Under out conditions, the site balance includes adsorbed hydrogen and the organic reactant.

$$1 = \theta_* + \theta_H + \theta_{RCHO} \qquad (S2.51)$$

Substituting the hydrogen coverage θ_H (Eq. (S2.50)) and the organic coverage θ_{RCHO} (Eq. (S2.49)) provide the empty site coverage θ_* (Eq. (S2.52)).

$$\theta_* = \frac{1}{1 + K_{RCHO}\, a_{RCHO} + \frac{K_{Vr}^{o}\, e^{-f\eta}\, a_{H_3O^+}}{a_{H_2O}}} \qquad (S2.52)$$

Here, we assume a neutral first hydrogen addition as rate limiting step for ECH (Sxi).

$$r_{ECH_1} = k_{ECH_1}\, \theta_{RCHO}\, \theta_H \qquad (S2.53)$$

where, r_{ECH_1} and k_{ECH_1} are the ECH rate and rate constant of the first hydrogen addition step, respectively. Substitution with the organic coverage θ_{RCHO} (Eq. (S2.49)), hydrogen coverage θ_H (Eq. (S2.50)) and the empty site coverage θ_* (Eq. (S2.52)), results in the final hydrogenation rate equation (Eq. (S2.54)):

$$r_{ECH_1} = \frac{k_{ECH_1}\, K_{RCHO}\, a_{RCHO}\, K_{Vr}^{o}\, e^{-f\eta}\, a_{H_3O^+}}{a_{H_2O}\left(1 + K_{RCHO}\, a_{RCHO} + \frac{K_{Vr}^{o}\, e^{-f\eta}\, a_{H_3O^+}}{a_{H_2O}}\right)^2} \qquad (S2.54)$$

The HER equation is outlined below (Eq. (S2.55)). Substituting the hydrogen coverage θ_H (Eq. (S2.50)), followed by the active site coverage θ_* (Eq. (S2.52)) gives the HER rate expression (Eq. (S2.56)).

$$r_{HER} = k_{Hy}\, \theta_H\, a_{H_3O^+} \qquad (S2.55)$$

$$r_{HER} = \frac{k_{Hy}^{o}\, e^{-f\eta(\alpha+1)}\, K_{Vr}^{\circ}\, a_{H_3O^+}^{2}}{a_{H2O}\left(1 + K_{RCHO}\, a_{RCHO} + \frac{K_{Vr}^{\circ}\, e^{-f\eta}\, a_{H_3O^+}}{a_{H2O}}\right)} \qquad (S2.56)$$

where, k_{Hy} is the potential dependent Heyrovsky rate constant and α_{HER} the charge transfer coefficient.

Models with neutral H addition were not able to capture the different offsets of hydrogenation and HER along with potential.

2.5.6. Determination of organic adsorption constants on Pd/C using a rotating disc electrode

The adsorption constants of the organic compounds were measured by cyclic voltammetry (CV) on a rotating disc electrode based on Ref.[17, 34] The RDE setup was used as described in the experimental section. The working electrode was a polished glassy carbon electrode, drop-casted with 20 wt.% Pd/C (Premetek) with a Pd loading of 19 µg cm^{-2}. The catalyst ink and drop-casting preparation are reported in Ref.[34] A 2 M sodium acetate buffer (pH 5.2), purged with Ar during the measurement, was utilized as electrolyte. The CV scan rate was 0.05 V s^{-1} for all experiments.

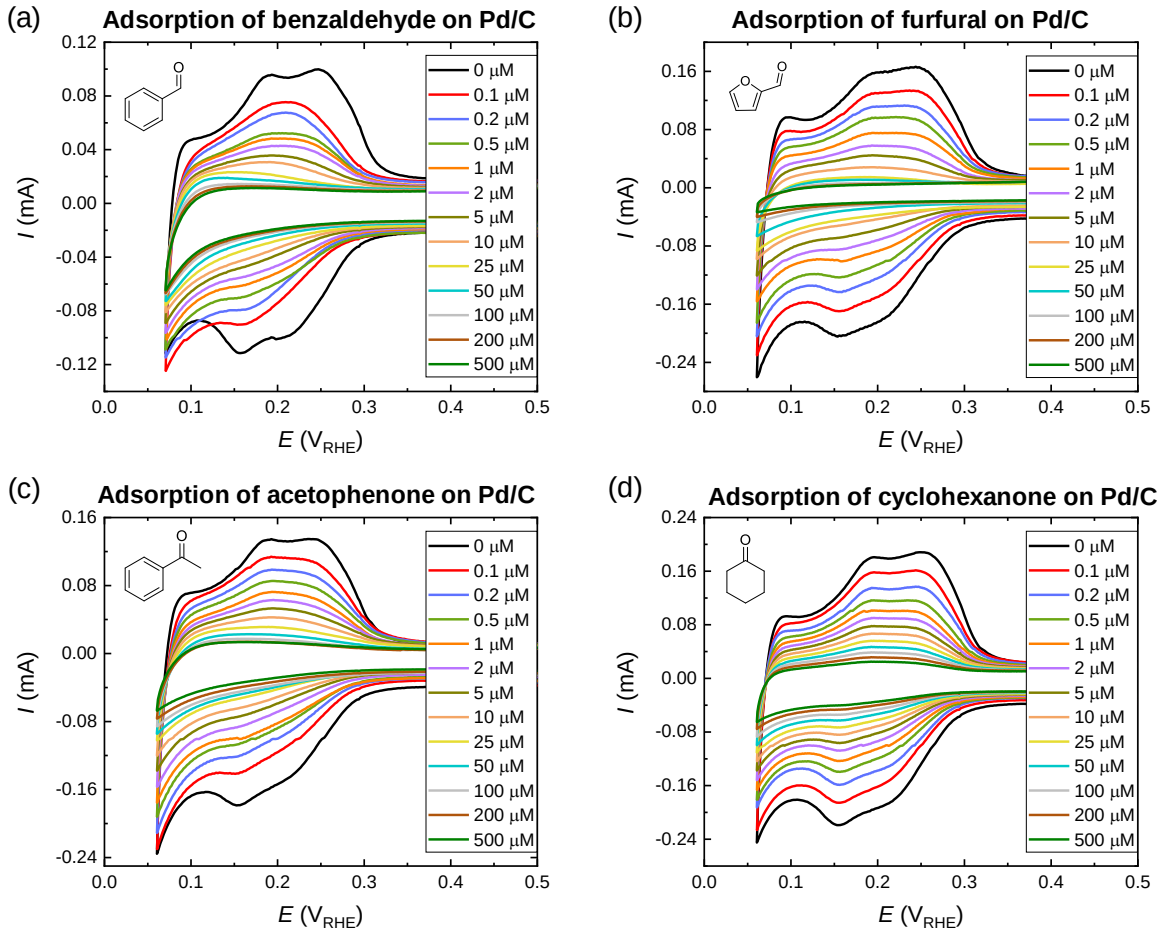

Figure S2.7. Cyclic voltammograms in the H_{upd} region with increasing (0 µM to 500 µM) organic concentrations – (a) benzaldehyde, (b) furfural, (c) acetophenone and (d) cyclohexanone. CVs were measured on 20 wt% Pd/C in 2 M sodium acetate buffer and at a scan rate of 0.05 V s^{-1}.

Figure S2.7 shows the cyclic voltammograms in the hydrogen underpotential deposition (H_{upd}) region in absence and varying concentrations of benzaldehyde, furfural, acetophenone, and cyclohexanone. The amount of H_{upd} atoms deposited was determined by measuring the charge

during the desorption sweep and subtracting it from the capacitance current baseline. In absence of organics (0 μM) the H_{upd} charge corresponds to the total concentration of adsorbed hydrogen on Pd. As the organic concentration increases from 0.1 μM to 500 μM the H_{upd} decreases, thus the total amount of adsorbed hydrogen, decreases. We assumed that the decrease in H_{upd} area is proportional to the coverage of organics and by comparing this with the initial H_{upd} charge without organics, the fraction of charge inhibited by organics can be estimated.

The surface coverages of the organic molecules were calculated as follows:

$$\theta_i = \frac{Q_{H_{upd}}^{total} - Q_{H_{upd}}^{i\,\mu M}}{Q_{H_{upd}}^{total}} \qquad (S2.57)$$

where, θ_i describes the coverage of organic compounds, $Q_{H_{upd}}^{total}$ and $Q_{H_{upd}}^{i\,\mu M}$ represents the H_{upd} charge in absence of organics and in presence of $i\ \mu M$ organic, respectively.

Using a two-site Langmuir model, the experimental organic coverages were fitted using Eq. (S2.58).

$$\theta_i = \frac{K_{i,a} x_{a,max} C_i}{1 + K_{i,a} C_i} + \frac{K_{i,b} x_{b,max} C_i}{1 + K_{i,b} C_i} \qquad (S2.58)$$

where θ_i represents the coverage of the organic compound, $K_{i,a}$ and $K_{i,b}$ are the adsorption equilibrium constants of the organic compound on two different sites (a and b respectively), and C_i is the concentration of the organic compound. The terms $x_{i,a,max}$ and $x_{i,b,max}$ are the maximum contributions of the two adsorption sites. Table S2.4 summarizes the fitted adsorption parameters along with the corresponding Gibbs free energy ΔG° of adsorption. For the kinetic fitting, the adsorption constants of the second site were utilized due to their larger magnitude.

Table S2.4. Fitted adsorption parameters (x: contribution of adsorption on a given site, K: adsorption equilibrium constant, ΔG°: Gibbs free energy) for benzaldehyde, furfural, acetophenone and cyclohexanone on Pd/C utilizing a two-site Langmuir model.

	Benzaldehyde			**Furfural**		
	x	K	ΔG° [kJ mol^{-1}]	x	K	ΔG° [kJ mol^{-1}]
Site 1	0.5	0.10 x 10^6	-31	0.4	0.22 x 10^6	-29
Site 2	0.5	13.0 x 10^6	-41	0.6	5.5 x 10^6	-39
	Acetophenone			**Cyclohexanone**		
	x	K	ΔG° [kJ mol^{-1}]	x	K	ΔG° [kJ mol^{-1}]
Site 1	0.4	0.11 x 10^6	-29	0.3	0.06 x 10^6	-28
Site 2	0.6	5.3 x 10^6	-38	0.6	2.6 x 10^6	-37

2.5.7. X-ray Absorption Spectroscopy

X-ray absorption near-edge structure spectroscopy (XANES) and extended X-ray absorption fine structure (EXAFS) measurements were conducted in a custom built flow electrochemical cell.[53] After depositing the Pd/C catalyst onto the carbon felt via infiltration, the electrode was reduced, followed by a cleaning step of 5 min at 1.8 V_{RHE} and 5 min at -0.3 V_{RHE} in 0.1 M sodium acetate buffer with pH 5. For every measurement, a new solution, which was purged with argon and degassed beforehand, was introduced to the cell with various concentrations of organic compounds at room temperature. During all experiments the potential was held at 0.15 V_{RHE} or -0.1 V_{RHE}. The spectra were recorded at Sector 20 of the Advanced Photon Source in the Argonne National Laboratory. The data were analyzed using the Athena software and Artemis was utilized for EXAFS fitting.[54]

We calculated the Pd-Pd lattice distance (l_0) of hydride-free Pd as 2.63 Å. Then, we also calculated the Pd-Pd lattice distance when the catalyst was subjected to external potential in the absence and the presence of organic compounds (l). Based on the lattice expansion (∂l), the molar ratio of incorporated hydrogen in the bulk of Pd ([H]/[Pd]) was determined by Eq. (S2.59).[44, 45] The molar ratios are graphically presented in Figure S2.8.

$$\frac{\partial l}{l_0} = 0.0666\frac{[H]}{[Pd]} - 0.0164\left(\frac{[H]}{[Pd]}\right)^2 \qquad (S2.59)$$

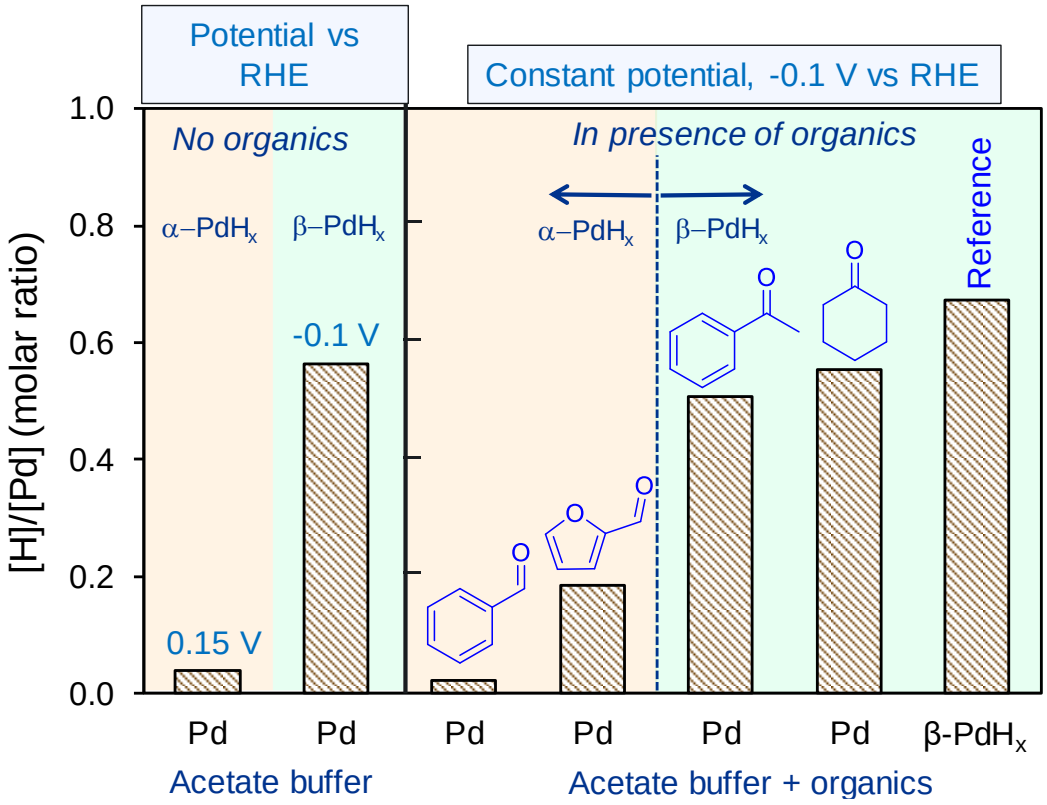

Figure S2.8. Molar ratio of hydrogen incorporated in palladium in the presence and absence of organic compounds. Left side: molar ratio in pure sodium acetate buffer (pH 5) at 0.15 V_{RHE} and -0.1 V_{RHE}; Right side: molar ratio in the presence of benzaldehyde, furfural, acetophenone, or cyclohexanone. The reference is Pd foil at -0.1 V_{RHE}.

2.6. References

1. Lam, C. H.; Das, S.; Erickson, N. C.; Hyzer, C. D.; Garedew, M.; Anderson, J. E.; Wallington, T. J.; Tamor, M. A.; Jackson, J. E.; Saffron, C. M., Towards sustainable hydrocarbon fuels with biomass fast pyrolysis oil and electrocatalytic upgrading. *Sustainable Energy & Fuels* **2017,** *1* (2), 258-266.
2. Akhade, S. A.; Singh, N.; Gutiérrez, O. Y.; Lopez-Ruiz, J.; Wang, H.; Holladay, J. D.; Liu, Y.; Karkamkar, A.; Weber, R. S.; Padmaperuma, A. B.; Lee, M.-S.; Whyatt, G. A.; Elliott, M.; Holladay, J. E.; Male, J. L.; Lercher, J. A.; Rousseau, R.; Glezakou, V.-A., Electrocatalytic Hydrogenation of Biomass-Derived Organics: A Review. *Chemical Reviews* **2020,** *120* (20), 11370-11419.
3. Orella, M. J.; Román-Leshkov, Y.; Brushett, F. R., Emerging opportunities for electrochemical processing to enable sustainable chemical manufacturing. *Current Opinion in Chemical Engineering* **2018,** *20*, 159-167.
4. Wang, H.; Lee, S.-J.; Olarte, M. V.; Zacher, A. H., Bio-oil Stabilization by Hydrogenation over Reduced Metal Catalysts at Low Temperatures. *ACS Sustainable Chemistry & Engineering* **2016,** *4* (10), 5533-5545.
5. Wang, H.; Male, J.; Wang, Y., Recent Advances in Hydrotreating of Pyrolysis Bio-Oil and Its Oxygen-Containing Model Compounds. *ACS Catalysis* **2013,** *3* (5), 1047-1070.
6. Lister, T. E.; Diaz, L. A.; Lilga, M. A.; Padmaperuma, A. B.; Lin, Y.; Palakkal, V. M.; Arges, C. G., Low-Temperature Electrochemical Upgrading of Bio-oils Using Polymer Electrolyte Membranes. *Energy & Fuels* **2018,** *32* (5), 5944-5950.

7. Frontana-Uribe, B. A.; Little, R. D.; Ibanez, J. G.; Palma, A.; Vasquez-Medrano, R., Organic electrosynthesis: a promising green methodology in organic chemistry. *Green Chemistry* **2010,** *12* (12), 2099-2119.
8. Kwon, Y.; Birdja, Y. Y.; Raoufmoghaddam, S.; Koper, M. T. M., Electrocatalytic Hydrogenation of 5-Hydroxymethylfurfural in Acidic Solution. *ChemSusChem* **2015,** *8* (10), 1745-1751.
9. Song, Y.; Sanyal, U.; Pangotra, D.; Holladay, J. D.; Camaioni, D. M.; Gutiérrez, O. Y.; Lercher, J. A., Hydrogenation of benzaldehyde via electrocatalysis and thermal catalysis on carbon-supported metals. *Journal of Catalysis* **2018,** *359*, 68-75.
10. Lopez-Ruiz, J. A.; Sanyal, U.; Egbert, J.; Gutiérrez, O. Y.; Holladay, J., Kinetic Investigation of the Sustainable Electrocatalytic Hydrogenation of Benzaldehyde on Pd/C: Effect of Electrolyte Composition and Half-Cell Potentials. *ACS Sustainable Chemistry & Engineering* **2018,** *6* (12), 16073-16085.
11. May, A. S.; Watt, S. M.; Biddinger, E. J., Kinetics of furfural electrochemical hydrogenation and hydrogenolysis in acidic media on copper. *Reaction Chemistry & Engineering* **2021,** *6* (11), 2075-2086.
12. Chadderdon, X. H.; Chadderdon, D. J.; Matthiesen, J. E.; Qiu, Y.; Carraher, J. M.; Tessonnier, J.-P.; Li, W., Mechanisms of Furfural Reduction on Metal Electrodes: Distinguishing Pathways for Selective Hydrogenation of Bioderived Oxygenates. *Journal of the American Chemical Society* **2017,** *139* (40), 14120-14128.
13. Roylance, J. J.; Kim, T. W.; Choi, K.-S., Efficient and Selective Electrochemical and Photoelectrochemical Reduction of 5-Hydroxymethylfurfural to 2,5-Bis(hydroxymethyl)furan using Water as the Hydrogen Source. *ACS Catalysis* **2016,** *6* (3), 1840-1847.
14. Bondue, C. J.; Koper, M. T. M., A mechanistic investigation on the electrocatalytic reduction of aliphatic ketones at platinum. *Journal of Catalysis* **2019,** *369*, 302-311.
15. Cantu, D. C.; Padmaperuma, A. B.; Nguyen, M.-T.; Akhade, S. A.; Yoon, Y.; Wang, Y.-G.; Lee, M.-S.; Glezakou, V.-A.; Rousseau, R.; Lilga, M. A., A Combined Experimental and Theoretical Study on the Activity and Selectivity of the Electrocatalytic Hydrogenation of Aldehydes. *ACS Catalysis* **2018,** *8* (8), 7645-7658.
16. Pinna, F.; Menegazzo, F.; Signoretto, M.; Canton, P.; Fagherazzi, G.; Pernicone, N., Consecutive hydrogenation of benzaldehyde over Pd catalysts: Influence of supports and sulfur poisoning. *Applied Catalysis A: General* **2001,** *219* (1), 195-200.
17. Singh, N.; Sanyal, U.; Fulton, J. L.; Gutiérrez, O. Y.; Lercher, J. A.; Campbell, C. T., Quantifying Adsorption of Organic Molecules on Platinum in Aqueous Phase by Hydrogen Site Blocking and in Situ X-ray Absorption Spectroscopy. *ACS Catalysis* **2019,** *9* (8), 6869-6881.
18. Koh, K.; Sanyal, U.; Lee, M.-S.; Cheng, G.; Song, M.; Glezakou, V.-A.; Liu, Y.; Li, D.; Rousseau, R.; Gutiérrez, O. Y.; Karkamkar, A.; Derewinski, M.; Lercher, J. A., Electrochemically Tunable Proton-Coupled Electron Transfer in Pd-Catalyzed Benzaldehyde Hydrogenation. **2020,** *59* (4), 1501-1505.
19. Lopez-Ruiz, J. A.; Andrews, E.; Akhade, S. A.; Lee, M.-S.; Koh, K.; Sanyal, U.; Yuk, S. F.; Karkamkar, A. J.; Derewinski, M. A.; Holladay, J.; Glezakou, V.-A.; Rousseau, R.; Gutiérrez, O. Y.; Holladay, J. D., Understanding the Role of Metal and Molecular Structure on the Electrocatalytic Hydrogenation of Oxygenated Organic Compounds. *ACS Catalysis* **2019,** *9* (11), 9964-9972.
20. Andrews, E.; Lopez-Ruiz, J. A.; Egbert, J. D.; Koh, K.; Sanyal, U.; Song, M.; Li, D.; Karkamkar, A. J.; Derewinski, M. A.; Holladay, J.; Gutiérrez, O. Y.; Holladay, J. D., Performance of Base and Noble Metals for Electrocatalytic Hydrogenation of Bio-Oil-Derived Oxygenated Compounds. *ACS Sustainable Chemistry & Engineering* **2020,** *8* (11), 4407-4418.
21. Li, Z.; Kelkar, S.; Lam, C. H.; Luczek, K.; Jackson, J. E.; Miller, D. J.; Saffron, C. M., Aqueous electrocatalytic hydrogenation of furfural using a sacrificial anode. *Electrochimica Acta* **2012,** *64*, 87-93.
22. Jung, S.; Biddinger, E. J., Electrocatalytic Hydrogenation and Hydrogenolysis of Furfural and the Impact of Homogeneous Side Reactions of Furanic Compounds in Acidic Electrolytes. *ACS Sustainable Chemistry & Engineering* **2016,** *4* (12), 6500-6508.

23. Sáez, A.; García-García, V.; Solla-Gullón, J.; Aldaz, A.; Montiel, V., Electrocatalytic hydrogenation of acetophenone using a Polymer Electrolyte Membrane Electrochemical Reactor. *Electrochimica Acta* **2013,** *91*, 69-74.
24. Villalba, M.; del Pozo, M.; Calvo, E. J., Electrocatalytic hydrogenation of acetophenone and benzophenone using palladium electrodes. *Electrochimica Acta* **2015,** *164*, 125-131.
25. Cheng, G.; Jentys, A.; Gutiérrez, O. Y.; Liu, Y.; Chin, Y.-H.; Lercher, J. A., Critical role of solvent-modulated hydrogen-binding strength in the catalytic hydrogenation of benzaldehyde on palladium. *Nature Catalysis* **2021,** *4* (11), 976-985.
26. Sanyal, U.; Lopez-Ruiz, J.; Padmaperuma, A. B.; Holladay, J.; Gutiérrez, O. Y., Electrocatalytic Hydrogenation of Oxygenated Compounds in Aqueous Phase. *Organic Process Research & Development* **2018,** *22* (12), 1590-1598.
27. Bondue, C. J.; Koper, M. T. M., Electrochemical Reduction of the Carbonyl Functional Group: The Importance of Adsorption Geometry, Molecular Structure, and Electrode Surface Structure. *Journal of the American Chemical Society* **2019,** *141* (30), 12071-12078.
28. Singh, N.; Sanyal, U.; Ruehl, G.; Stoerzinger, K. A.; Gutiérrez, O. Y.; Camaioni, D. M.; Fulton, J. L.; Lercher, J. A.; Campbell, C. T., Aqueous phase catalytic and electrocatalytic hydrogenation of phenol and benzaldehyde over platinum group metals. *Journal of Catalysis* **2020,** *382*, 372-384.
29. Song, Y.; Chia, S. H.; Sanyal, U.; Gutiérrez, O. Y.; Lercher, J. A., Integrated catalytic and electrocatalytic conversion of substituted phenols and diaryl ethers. *Journal of Catalysis* **2016,** *344*, 263-272.
30. Durst, J.; Simon, C.; Hasché, F.; Gasteiger, H. A., Hydrogen Oxidation and Evolution Reaction Kinetics on Carbon Supported Pt, Ir, Rh, and Pd Electrocatalysts in Acidic Media. *Journal of The Electrochemical Society* **2015,** *162* (1), F190-F203.
31. Rheinländer, P. J.; Herranz, J.; Durst, J.; Gasteiger, H. A., Kinetics of the Hydrogen Oxidation/Evolution Reaction on Polycrystalline Platinum in Alkaline Electrolyte Reaction Order with Respect to Hydrogen Pressure. *Journal of The Electrochemical Society* **2014,** *161* (14), F1448-F1457.
32. Shinagawa, T.; Garcia-Esparza, A. T.; Takanabe, K., Insight on Tafel slopes from a microkinetic analysis of aqueous electrocatalysis for energy conversion. *Scientific Reports* **2015,** *5*, 13801.
33. Nguyen, M.-T.; Akhade, S. A.; Cantu, D. C.; Lee, M.-S.; Glezakou, V.-A.; Rousseau, R., Electro-reduction of organics on metal cathodes: A multiscale-modeling study of benzaldehyde on Au (111). *Catalysis Today* **2020,** *350*, 39-46.
34. Sanyal, U.; Yuk, S. F.; Koh, K.; Lee, M.-S.; Stoerzinger, K.; Zhang, D.; Meyer, L. C.; Lopez-Ruiz, J. A.; Karkamkar, A.; Holladay, J. D.; Camaioni, D. M.; Nguyen, M.-T.; Glezakou, V.-A.; Rousseau, R.; Gutiérrez, O. Y.; Lercher, J., Hydrogen bonding enhances the electrochemical hydrogenation of benzaldehyde in the aqueous phase. *Angewandte Chemie International Edition* **2020,** *n/a* (n/a).
35. DeBlois, M.; Lessard, J.; Jerkiewicz, G., Influence of benzene on the HUPD and anion adsorption on Pt(110), Pt(100) and Pt(111) electrodes in aqueous H2SO4. *Electrochimica Acta* **2005,** *50* (16), 3517-3523.
36. Obradović, M. D.; Lessard, J.; Jerkiewicz, G., Cyclic-voltammetry behavior of Pt(111) in aqueous HClO4+C6H6: Influence of C6H6 concentration, scan rate and temperature. *Journal of Electroanalytical Chemistry* **2010,** *649* (1), 248-256.
37. Sasaki, K.; Kunai, A.; Harada, J.; Nakabori, S., Electrolytic hydrogenation of phenols in aqueous acid solutions. *Electrochimica Acta* **1983,** *28* (5), 671-674.
38. Akinola, J.; Barth, I.; Goldsmith, B. R.; Singh, N., Adsorption Energies of Oxygenated Aromatics and Organics on Rhodium and Platinum in Aqueous Phase. *ACS Catalysis* **2020,** *10* (9), 4929-4941.
39. Akhade, S. A.; Lee, M.-S.; Meyer, L. C.; Yuk, S. F.; Nguyen, M.-T.; Sanyal, U.; Egbert, J. D.; Gutiérrez, O. Y.; Glezakou, V.-A.; Rousseau, R., Impact of functional groups on the electrocatalytic hydrogenation of aromatic carbonyls to alcohols. *Catalysis Today* **2021**.
40. Bugaev, A. L.; Guda, A. A.; Lomachenko, K. A.; Shapovalov, V. V.; Lazzarini, A.; Vitillo, J. G.; Bugaev, L. A.; Groppo, E.; Pellegrini, R.; Soldatov, A. V.; van Bokhoven, J. A.; Lamberti, C., Core–

Shell Structure of Palladium Hydride Nanoparticles Revealed by Combined X-ray Absorption Spectroscopy and X-ray Diffraction. *The Journal of Physical Chemistry C* **2017,** *121* (33), 18202-18213.
41. Tew, M. W.; Miller, J. T.; van Bokhoven, J. A., Particle Size Effect of Hydride Formation and Surface Hydrogen Adsorption of Nanosized Palladium Catalysts: L3 Edge vs K Edge X-ray Absorption Spectroscopy. *The Journal of Physical Chemistry C* **2009,** *113* (34), 15140-15147.
42. Nag, N. K., A Study on the Formation of Palladium Hydride in a Carbon-Supported Palladium Catalyst. *The Journal of Physical Chemistry B* **2001,** *105* (25), 5945-5949.
43. Johansson, M.; Skúlason, E.; Nielsen, G.; Murphy, S.; Nielsen, R. M.; Chorkendorff, I., Hydrogen adsorption on palladium and palladium hydride at 1bar. *Surface Science* **2010,** *604* (7), 718-729.
44. Chase, Z. A.; Fulton, J. L.; Camaioni, D. M.; Mei, D.; Balasubramanian, M.; Pham, V.-T.; Zhao, C.; Weber, R. S.; Wang, Y.; Lercher, J. A., State of Supported Pd during Catalysis in Water. *The Journal of Physical Chemistry C* **2013,** *117* (34), 17603-17612.
45. Feenstra, R.; Griessen, R.; Groot, D. G. d., Hydrogen induced lattice expansion and effective H-H interaction in single phase PdHc. *Journal of Physics F: Metal Physics* **1986,** *16* (12), 1933-1952.
46. Sanyal, U.; Song, Y.; Singh, N.; Fulton, J. L.; Herranz, J.; Jentys, A.; Gutiérrez, O. Y.; Lercher, J. A., Structure Sensitivity in Hydrogenation Reactions on Pt/C in Aqueous-phase. *ChemCatChem* **2019,** *11* (1), 575-582.
47. Mittermeier, T.; Weiß, A.; Gasteiger, H. A.; Hasché, F., Monometallic Palladium for Oxygen Reduction in PEM Fuel Cells: Particle-Size Effect, Reaction Mechanism, and Voltage Cycling Stability. *Journal of The Electrochemical Society* **2017,** *164* (12), F1081-F1089.
48. Jung, S.; Biddinger, E. J., Controlling Competitive Side Reactions in the Electrochemical Upgrading of Furfural to Biofuel. *Energy Technology* **2018,** *6* (7), 1370-1379.
49. Dunlop, A. P., Furfural formation and behavior. *Industrial and Engineering Chemistry* **1948,** *40* (2), 204-209.
50. Danon, B.; Marcotullio, G.; de Jong, W. J. G. C., Mechanistic and kinetic aspects of pentose dehydration towards furfural in aqueous media employing homogeneous catalysis. **2014,** *16* (1), 39-54.
51. Hu, X.; Westerhof, R. J. M.; Wu, L.; Dong, D.; Li, C.-Z., Upgrading biomass-derived furans via acid-catalysis/hydrogenation: the remarkable difference between water and methanol as the solvent. *Green Chemistry* **2015,** *17* (1), 219-224.
52. van Zandvoort, I.; Wang, Y.; Rasrendra, C. B.; van Eck, E. R. H.; Bruijnincx, P. C. A.; Heeres, H. J.; Weckhuysen, B. M., Formation, Molecular Structure, and Morphology of Humins in Biomass Conversion: Influence of Feedstock and Processing Conditions. **2013,** *6* (9), 1745-1758.
53. Singh, N.; Nguyen, M.-T.; Cantu, D. C.; Mehdi, B. L.; Browning, N. D.; Fulton, J. L.; Zheng, J.; Balasubramanian, M.; Gutiérrez, O. Y.; Glezakou, V.-A.; Rousseau, R.; Govind, N.; Camaioni, D. M.; Campbell, C. T.; Lercher, J. A., Carbon-supported Pt during aqueous phenol hydrogenation with and without applied electrical potential: X-ray absorption and theoretical studies of structure and adsorbates. *Journal of Catalysis* **2018,** *368*, 8-19.
54. Ravel, B.; Newville, M., ATHENA, ARTEMIS, HEPHAESTUS: data analysis for X-ray absorption spectroscopy using IFEFFIT. *Journal of Synchrotron Radiation* **2005,** *12* (4), 537-541.

3. Role of Hydronium ions for Controlling and Enhancing Catalytic Hydrogenation in Aqueous Phase

Abstract

Hydrogenation of organic molecules in water offers the possibility of controlling catalysis on metals by applying an electric potential. However, the mechanisms of control are still under debate. We report the comparison of thermocatalytic and electrocatalytic hydrogenation on Pd in water to show that neutral and electrochemical hydrogenation steps (H· versus H^++e^-) are not mutually exclusive, both contribute to hydrogenation regardless of the origin of the reducing equivalents. Electrochemical routes (i.e., proton coupled electron transfer) prevail at low H_2 pressure and acidic conditions. Thus, one can control, e.g., C=O bond hydrogenation (and C-O bond cleavage) with applied potential and with concentration of hydronium ions (as reactants and regulators of electrochemical potential). Decreasing pH from neutral to acidic conditions increases the rates of reaction by up to four times (in the presence and in the absence of external potential), whereas overpotential and H_2 pressure increase catalytic rates exponentially. The correlation of conversion rates with pH is concluded to stem from weakening of metal-H binding as the pH decreases. In brief, thermocatalytic and electrocatalytic hydrogenation, in water, are not fundamentally different.

3.1. Introduction

The ubiquitous presence of water in bio-derived and waste carbon resources poses significant challenges for their utilization as feedstocks for production of fuels and chemicals [1-3]. Water, however, also offers new opportunities to perform and control catalysis using parameters such as applied potential and concentration of ions in solution. These two parameters are the core of the concept of electrocatalytic hydrogenation (ECH) [4-8]. Applied potential provides reduction equivalents for reduction of, e.g., aromatic rings, and carbonyl groups, by producing hydrogen at metal surfaces [9-13], enabling proton coupled electron transfer (PCET) [14-16], and driving outer sphere electron transfer [17].

In thermocatalytic hydrogenation (i.e., hydrogenation with H_2 and without applied potential), the concentration of hydronium ions influences hydrogenation rates. For instance, increasingly acidic

environments enhance the reactivity of Pt for hydrogenation of aromatic rings and carbonyl groups in oxygenated compounds [18-20]. This has been related with the weakening of the H-metal bond, which decreases the hydrogenation barriers by Brønsted-Evans-Polanyi relationships [21]. Interestingly, the same argument is put forward to explain the faster rates of electrochemical H_2 evolution and oxidation on Pt-group metals in acid than in alkaline media [22-26]. Thus, there is a key fundamental overlap between hydrogenation of organic compounds and electrochemistry on metals that needs to be better understood to enhance catalytic performance in water at mild conditions. Understanding the combined effects of varying pH and applied potential could be a particularly powerful combination to be utilized on electrocatalytic hydrogenation.

In this work we study both thermocatalytic and electrocatalytic hydrogenation of aromatic carbonyl groups in aqueous phase. We used Pd because we previously observed a particular interaction between benzaldehyde and Pd, which suppresses H_2 evolution during ECH at certain conditions [11, 27]. In previous reports, higher intrinsic rates, lower activation energies in ECH than in thermocatalytic hydrogenation and a key impact of Brønsted acid sites on hydrogenation [15] allowed us to hypothesize that a proton coupled electron transfer replaces the reductive elimination as the hydrogen transfer mechanism at the metal surface. For this follow up work, we proposed that increasing hydronium ion concentration could further enhance the rates of hydrogenation via the PCET mechanism. Hence, we probed the influence of pH on the activity of Pd for the reductive conversion of benzaldehyde and acetophenone under ECH and with molecular H_2 (i.e., under open circuit voltage, OCV, conditions). Our results indeed showed increasing ECH rates with increasingly acidic conditions. Unexpectedly, the same effect was observed under OCV. The analysis of the results, complemented with isotope-labeled and high pressure experiments, showed that both PCET and H-addition mechanism coexist in water and that both are affected by the concentration of hydronium ions. This pH effect is indeed found to originate from the change in the Pd-H binding energy with varying hydronium ion concentration. Further, we observed that strongly acidic conditions enable the C-O bond cleavage of the primary alcohol products and that the rate of this step is also enhanced by hydronium ion concentration. Thus, we show that hydronium ions have a key role for reductive transformations in water as reactants as well as influencing the energy levels of surface intermediates. The combination of thermocatalytic and electrochemical pathways, both sensitive to pH and applied potential, provides a highly efficient way of controlling hydrogenation in water.

3.2. Results and discussion

3.2.1. Electrocatalytic hydrogenation of benzaldehyde and acetophenone

The ECH rates of benzaldehyde and acetophenone increased with increasingly negative potential in the explored potential window (e.g., more than twofold as the potential decreased by ~0.1 V) (Figure 3.1). ECH rates were higher than those measured under OCV and acetophenone was less reactive than benzaldehyde, which is attributed to the steric hindrance by the methyl group adjacent to the carbonyl [28]. The reaction rates at pH 1.6 and 2.5 were higher than at pH 5.2 and this effect is more marked as the potential is made more negative.

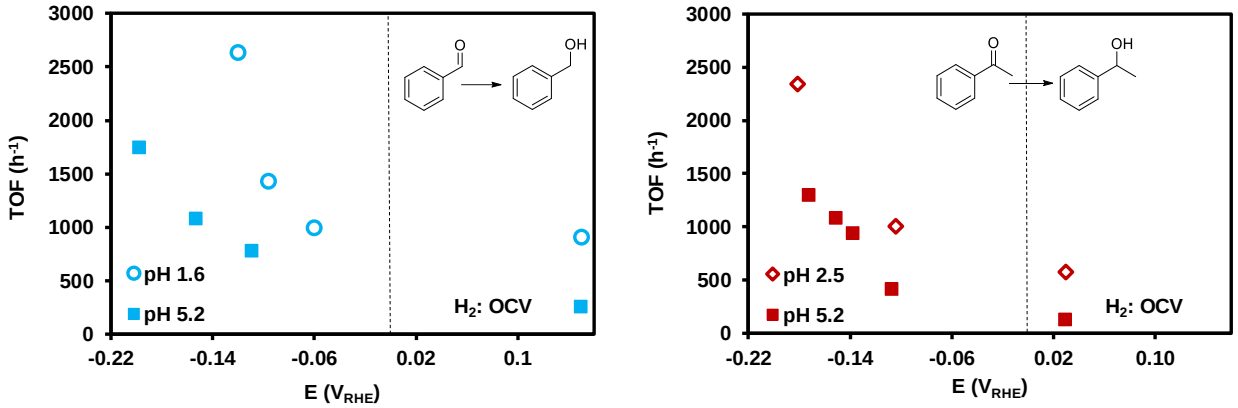

Figure 3.1. Left: Turn over frequencies (TOF) for the hydrogenation of benzaldehyde at pH 1.6 and 5.2. Right: TOF for acetophenone hydrogenation at pH 1.6 and pH 5.2. In both figures, the data plotted at negative potentials denote electrocatalytic hydrogenation at the potential shown in the x-axis (under 1 bar bubbling N_2). The points at positive potential correspond to rates and open circuit potentials measured under 1 bar H_2. Experiments were performed in buffer solutions of phosphoric acid (pH 1.6, pH 2.5) or acetate buffer (pH 5.2) over Pd/C (5 wt.%) at room temperature and atmospheric pressure.

Expectedly, the same effects of potential and pH were observed for the rates of the H_2 evolution reaction (HER), i.e., more negative potentials and acidic conditions enhance the evolution of H_2 (Figure S3.1). In the case of benzaldehyde, applied potential has approximately the same effect over ECH and HER rates. Consequently, the Faradaic efficiencies (FEs) remained constant at ~100% and 80% for pH 5.2 and 1.6, respectively (Figure S3.2). The exception is the reaction at -0.2 V at pH 5.2, where the FE dropped to 85%. For acetophenone, applied potential has a slightly stronger effect on HER than on ECH. Therefore, the FEs decreased from > 90% at -0.1 V to 60-80% (Figure S3.2). We did not observe a clear effect of pH on FE during the ECH of acetophenone. The general observation that relatively negative potentials favor HER over ECH is in line with observations made on other metals [29].

In the first step, the carbonyl groups are hydrogenated to hydroxyls yielding benzyl alcohol and 1-phenylethanol as primary products in the hydrogenation of benzaldehyde and acetophenone, respectively. Those alcohols are also the final products at pH 5.2 as shown in Figure S3.3 and Figure S3.4. At acidic pH, however, the alcohols are dehydrated. Benzyl alcohol conversion yields toluene as secondary product, whereas 1-phenylethanol yields styrene and ethylbenzene in consecutive steps (Figure S3.5). These pathways and their dependence on pH are insensitive to the origin of the reduction equivalents, i.e., H_2 under OCV and electric potential in ECH lead to the same concentration profiles (Figure S3.4).

3.2.2. Conversion of benzaldehyde and benzyl alcohol at varying pH

Having established that ECH is controlled by potential yielding higher conversion rates than at OCV (Figure 3.1) in most of the explored potential window, we studied the effect of pH on benzaldehyde hydrogenation with 1 bar H_2 (OCV) and with -0.06 V vs RHE (ECH). We selected this low potential because it rendered ECH rates comparable to those obtained at OCV. Surprisingly, both operation modes showed the same dependence on pH, i.e., in both cases, the conversion rates increased approximately twofold as the pH decreased from 7 to 1 (Figure 3.2). This increase in rate was independent from the nature of the electrolyte (see also Table S3.1 and Table S3.2 in the supporting information).

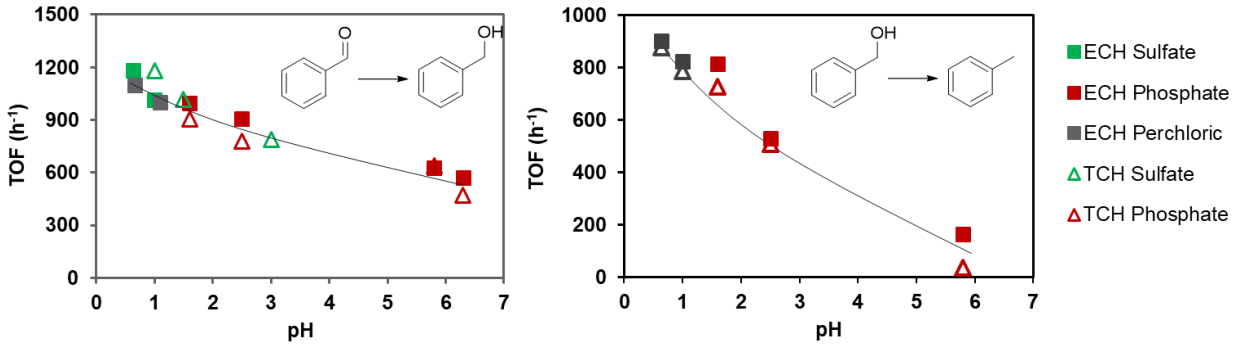

Figure 3.2. Turnover frequency (TOF) of benzaldehyde hydrogenation to benzyl alcohol (left) and of benzyl alcohol reduction to toluene (right) as a function of pH and electrolyte. Reactions at open circuit voltage (OCV) were performed under 1 bar H_2 and electrocatalytic hydrogenation (ECH) was performed at -0.06 V vs RHE. All experiments were performed using Pd/C (5 wt. % Pd) at room temperature with 20 mM benzaldehyde in aqueous solutions containing the selected electrolytes (green points were measured in sulfate buffers, grey points in perchloric buffers, and red points in phosphate buffer).

In a series of experiments using benzyl alcohol as initial reactant (Figure 3.2, right), we observed that benzyl alcohol appreciably reacted only below pH 6 with toluene as the only product (i.e., ring

hydrogenation was not observed). The conversion rate increased almost linearly as the pH decreased to pH 1.6 (see Table S3.5 in the supporting information for tabulated data). This marked dependence of C-O cleavage rates on pH strongly suggested that the reaction is acid-catalyzed. However, in control experiments, benzyl alcohol did not convert in acidic media in the absence of Pd, with and without the presence of 1 bar H_2 or cathodic potential. Thus, the cleavage of the C-O bond in benzyl alcohol requires both, acid sites and reduction equivalents produced at the Pd surface.

It is worth noting that the rates of toluene production were higher when starting from benzyl alcohol than from benzaldehyde, where the C-O bond cleavage step occurred at appreciable rates only at pH below 3. This points to a stronger adsorption of the carbonyl compound than of the alcohol, which is in line with the zero reaction order in benzaldehyde (surface saturated with benzaldehyde) observed at these conditions [14].

3.2.3. Effect of pH on hydrogen binding energy

In the series of ECH experiments for benzaldehyde and benzyl alcohol conversion we considered the change in equilibrium potential with varying pH according to the Nernst equation and consistently applied the same overpotential. Thus, we can rule out that the enhancement in hydrogenation rates with increasing concentration of hydronium ions originates from an increase in hydrogen chemical potential. The invariant Faradaic efficiencies in the studied potential range (Figure S3.2, Table S3.2) indicate that accelerating the provision of reduction equivalents by making the potential more negative, the rates of H_2 evolution and ECH increase in an identical way. The FE tends to decrease as the potential becomes more negative but because of a higher increase of HER than ECH rather than net decreasing rates of ECH. This shows that the changes of ECH and HER rates with varying hydronium ion concentration have the same underlying origin.

Thus, we turn to the effect of pH on the H-metal binding energy (HBE), which has been put forward for the enhancing effect of pH on the H_2 evolution reaction and the hydrogenation rates of phenol on Pt [21, 30]. In the following analysis we have used the HBE calculated from the desorption signals of underpotential deposited hydrogen as reported in Ref. [30] (see SI chapter 3.5.3 for details).

The correlations of TOF and pH shown in Figure 3.2 closely resemble the dependence of HBE with pH and electrolyte presented in the supporting information (Figure S6). Indeed, the conversion rates of benzaldehyde under OCV (1 bar H_2) and ECH (-0.06 V_{RHE}) are inversely proportional to the HBE (Figure 3.3) from -35 kJ mol^{-1} to -20 kJ mol^{-1}. Further decrease in HBE does not seem to enhance the TOF further. The correlation in Figure 3.3 strongly suggests that the effect of pH on hydrogenation rates, irrespective of the origin of the reduction equivalents, originates from weakened HBE.

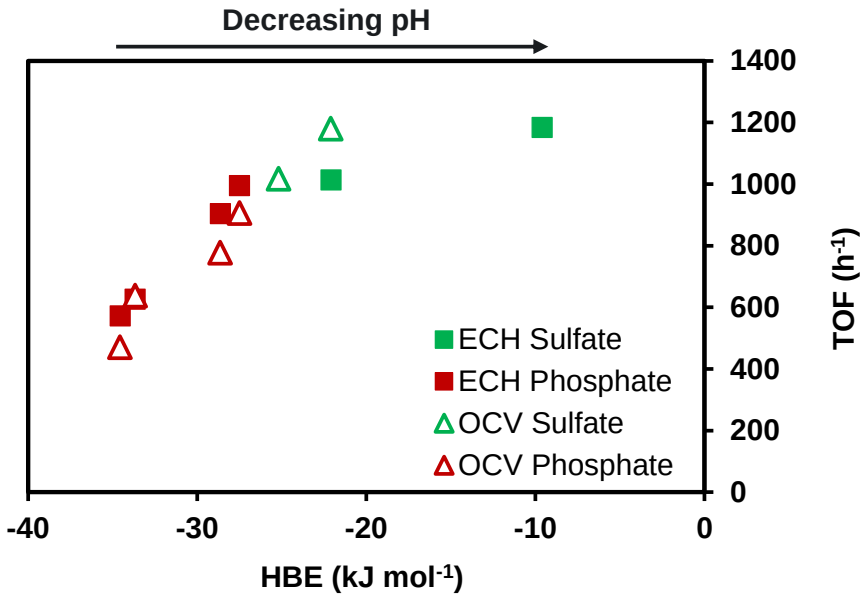

Figure 3.3. Correlation of hydrogen binding energy (HBE) with benzaldehyde hydrogenation rates during open circuit voltage (OCV) at 1 bar H_2 and electrocatalytic hydrogenation (ECH) at -0.06 V_{RHE}. Pd/C (5 wt.% Pd), 20 mM benzaldehyde and as described electrolytes were used at room temperature.

3.2.4. Mechanisms for reduction in water

The identical effects of hydronium ion concentration, via H-Pd binding energy, on the conversion rates of benzaldehyde and benzyl alcohol under OCV and ECH indicate that the reaction mechanisms are the same under both conditions. In line with this conclusion, the activation energies for the hydrogenation of benzaldehyde under ECH and OCV were similar. That is, ~13 kJ mol^{-1} at -0.06 V and -0.18 V vs RHE for ECH and 18 kJ mol^{-1} for OCV (Figure 3.4) (we reported 21 kJ mol^{-1} at pH 5 for OCV before) [14]. In comparison, the hydrogenation of benzaldehyde in decalin showed the activation energy of 32 kJ mol^{-1} (Figure 3.4). Thus, we conclude that the mechanisms of hydrogenation in water are similar under OCV and ECH while both being

fundamentally different to the mechanism in the organic phase, within the explored potential range. The differences in ECH and OCV (~13 kJ mol^{-1} and 21 kJ mol^{-1}), interpreted differently in Ref. [14], are tentatively attributed to changes in the chemical potential of reacting species due to the applied potential.

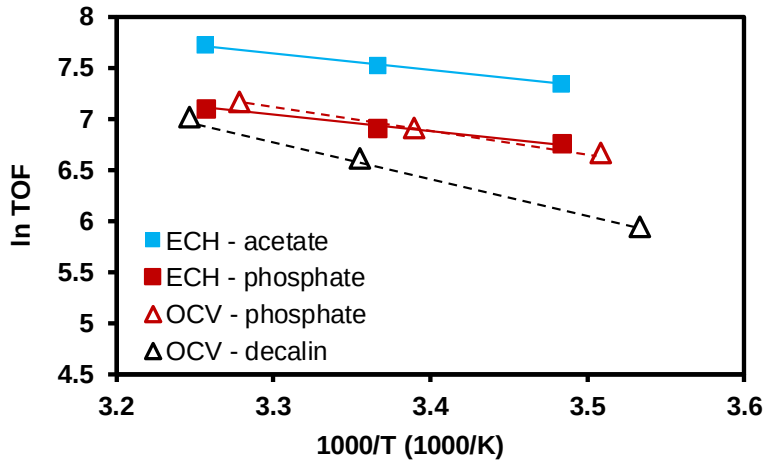

	E_A (kJ mol^{-1})
ECH - phosphate	13
ECH - acetate	14
OCV – phosphate	18
OCV – decalin	32

Figure 3.4. Activation energies for the hydrogenation of benzaldehyde in different solvents during open circuit voltage (OCV) performed under 1 bar H_2 and electrocatalytic hydrogenation (ECH) at -0.06 V vs RHE (phosphate, pH 1.6) and -0.18 V vs RHE (acetate, pH 5.2). Latter is taken from Ref. [14].

In another set of experiments, we performed kinetic isotope effect (KIE) reactions for the hydrogenation of benzaldehyde under OCV in acidic and neutral solvents. The hydrogenation was studied at OCV by contacting H_2 or D_2 with solutions prepared in H_2O or D_2O, i.e., we performed the combinations: H_2-H_2O, D_2-H_2O, D_2-D_2O, H_2-D_2O. In neutral solutions (pH 6.3), the solvent (H_2O or D_2O) had little influence on the rates of hydrogenation, i.e., the ratios of the rates observed in H_2O and D_2O was ~1 using both H_2 and D_2 (Figure 3.5). In contrast, when varying the gas composition, the rates of hydrogenation with D_2 were significantly lower than the rates with H_2 (KIE of ~3 in H_2O and D_2O). When the reactions were performed in acidic conditions (pH 1.6), the rates were higher in H_2O than in D_2O using either H_2 or D_2 with a rate ratio of ~1.4 (Figure 3.5, right). In each solvent (H_2O or D_2O), D_2 led to lower reaction rates than H_2, and the KIE is much smaller (~1.2) than that under neutral pH showing that the impact of the gas composition is small in acidic conditions. These results suggest that the solvent is effectively involved in the reaction at acidic conditions even if the reaction is driven by H_2 (or D_2), as kinetic isotope experiments of reactions containing charge transfer steps are often insensitive and show KIE values close to unity (Figure 3.5, right) [31].

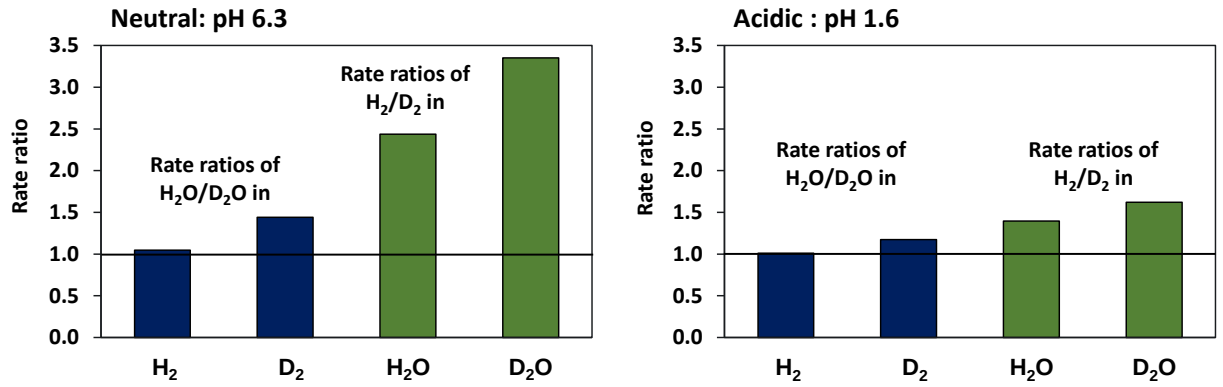

Figure 3.5. Ratios of the rates of benzaldehyde hydrogenation performed under 1 bar H_2 or D_2 in H_2O or D_2O. The reactions were performed in neutral conditions (left) and in the presence of 0.2 M phosphoric acid at pH 1.6 (right). All experiments were performed using Pd/C (5 wt. % Pd/C) at room temperature with 20 mM benzaldehyde.

Thus, we conclude that a PCET mechanism (where the hydronium ions participate in the reaction) dominates the hydrogenation of benzaldehyde in water at acidic conditions and in the presence of an external potential. We depict the PCET mechanism as shown in Figure 3.6, where the first step is the adsorption of benzaldehyde on the metal. Hydrogenation occurs in a sequence of hydrogen addition steps, wherein the kinetically relevant hydrogenation proceeds with the addition of a proton from a hydronium ion and an electron from the metal. Finally, the fully hydrogenated product (benzyl alcohol in this case) desorbs from the metal. In homogenous phase, the one-electron reduction of carbonyl by PCET (i.e., $CH_2O+H^++e^-\rightarrow\cdot CH_2OH$) is energetically more demanding than the one-electron reduction of the resulting radical (i.e., $\cdot CH_2OH +H^++e^-\rightarrow CH_3OH$) carbonyl [32]. Thus, we postulate that the first hydrogenation is the rate determining step as shown in Figure 3.6 and Table S3.6. This protonation and electron transfer in the PCET step can be consecutive or simultaneous. A simultaneous proton-electron addition is energetically more favorable than any consecutive addition [14]. The metal-H binding energy will directly impact the concentration of hydronium ions in the outer Helmholtz plane of the electrical double layer relative to the concentration of adsorbed hydrogen. That is, the hydrogen equilibrium (Volmer reaction) shown in Figure 3.6 will favor the side of the hydronium ion as the metal-H binding weakens.

In support for the PCET mechanism postulated in Figure 3.6, recent studies on electrochemical hydrogenation have shown that low-energy pathways for electrocatalytic reduction indeed include reduction of protonated species [16]. Conversely, in agreement with our conclusion of the same mechanism operating under OCV conditions, PCET has also been reported for thermocatalytic hydrogenation with contributions depending on the composition of the liquid phase [33].

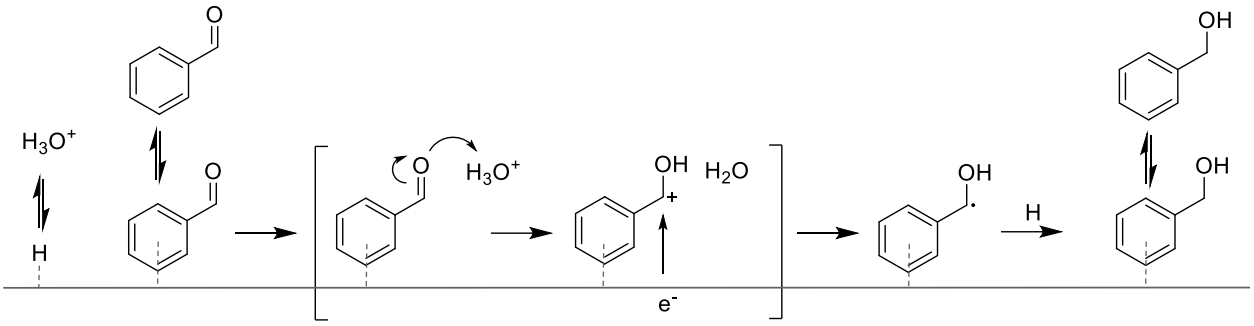

Figure 3.6. Proposed elementary steps for the hydrogenation of benzaldehyde in aqueous phase: upon adsorption at the metal benzaldehyde is protonated and the resulting carbocation reduced by an electron at the surface. Adsorbed alcohol is formed upon the second hydrogen addition.

We have reported that ECH rates are significantly affected by the presence of Brønsted acidic species near the metal, e.g., functional groups at the support or co-adsorbed molecules [15, 34]. On that basis, we hypothesized that hydrogenation under such conditions occurs through a PCET mechanism. We also observed that if adsorbed H is formed at the surface of Pd, its addition to adsorbed benzaldehyde is not less energetically favored than a PCET step [34]. Thus, we do not discard the reaction of the organic compound with adsorbed hydrogen under ECH conditions, which seems indeed, the dominant mechanism for the hydrogenation of aromatic rings on Pt and Rh [9, 11, 35]. This is also the most likely mechanism for benzaldehyde hydrogenation at OCV and neutral conditions (Figure 3.5). Let us call this hydrogenation via H-addition a Langmuir-Hinshelwood (L-H) mechanism, because both H and benzaldehyde react from a state bound to the metal surface (Table S3.6).

Therefore, both PCET and L-H mechanisms coexist in both ECH and OCV conditions and their contributions to the overall hydrogenation in water depends on the potential of the system and availability of adsorbed hydrogen. A possible unified rate equation is shown in Eq. (3.1). The numerator of the first term at the right side of the equation is the contribution of the PCET step, where k'_{PCET} is a potential-dependent rate constant. The numerator of the second term contains the contribution of the L-H step, which explicitly depends on the pressure of H_2 (P_{H2}). In both cases, K_i are the adsorption equilibrium constants of reactants (K is a combination of constants). Detailed derivations of Eq. (3.1) are shown in the supporting information, chapter 3.5.5.

$$r_{HYD} = \frac{k'_{PCET} K_{RCHO} [RCHO][H^+]}{1+K_{RCHO}[RCHO]} + \frac{k_{L-H}\, K_{RCHOH}\, K_{RCHO}\, K_{H2}\, [RCHO]\, P_{H2}}{\left[1 + K_{RCHO}\, [RCHO] + (K_{H2}\, P_{H2})^{\frac{1}{2}}\right]^2} \qquad (S3.1)$$

Equation (3.1) illustrates that contributions of the two pathways to the overall transformation primarily depend on the reaction conditions. The contribution of the PCET mechanism increases with increasing applied potential (which increases the electrochemical rate constant) and increasing concentration of hydronium ions. The contribution of the L-H mechanism increases with increasing H_2 pressure but, in more general terms, with increasing coverage of adsorbed hydrogen (that can also be produced upon proton reduction).

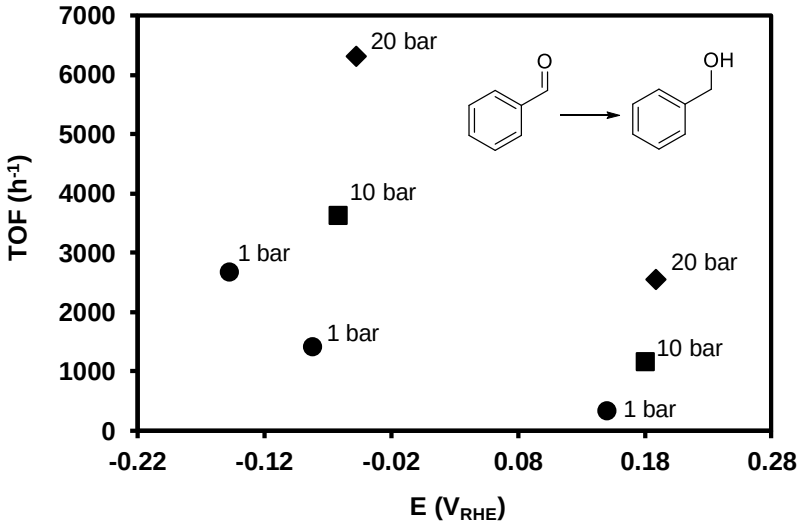

Figure 3.7. Turn over frequencies (TOF) for the hydrogenation of benzaldehyde at pH 5.2 and varying H_2 pressure (values shown in the plot). The data plotted at negative potentials denote electrocatalytic hydrogenation at the potential shown in the x-axis. The points at positive potential correspond to rates at open circuit potentials. Experiments were performed over Pd/C (5 wt.%) at room temperature.

We verified the effects of applied potential and pressure by performing the hydrogenation of benzaldehyde on Pd at varying pressure under OCV conditions and with an applied electric potential. Figure 3.7 shows that in both cases the reaction rates increase with increasing H_2 pressures. The corresponding reactions orders in H_2 were 0.64 and 0.47 in the absence of an applied potential and with -0.06 V_{RHE}, respectively (Figure S3.8). Interestingly, the effects of pressure and potential are not additive, i.e., the absolute rate increases observed by increasing pressure from 1 to 10 and 20 bar are higher at -0.06 V_{RHE} than under OCV. Note that the potential remained constant, and therefore also the potential-dependent rate constant (k'_{PCET}). Thus, the higher than expected effect of pressure, according to Eq. (3.1), is attributed to effects of the applied potential on the rates of the L-H pathway. We propose that this effect derives from the impact of the applied potential on the chemical potential of adsorbed hydrogen, which in turn, increases the reaction rate constants of L-H (H-addition steps). In line with this proposal, we have observed a decrease in the

apparent activation energies for ECH of phenol over Pt by ca. 18 kJ mol^{-1} with increasingly negative potential [12].

3.3. Conclusion

The metal-catalyzed hydrogenation of functionalized compounds in water enables a conversion route that comprises the proton couple electron transfer (PCET) to the polar (aldehyde, alcohol) moiety of the molecule. This reductive route may surpass the hydrogenation route, where adsorbed H is added from the surface to the adsorbed organic compound. However, both routes are not mutually exclusive, and both contribute to the overall reaction. Fundamentally, their net contributions depend on the applied potential of the system and on the coverage of hydrogen. The electrochemical nature of the PCET mechanism makes it very sensitive to the overpotential, thus making electrochemical hydrogenation faster than hydrogenation with H_2 at 1 bar (open circuit voltage, OCV conditions). The hydrogenation rates also increase with increasing concentration of hydronium ions, resulting from the weakening of the metal-hydrogen bond. This leads to easier transfer of hydrogen to the organic compound in case of L-H mechanism. In the PCET pathway the weakened metal-H binding energy shifts the equilibrium of the Volmer reaction to the side of the hydronium ion effectively increasing the concentration of reducing equivalents at the OHP.

Overall, the occurrence of electrochemical steps in the reduction of organic molecules in water, regardless of the origin of the reduction equivalents open the possibilities for a new approach for catalysis, where thermocatalysis and electrocatalysis are not fundamentally different and, where applied potential is used as an additional level to control catalytic rates.

3.4. Acknowledgements

The research described in this paper is part of the Chemical Transformation Initiative at Pacific Northwest National Laboratory (PNNL), conducted under the Laboratory Directed Research and Development Program at PNNL, a multiprogram national laboratory operated by Battelle for the U.S. Department of Energy. J.A.L. was supported by the U.S. Department of Energy (DOE), Office of Science, Office of Basic Energy Sciences, Division of Chemical Sciences, Geosciences and Biosciences (Transdisciplinary Approaches to Realize Novel Catalytic Pathways to Energy Carriers, FWP 47319). We thank Yue Liu and Donald M. Camaioni for fruitful discussions.

3.5. Supporting Information

3.5.1. Experimental methods

Reagents and materials

Chemicals were purchased from Sigma and used as received: benzaldehyde (≥99.0%), benzyl alcohol (≥99.0%), ethyl acetate (≥99.9%), NaCl (≥99.9%) and KCl (≥99.9%). Phosporic acid (H_3PO_4, ≥99.9%), sodium dihydrogen phosphate (NaH_2PO_4, ≥99.9%), disodium hydrogen phosphate (Na_2HPO_4, ≥99.9%), sulfuric acid (H_2SO_4, ≥99.9%), sodium sulfate (Na_2SO_4, ≥99.9%), acetic acid (CH_3COOH, ≥99.9%), sodium acetate (CH_3COONa ≥99.9%) and phecoloric acid ($HClO_4$, ≥99.9%) were used as received to prepare the buffer solutions. The calculation about pH of the buffer solution is according to the Henderson-Hasselbalch equation ($pH=pKs+lg(C_{A^-}/C_{HA})$), and then estimated by pH value meter. High purity water, obtained with a Milli-Q water purification system with a resistivity of 18.2 MΩ·cm, was used for all experimental procedures. H_2 (Air Liquide, >99.99%) was used for thermal hydrogenation, He (Air Liquide, >99.99%) was used as protection gas to remove O_2 from the electrolyte before ECH.

Catalyst characterization

We used a carbon supported Pd catalysts with the metal loading of 5 wt. %. The supported metal phase had a dispersion of 30 % and an average particle size of 3.3 nm as measured by hydrogen chemisorption and transmission electron microscopy. Details of the physicochemical properties of this catalysts can be found in Ref [14].

Electrocatalytic hydrogenation measurements

Experiments were carried out in a two-compartment galvanostatic cell. The cathodic and anodic compartments were separated by a Nafion 117 proton exchange membrane (Ion Power, Inc.), which had been pretreated in a H_2O_2 solution (3 vol.%) and in sulfuric acid (2 M) to obtain higher proton conductivity, fast ion crossover and large membrane area. A piece of carbon felt (Alfa Aesar >99.0%, 3.2 mm thickness) infiltrated with 10 mg Pd/C connected to a graphite rod (Sigma Aldrich, 99.99%) was used as working electrode in the cathode compartment. A platinum wire (Alfa Aesar, 99.9 %) was used as counter electrode in the anodic compartment. The reference electrode was a lab-made Ag/AgCl electrode with a double junction protection. The cathode and

anode compartments were filled with 60 mL electrolyte solution each of the same electrolyte during all procedures. All reactions were performed at atmospheric pressure at constant potential referred to the reverse hydrogen electrode (RHE). For this, the reference electrode was calibrated against a RHE in sodium acetate buffer and all potentials throughout this work are reported on the RHE reference scale. Prior to ECH, polarization of the catalyst was performed under a constant current of -40 mA for 10 min. Benzaldehyde was typically added into the cathode compartment to obtain a final concentration of 20 $mmol \cdot L^{-1}$. Temperature was controlled with a cooling/heating circulator (Julabo F25-ED). All electrochemical procedures were performed with an electrochemical workstation VSP-300, Bio Logic. Prior to the experimental procedures, the electrodes were alternatively immersed in H_2SO_4 (5 M) and KOH (5 M) for 15 min. After each immersion, the materials were thoroughly cleaned (Pt electrodes were further ultrasonically treated) in ultrapure water for 15 min. In order to eliminate the effect of electrolyte resistance, ohmic loss was measured by the IR compensation (PEIS) high frequency impedance method from Bio-Logic potentiostat using scanning from 100 mHz to 800 kHz. Afterwards, 85% of the iR drop was compensated and the applied potential was corrected during all measurements.

To discuss the utilization of cathodic potential to reduce organic compounds we defined Faradic efficiency (FE) as the percentage of the total current that is used for conversion of the organic compounds. The difference between the total current passed and that utilized for ECH was consumed for H_2 evolution in all cases.

Catalytic hydrogenation under open circuit voltage conditions

Experiments were carried out in a glass batch reactor with 10 mg Pd/C during stirring at 600 rpm. Typical measurements were performed at atmospheric pressure with H_2 (10 $mL \cdot min^{-1}$) flowing through the reactant solution at 296 K. The benzaldehyde concentrations were the same as those described for ECH. The temperature was controlled with the cooling/heating circulator Julabo F25-ED.

Product analysis

The courses of ECH and TCH experiments were followed by periodically withdrawing aliquots of 1 mL from the cathode compartment. The products were extracted with 3 mL of ethyl acetate. The organic phase was separated from the aqueous phase and then dried over Na_2SO_4. Quantitative

analyses of the samples were performed by gas chromatography equipped with a Wax capillary column (30m x 250 μm) and a flame ionization detector. P-cresol (Sigma Aldrich, >99 %) was used as internal standard for quantification.

Calculations

Conversion, reaction rate of ECH, OCV/TCH and HER, turnover frequency (TOF), and Faradaic efficiency (FE) were calculated as follows.

$$\text{Conversion} = \frac{\text{moles of reactant consumed}}{\text{initial moles of reactant}} \text{ x } 100 \quad [\%]$$

$$\text{ECH reaction rate} = \frac{\text{moles of reactant consumed by ECH}}{\text{time x mass of metal}} \quad [\text{mol s}^{-1}\ g_{metal}^{-1}]$$

$$\text{TCH reaction rate} = \frac{\text{moles of reactant consumed by TCH}}{\text{time x mass of metal}} \quad [\text{mol s}^{-1}\ g_{metal}^{-1}]$$

$$\text{HER reaction rate} = \frac{\text{moles of hydrogen gas produced by HER}}{\text{time x mass of metal}} \quad [\text{mol s}^{-1}\ g_{metal}^{-1}]$$

$$\text{TOF} = \frac{\text{moles of reactant consumed}}{\text{time x moles of exposed metal}} \quad [h^{-1}]$$

$$\text{FE} = \frac{\text{electrons consumed by ECH}}{\text{total electrons passed}} \text{ x } 100 \quad [\%]$$

Isotopic experiments

Kinetic isotope experiments were performed analogous to open circuit voltage hydrogenation reactions. 10 mg Pd/C were dispersed in 60 ml of 0.1 M phosphoric acid (pH 1.6) or 0.1 M phosphate buffer (pH 6.3) prepared in H_2O or D_2O at 600 rpm and 1 bar H_2 or D_2 were introduced into the reactor. 20 mM benzaldehyde was utilized, and aliquots taken during the reaction and analyzed in a GC-FID.

High pressure electrochemical hydrogenation

Experiments were performed in closed H-cell connected to a back pressure regulator. In this cell, threaded inlets were installed to connect working, counter and reference electrodes with ferrules and nuts (IDEX) as well as with gas inlet, gas outlet and sampling lines and valves. The working electrode was prepared by electrodepositing Pd on glassy carbon foam in a 2 mM $Pd(NO_3)_2$ in 0.5 M H_2SO_4 solution at -150 mA for 20 minutes (acetate buffer with pH 5.2 was used as

electrolyte). After assembly, the electrochemical pretreatments and experiments were conducted following the same procedures as those described above for ECH measurements at atmospheric conditions.

3.5.2. Influence of pH on benzaldehyde and acetophenone hydrogenation rates and pathways

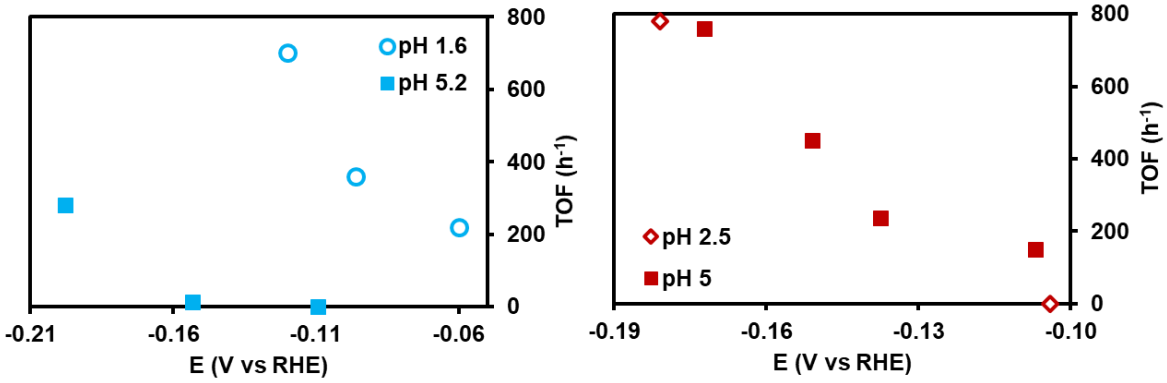

Figure S3.1. Metal normalized rates of the H_2 evolution reaction (TOF) observed during the electrocatalytic hydrogenation of benzaldehyde (left) and acetophenone (right) as a function of cathodic potential. Experiments were conducted in buffer solutions of phosphoric acid (pH 1.6, pH 2.5) or acetic acid (pH 5.2) over Pd/C (5 wt. %) at room temperature and atmospheric pressure.

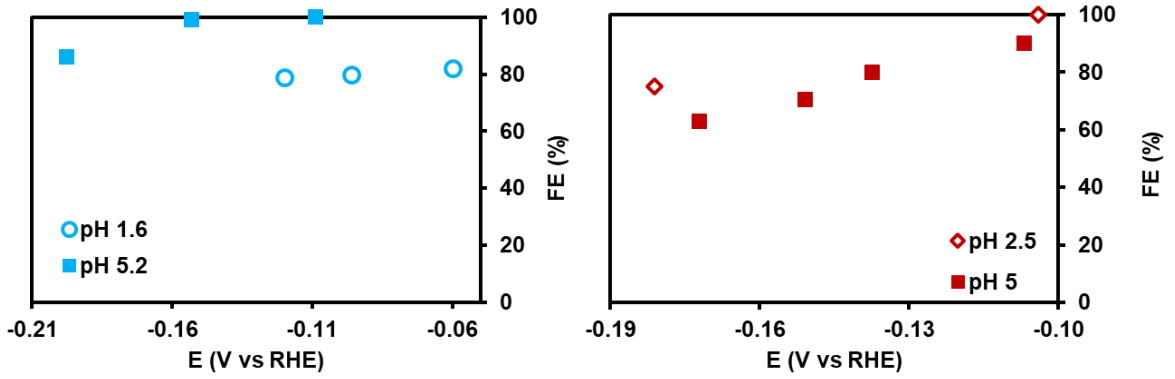

Figure S3.2. Faradaic efficiencies (FE) observed during the electrocatalytic hydrogenation of benzaldehyde (left) and acetophenone (right) as a function of cathodic potential. Experiments were conducted in buffer solutions of phosphoric acid (pH 1.6, pH 2.5) or acetic acid (pH 5.2) over Pd/C (5 wt. %) at room temperature and atmospheric pressure.

In the ECH of benzaldehyde, Faradaic efficiencies (FEs) above 80% were observed at the tested conditions, whereas in the ECH of acetophenone FEs were above 60% (Figure S3.2). For both compounds, the FE remained constant as the potential varied in the window of -0.06 V to -0.16 V RHE, while there are declining trends at more negative potentials. Thus, at moderate potentials,

increasing the driving force for electrochemical reduction has the same impact on ECH and HER rates, while very negative potentials enhance HER over ECH in line with observations reported on other metals [14]. These effects of potential, which will be studied in detail in a future contribution, is attributed to changes in the coverage of adsorbed hydrogen that increases with cathodic potential affecting the availability of sites for binding organic compounds [13].

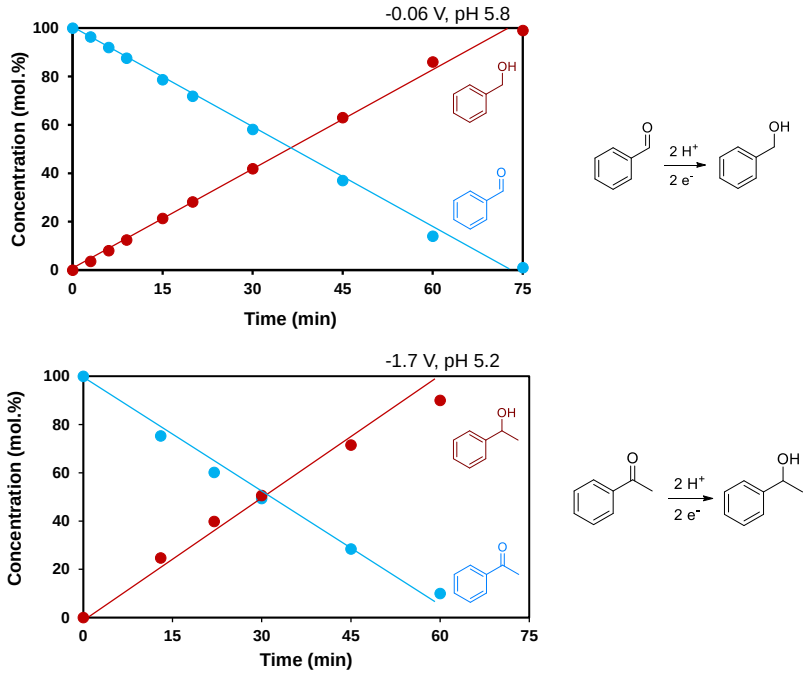

Figure S3.3. Concentration profiles during electrocatalytic hydrogenation of benzaldehyde and acetophenone at pH 5.2. Both sets of experiments were performed using Pd/C (5 wt. % Pd) at room temperature with 20 mM organic in aqueous solutions.

Along the reaction network, the carbonyl groups are hydrogenated to hydroxyls in the first reaction step with benzyl alcohol and 1-phenylethanol as the primary products in the hydrogenation of benzaldehyde and acetophenone, respectively. Those alcohols were also the final products at pH 5.2 as shown in Figure S3.3 and Figure S3.4. At acidic pH, however, the alcohols were further converted through a secondary C-O bond cleavage. That is, benzyl alcohol conversion yields toluene as secondary product, whereas 1-phenylethanol yields styrene and ethylbenzene in consecutive steps (illustrated for pH 1.6 and 2.5 in Figure S3.5). These reaction networks and their dependence on pH are insensitive to the origin of the reduction equivalents, i.e., H_2 under OCV and electric potential in ECH. The concentration profiles are also insensitive to origin of reduction equivalents (Figure S3.4). Table S3.1, Table S3.2, Table S3.3, Table S3.4 and Table S3.5 summarize the data shown in the figures.

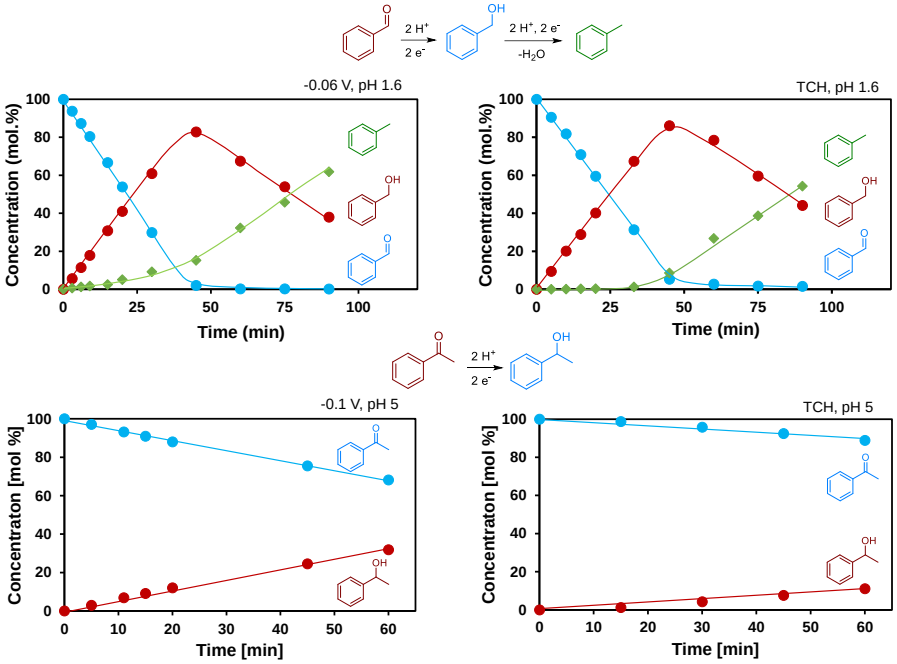

Figure S3.4. Top: Concentration profiles observed during the hydrogenation of benzaldehyde at pH 1.6 during electrocatalytic hydrogenation (-0.06 V) and open circuit voltage (OCV, 1 bar H_2). Bottom: Concentration profiles observed during the hydrogenation of acetophenone at pH 5.2 during electrocatalytic hydrogenation (-0.06 V) and open circuit voltage (OCV, 1 bar H_2). The experiments were performed using Pd/C (5 wt. % Pd) at room temperature with 20 mM organic in aqueous solutions with 0.2 M of phosphate electrolyte (pH 1.6) and 3 M acetate electrolyte (pH 5.2).

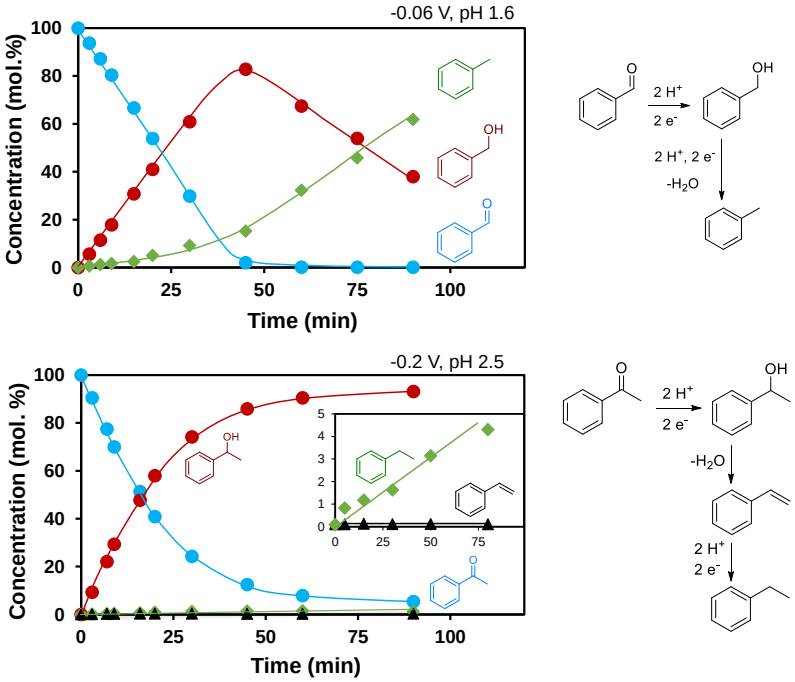

Figure S3.5. Concentration profiles observed during electrocatalytic conversion of benzaldehyde (top), acetophenone (bottom) and 1-phenylethanol (inset). The experiments were performed using Pd/C (5 wt. % Pd) at room temperature with 20 mM of the reactant in aqueous solutions with phosphate electrolytes.

Table S3.1. Summary of data obtained for the hydrogenation of benzaldehyde under open circuit potential conditions (1 bar H_2, room temperature).

pH	Rate (μmol $g^{-1}s^{-1}$)	TOF (h^{-1})	Electrolyte
1	1080	1248	H_2SO_4
1.5	993	1148	Na_2SO_4/H_2SO_4
3	720	832	Na_2SO_4/H_2SO_4
1.6	860	994	H_3PO_4
2.5	712	823	H_2NaPO_4/H_3PO_4
5.8	582	673	H_2NaPO_4/HNa_2PO_4
6.3	478	552	H_2NaPO_4/HNa_2PO_4
5	976	1128	AcOH/NaOAc
6	804	930	AcOH/NaOAc
7	480	555	AcOH/NaOAc

Table S3.2. Summary of data obtained for the hydrogenation of benzaldehyde under electrocatalytic hydrogenation (-0.06 V vs. RHE, room temperature).

pH	Rate (μmol $g^{-1}s^{-1}$)	TOF (h^{-1})	Current (mA)	FE (%)	Electrolyte
0.63	1024	1184	-111	91	0.2 M H_2SO_4
0.66	948	1096	-105	82	0.2 M $HClO_4$
1	877	1014	-88	81	0.1 M $HClO_4$
1.1	866	1002	-99	74	0.1 M H_2SO_4
1.6	861	996	-102	76	0.2 M H_3PO_4
2.5	783	905	-84	81	0.2 M H_2NaPO_4/H_3PO_4
5.8	542	627	-58	77	0.2 M H_2NaPO_4/HNa_2PO_4
6.3	496	573	-53	79	0.2 M H_2NaPO_4/HNa_2PO_4

Table S3.3. Summary of data obtained for the hydrogenation of acetophenone under electrocatalytic hydrogenation (-0.1 V vs. RHE, room temperature).

pH	Rate (μmol $g^{-1}s^{-1}$)	TOF (h^{-1})	Current (mA)	FE (%)	Electrolyte
2.5	557	1002	-52	100	0.1 M H_3PO_4/NaH_2PO_4
5.2	226	407	-34	62	3 M HOAc/NaOAc

Table S3.4. Summary of data obtained for the hydrogenation of acetophenone under electrocatalytic hydrogenation (-0.2 V vs. RHE, room temperature).

pH	Rate (μmol $g^{-1}s^{-1}$)	TOF (h^{-1})	Current (mA)	FE (%)	Electrolyte
2.5	1302	2342	-164	75	0.1 M H_3PO_4/NaH_2PO_4
5.2	758	1363	-146	50	3 M HOAc/NaOAc

Table S3.5. Summary of benzyl alcohol reductive dehydration in catalytic hydrogenation with H_2 (TCH) and electrocatalytic hydrogenation (ECH).

	pH	Rate (mol g^{-1} h^{-1})	TOF (h^{-1})	Buffer
	0.63	2.81	901	$HClO_4$
	1	2.56	823	$HClO_4$
ECH	1.6	2.53	814	H_3PO_4
	2.5	1.66	532	H_2NaPO_4/H_3PO_4
	5.8	0.52	166	H_2NaPO_4/HNa_2PO_4
	0.63	2.74	878	$HClO_4$
	1	2.45	786	$HClO_4$
TCH	1.6	2.26	726	H_3PO_4
	2.5	1.58	509	H_2NaPO_4/H_3PO_4
	5.8	0.11	35	H_2NaPO_4/HNa_2PO_4

3.5.3. Determination of the hydrogen binding energy on Pd at varying pH

The hydrogen binding energy (HBE) refers to the strength of H binding on the metal surface. HBE can be calculated according to desorption peak potentials for underpotential deposited hydrogen (H_{upd}) obtained from the respective cyclic voltammetry (CV) in buffered electrolytes with varied pH values using the equation of $HBE = - F E_{peak}$ (F, Faraday constant, 96485 C mol^{-1}), derived from $-F E_{peak} = \Delta H$ [24].

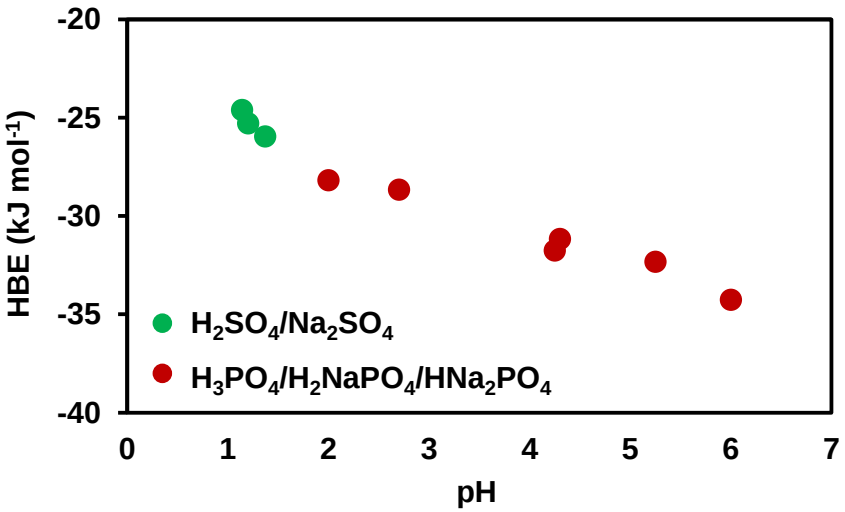

Figure S 3.6. Hydrogen binding energies (HBE) on Pd as a function of pH and electrolytes calculated on basis of E_{peak} according to Ref. [30]

3.5.4. Kinetic isotope effect in neutral and acidic pH

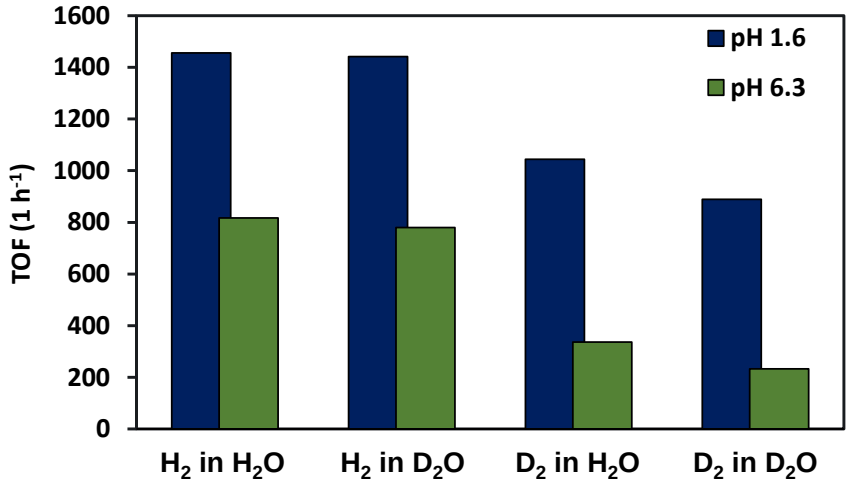

Figure S3.7. Turnover frequency (TOF) of benzaldehyde hydrogenation performed under 1 bar H_2 or D_2 in H_2O or D_2O. The reactions were performed in 0.1M phosphate buffer (pH 6.3 - green) and in the presence of 0.1 M phosphoric acid (pH 1.6 - blue). Pd/C (5 wt. % Pd/C) were used at room temperature with 20 mM benzaldehyde.

3.5.5. Kinetic derivation of hydrogenation mechanisms in water

Table S3.6. Elementary steps for two possible hydrogenation mechanisms in water. PCET is proton couple electron transfer.

a) Concerted PCET		b) Langmuir-Hinshelwood	
RCHO + * ⇄ RCHO*	(1)	RCHO + * ⇄ RCHO*	(1)
RCHO* + H^+ + e^- → RCHOH*	(2)	H_2 + 2* ⇄ 2H*	(1b)
RCHOH* + H* ⇄ RCH_2OH* + *	(3)	RCHO* + H* ⇄ RCHOH*+ *	(2b)
RCH_2OH* ⇄ RCH_2OH + *	(4)	RCHOH* + H* → RCH_2OH * + *	(3)
		RCH_2OH* ⇄ RCH_2OH + *	(4)
H^+ + e^- + * → H*	(5)		

Let us consider the two mechanisms of hydrogenation shown in Table S3.6. In both cases we consider that the organic compounds are adsorbed on the surface and that this adsorption is equilibrated as shown in reaction (1). This equilibrium is described as:

$$K_{RCHO} = \frac{\theta_{RCHO}}{[RCHO]\theta_*} \qquad (S3.1)$$

where K_{RCHO} is the adsorption equilibrium constant, θ_{RCHO} is the coverage of the organic compound on the catalyst, $[RCHO]$ is the concentration of the organic compound in solution, and θ_* is the fraction of available sites.

Assuming that the first proton and electron transfer is the rate determining step in the proton coupled electron addition pathway, the rate of the reaction ($r_{HYD_{PCET}}$) is:

$$r_{HYD_{PCET}} = k'_{PCET}\theta_{RCHO}[H^+] \qquad (S3.2)$$

where k'_{PCET} is the potential dependent rate constant, and $[H^+]$ is the concentration of hydronium ions. Using Eq. (S3.1) to replace the coverage of the organic in Eq. (S3.2), we obtain:

$$r_{HYD_{PCET}} = k'_{PCET}K_{RCHO}[RCHO]\theta_*[H^+] \qquad (S3.3)$$

The simplest site balance that we can propose is:

$$1 = \theta_{RCHO} + \theta_* \qquad (S3.4)$$

Which can be simplified to:

$$1 = K_{RCHO}[RCHO]\theta_* + \theta_* \qquad (S3.5)$$

Substituting Eq. (S3.5) in Eq. (S3.3):

$$r_{HYD_{PCET}} = \frac{k'_{PCET} K_{RCHO} [RCHO][H^+]}{1 + K_{RCHO}[RCHO]} \quad (S3.6)$$

For the Langmuir-Hinshelwood mechanism in Table S3.6, the equilibrated adsorption of molecular H_2 (reaction 1b) is represented by:

$$K_{H2} = \frac{\theta_H^2}{P_{H2}\ \theta_*^2} \quad (S3.7)$$

where K_{H2} is the adsorption equilibrium constant, θ_H is the coverage of hydrogen on the catalyst, and P_{H2} is the pressure of H_2. If the second hydrogenation is the rate determining step [14], the rate of the reaction ($r_{HYD_{L-H}}$) is:

$$r_{HYD_{L-H}} = k_{L-H}\ \theta_{RCHOH}\ \theta_H \quad (S3.8)$$

where k_{L-H} is the reaction rate constant and θ_{RCHOH} is the coverage of the hydrogenated intermediate produced by reaction 2b in Table S3.6. That equilibrated reaction is represented by:

$$K_{RCHOH} = \frac{\theta_{RCHOH}\ \theta_*}{\theta_{RCHO}\ \theta_H} \quad (S3.9)$$

where θ_{RCHOH} is the coverage of the hydrogenated intermediate. Substituting Eq. (S3.9) and Eq. (S3.7) in Eq. (S3.8):

$$r_{HYD_{L-H}} = k_{L-H}\ K_{RCHOH}\ \theta_{RCHO}\ K_{H2}\ P_{H2}\ \theta_* \quad (S3.10)$$

The site balance in this case, omitting for simplicity the coverage of the hydrogenated intermediate, is:

$$1 = \theta_{RCHO} + \theta_H + \theta_* \quad (S3.11)$$

$$1 = K_{RCHO}\ [RCHO]\ \theta_* + (K_{H2}P_{H2})^{\frac{1}{2}}\ \theta_* + \theta_* \quad (S3.12)$$

Substituting Eq. (S3.1) and Eq. (S3.12) in Eq. (S3.10):

$$r_{HYD_{L-H}} = \frac{k_{L-H}\ K_{RCHOH}\ K_{RCHO}\ K_{H2}\ [RCHO]\ P_{H2}}{\left[1 + K_{RCHO}\ [RCHO] + (K_{H2}\ P_{H2})^{\frac{1}{2}}\right]^2} \quad (S3.13)$$

Thus, if both hydrogenation mechanisms coexist on the same kind sites, i.e., there is adsorbed H at the surface (mainly from H_2 activation), the net rate will be the sum of Eq. (S3.6) and Eq. (S3.13):

$$r_{HYD} = r_{HYD_{PCET}} + r_{HYD_{L-H}} = \frac{k'_{PCET} K_{RCHO} [RCHO][H^+]}{1+K_{RCHO}[RCHO]} + \frac{k_{L-H}\, K_{RCHOH}\, K_{RCHO}\, K_{H2}\, [RCHO]\, P_{H2}}{\left[1 + K_{RCHO}\,[RCHO] + (K_{H2}\, P_{H2})^{\frac{1}{2}}\right]^2} \quad (S3.14)$$

Eq. (S3.14) is shown as Eq. (3.1) in the main text (merging the equilibrium constants of the L-H contribution).

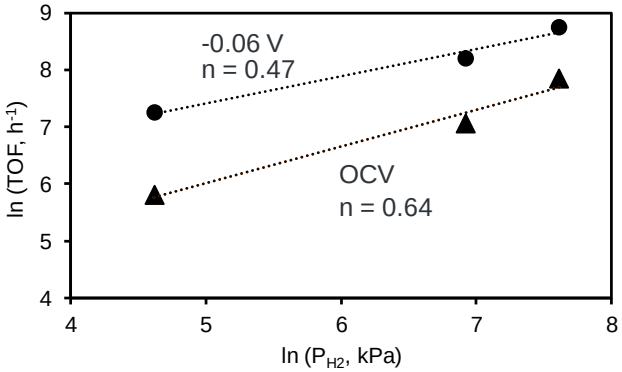

Figure S3.8. Natural logarithms of the rates of benzaldehyde hydrogenation (turn over frequencies, TOF) plotted along the natural logarithms of the H_2 pressure to derive the reaction orders in H_2. The reactions were performed in acetate buffer electrolyte (pH 5) under OCV conditions (triangles) and with the applied potential of -0.06 V vs RHE (circles).

3.6. References

1. Venderbosch, R.; Ardiyanti, A.; Wildschut, J.; Oasmaa, A.; Heeres, H., Stabilization of biomass-derived pyrolysis oils. *Journal of Chemical Technology and Biotechnology* **2010,** *85* (5), 674-686.
2. Haverly, M. R.; Okoren, K. V.; Brown, R. C., Thermal Stability of Fractionated Bio-Oil from Fast Pyrolysis. *Energy & Fuels* **2016,** *30* (11), 9419-9426.
3. Weber, R. S.; Holladay, J. E., Modularized Production of Value-Added Products and Fuels from Distributed Waste Carbon-Rich Feedstocks. *Engineering* **2018,** *4* (3), 330-335.
4. Orella, M. J.; Román-Leshkov, Y.; Brushett, F. R., Emerging opportunities for electrochemical processing to enable sustainable chemical manufacturing. *Current Opinion in Chemical Engineering* **2018,** *20*, 159-167.
5. Lam, C. H.; Das, S.; Erickson, N. C.; Hyzer, C. D.; Garedew, M.; Anderson, J. E.; Wallington, T. J.; Tamor, M. A.; Jackson, J. E.; Saffron, C. M., Towards sustainable hydrocarbon fuels with biomass fast pyrolysis oil and electrocatalytic upgrading. *Sustainable Energy & Fuels* **2017,** *1* (2), 258-266.
6. Dang, Q.; Wright, M. M.; Li, W., Technoeconomic Analysis of a Hybrid Biomass Thermochemical and Electrochemical Conversion System. *Energy Technology* **2018,** *6* (1), 178-187.
7. Sanyal, U.; Lopez-Ruiz, J. A.; Padmaperuma, A.; Holladay, J.; Gutiérrez, O. Y., Electrocatalytic Hydrogenation of Oxygenated Compounds in Aqueous Phase. *Organic Process Research & Development* **2018**.

8. Akhade, S. A.; Singh, N.; Gutiérrez, O. Y.; Lopez-Ruiz, J.; Wang, H.; Holladay, J. D.; Liu, Y.; Karkamkar, A.; Weber, R. S.; Padmaperuma, A. B.; Lee, M.-S.; Whyatt, G. A.; Elliott, M.; Holladay, J. E.; Male, J. L.; Lercher, J. A.; Rousseau, R.; Glezakou, V.-A., Electrocatalytic Hydrogenation of Biomass-Derived Organics: A Review. *Chemical Reviews* **2020,** *120* (20), 11370-11419.
9. Song, Y.; Chia, S. H.; Sanyal, U.; Gutiérrez, O. Y.; Lercher, J. A., Integrated catalytic and electrocatalytic conversion of substituted phenols and diaryl ethers. *Journal of Catalysis* **2016,** *344*, 263-272.
10. Singh, N.; Song, Y.; Gutiérrez, O. Y.; Camaioni, D. M.; Campbell, C. T.; Lercher, J. A., Electrocatalytic hydrogenation of phenol over platinum and rhodium: unexpected temperature effects resolved. *ACS Catalysis* **2016,** *6* (11), 7466-7470.
11. Song, Y.; Gutiérrez, O. Y.; Herranz, J.; Lercher, J. A., Aqueous phase electrocatalysis and thermal catalysis for the hydrogenation of phenol at mild conditions. *Applied Catalysis B: Environmental* **2016,** *182*, 236-246.
12. Sanyal, U.; Song, Y.; Singh, N.; Fulton, J. L.; Herranz, J.; Jentys, A.; Gutiérrez, O. Y.; Lercher, J. A., Structure Sensitivity in Hydrogenation Reactions on Pt/C in Aqueous-phase. *ChemCatChem* **2019,** *11* (1), 575-582.
13. Singh, N.; Nguyen, M.-T.; Cantu, D. C.; Mehdi, B. L.; Browning, N. D.; Fulton, J. L.; Zheng, J.; Balasubramanian, M.; Gutiérrez, O. Y.; Glezakou, V.-A.; Rousseau, R.; Govind, N.; Camaioni, D. M.; Campbell, C. T.; Lercher, J. A., Carbon-supported Pt during aqueous phenol hydrogenation with and without applied electrical potential: X-ray absorption and theoretical studies of structure and adsorbates. *Journal of Catalysis* **2018,** *368*, 8-19.
14. Song, Y.; Sanyal, U.; Pangotra, D.; Holladay, J. D.; Camaioni, D. M.; Gutiérrez, O. Y.; Lercher, J. A., Hydrogenation of benzaldehyde via electrocatalysis and thermal catalysis on carbon-supported metals. *Journal of Catalysis* **2018,** *359*, 68-75.
15. Koh, K.; Sanyal, U.; Lee, M.-S.; Cheng, G.; Song, M.; Glezakou, V.-A.; Liu, Y.; Li, D.; Rousseau, R.; Gutiérrez, O. Y.; Karkamkar, A.; Derewinski, M.; Lercher, J. A., Electrochemically Tunable Proton-Coupled Electron Transfer in Pd-Catalyzed Benzaldehyde Hydrogenation. *Angewandte Chemie International Edition* **2020,** *59* (4), 1501-1505.
16. Bondue, C. J.; Koper, M. T. M., A mechanistic investigation on the electrocatalytic reduction of aliphatic ketones at platinum. *Journal of Catalysis* **2019,** *369*, 302-311.
17. Chadderdon, X. H.; Chadderdon, D. J.; Matthiesen, J. E.; Qiu, Y.; Carraher, J. M.; Tessonnier, J.-P.; Li, W., Mechanisms of Furfural Reduction on Metal Electrodes: Distinguishing Pathways for Selective Hydrogenation of Bioderived Oxygenates. *Journal of the American Chemical Society* **2017,** *139* (40), 14120-14128.
18. Lin, H.-W.; Yen, C. H.; Tan, C.-S., Aromatic hydrogenation of benzyl alcohol and its derivatives using compressed CO2/water as the solvent. *Green Chemistry* **2012,** *14* (3), 682-687.
19. Hiyoshi, N.; Sato, O.; Yamaguchi, A.; Shirai, M., Acetophenone hydrogenation over a Pd catalyst in the presence of H2O and CO2. *Chemical Communications* **2011,** *47* (41), 11546-11548.
20. Poltarzewski, Z.; Galvagno, S.; Pietropaolo, R.; Staiti, P., Hydrogenation of α,β-unsaturated aldehydes over Pt-Sn/Nylon. *Journal of Catalysis* **1986,** *102* (1), 190-198.
21. Singh, N.; Lee, M.-S.; Akhade, S. A.; Cheng, G.; Camaioni, D. M.; Gutiérrez, O. Y.; Glezakou, V.-A.; Rousseau, R.; Lercher, J. A.; Campbell, C. T., Impact of pH on Aqueous-Phase Phenol Hydrogenation Catalyzed by Carbon-Supported Pt and Rh. *ACS Catalysis* **2019,** *9* (2), 1120-1128.
22. Sheng, W.; Myint, M.; Chen, J. G.; Yan, Y., Correlating the hydrogen evolution reaction activity in alkaline electrolytes with the hydrogen binding energy on monometallic surfaces. *Energy & Environmental Science* **2013,** *6* (5), 1509-1512.
23. Zheng, J.; Nash, J.; Xu, B.; Yan, Y., Perspective—towards establishing apparent hydrogen binding energy as the descriptor for hydrogen oxidation/evolution reactions. *Journal of The Electrochemical Society* **2018,** *165* (2), H27-H29.

24. Sheng, W.; Zhuang, Z.; Gao, M.; Zheng, J.; Chen, J. G.; Yan, Y., Correlating hydrogen oxidation and evolution activity on platinum at different pH with measured hydrogen binding energy. *Nature communications* **2015,** *6*, 5848.
25. Parsons, R., The rate of electrolytic hydrogen evolution and the heat of adsorption of hydrogen. *Transactions of the Faraday Society* **1958,** *54*, 1053-1063.
26. Cheng, T.; Wang, L.; Merinov, B. V.; Goddard, W. A., Explanation of Dramatic pH-Dependence of Hydrogen Binding on Noble Metal Electrode: Greatly Weakened Water Adsorption at High pH. *Journal of the American Chemical Society* **2018,** *140* (25), 7787-7790.
27. Lopez-Ruiz, J. A.; Sanyal, U.; Egbert, J. D.; Gutiérrez, O. Y.; Holladay, J., A Kinetic Investigation of the Sustainable Electrocatalytic Hydrogenation of Benzaldehyde on Pd/C. Effect of Electrolyte Composition and Half-cell Potentials. *ACS Sustainable Chemistry & Engineering* **2018**.
28. Sanyal, U.; Lopez-Ruiz, J.; Padmaperuma, A. B.; Holladay, J.; Gutiérrez, O. Y., Electrocatalytic Hydrogenation of Oxygenated Compounds in Aqueous Phase. *Organic Process Research & Development* **2018,** *22* (12), 1590-1598.
29. Andrews, E.; Lopez-Ruiz, J. A.; Egbert, J. D.; Koh, K.; Sanyal, U.; Song, M.; Li, D.; Karkamkar, A. J.; Derewinski, M. A.; Holladay, J.; Gutiérrez, O. Y.; Holladay, J. D., Performance of Base and Noble Metals for Electrocatalytic Hydrogenation of Bio-Oil-Derived Oxygenated Compounds. *ACS Sustainable Chemistry & Engineering* **2020,** *8* (11), 4407-4418.
30. Zheng, J.; Sheng, W.; Zhuang, Z.; Xu, B.; Yan, Y., Universal dependence of hydrogen oxidation and evolution reaction activity of platinum-group metals on pH and hydrogen binding energy. *Science Advances* **2016,** *2* (3), e1501602.
31. Tyburski, R.; Liu, T.; Glover, S. D.; Hammarström, L., Proton-Coupled Electron Transfer Guidelines, Fair and Square. *Journal of the American Chemical Society* **2021,** *143* (2), 560-576.
32. Schwarz, H.; Dodson, R., Reduction potentials of CO2-and the alcohol radicals. *The Journal of Physical Chemistry* **1989,** *93* (1), 409-414.
33. Shangguan, J.; Chin, Y.-H. C., Kinetic Significance of Proton–Electron Transfer during Condensed Phase Reduction of Carbonyls on Transition Metal Clusters. *ACS Catalysis* **2019,** *9* (3), 1763-1778.
34. Sanyal, U.; Yuk, S. F.; Koh, K.; Lee, M.-S.; Stoerzinger, K.; Zhang, D.; Meyer, L. C.; Lopez-Ruiz, J. A.; Karkamkar, A.; Holladay, J. D.; Camaioni, D. M.; Nguyen, M.-T.; Glezakou, V.-A.; Rousseau, R.; Gutiérrez, O. Y.; Lercher, J. A., Hydrogen Bonding Enhances the Electrochemical Hydrogenation of Benzaldehyde in the Aqueous Phase. *Angewandte Chemie International Edition* **2021,** *60* (1), 290-296.
35. Singh, N.; Song, Y.; Gutiérrez, O. Y.; Camaioni, D. M.; Campbell, C. T.; Lercher, J. A., Electrocatalytic Hydrogenation of Phenol over Platinum and Rhodium: Unexpected Temperature Effects Resolved. *ACS Catalysis* **2016,** *6* (11), 7466-7470.

4. Influence of Ionic Strength and Cation Type on Catalytic Hydrogenation

4.1. Results and discussion

Recent studies have reported an enhancement of reaction rates for the dehydration of cyclohexanol and methylcyclohexanols on zeolites with increasing ionic strength in aqueous phase. This was concluded to originate from a non-ideality induced by high ionic strength resulting in a decrease of the free energy barrier. [1, 2] For the electrochemical CO_2 reduction on Ag and Sn, which are selective for CO and formate anion generation, respectively, the formation of these products was reported to increase with increasing alkali metal cation size i.e., $Li^+ < Na^+ < K^+ < Cs^+$. On Cu, the same cation sequence leads to increasing selectivity of e.g., ethylene and ethanol and an overall increase in cathode activity. In these cases, the observed trends were attributed to a stabilization of adsorbed surface intermediates with large dipole moments by electrostatic interaction with hydrated alkali metal cations in the outer Helmholtz plane (OHP). The trends in activity with cation size are shown to arise from differences in ion concentration at the Helmholtz plane as larger hydrated cations are more energetically favored at the OHP than smaller ones. [3, 4] Further, for the oxygen evolution reaction (OER) in alkaline solution it is reported that alkali metal cations in the electrolyte enhance the activity also with increasing cation size. The results show that large Cs^+ cations can significantly affect the interfacial water layer structure so that OER kinetics are improved. [5, 6]

In the following report, effects of electrolyte ionic strength and cation type on the benzaldehyde hydrogenation under electrocatalytic hydrogenation (ECH) and thermocatalytic hydrogenation (TCH) conditions are studied. Note that these are preliminary data and reproductions as well as additional measurements are necessary for a comprehensive interpretation.

The ionic strength I of a solution is a measure of the concentration of ions in the solution. It is the sum of each individual ion i and their charge present in solution.

$$I = \frac{1}{2} \sum_{i=1}^{n} c_i \, z_i^2 \tag{4.1}$$

where c_i is the concentration of ion i and z_i is the charge number of ion i.

To investigate the influence of changes in the ionic strength during ECH reactions, benzaldehyde reduction was performed at -0.1 V_{RHE} in NaOAc/HOAc buffer at constant pH 5.2 and ionic strengths of 0.1 M, 0.5 M, 1 M and 2 M. In accordance with previous measurements, described in detail in chapter 2.5.1 and 3.5.1, 10 mg of 5 wt.% Pd/C were used as catalyst and drop casted on a carbon felt as the working electrode. Electrochemical pretreatments were performed before running the hydrogenation reaction of 20 mM benzaldehyde at -0.1 V_{RHE} (iR compensated and corrected) in 1 bar N_2 or 1 bar H_2 for up to 1 h in a two-compartment batch cell, while analyzing aliquots of the reaction mixture in a GC-FID.

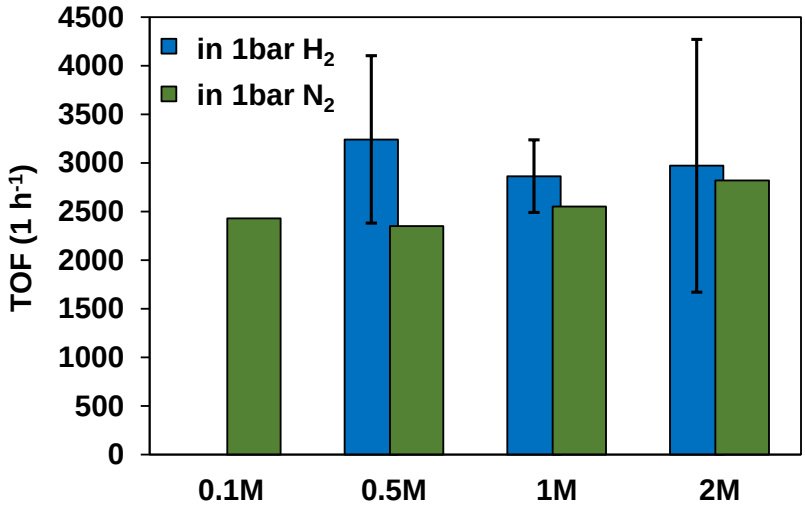

Figure 4.1. Electrocatalytic hydrogenation rates of benzaldehyde (20 mM) at -0.1 V_{RHE} under 1 bar N_2 (green) and 1 bar H_2 (blue) in sodium acetate buffer (pH 5.2) at different ionic strengths ranging from 0.1 M to 0.5 M, 1 M and 2 M. The standard deviations are depicted for the repeated reaction measurements.

Changing the ionic strength from 0.1 M to 2 M in NaOAc/HOAc buffer during electrocatalytic hydrogenation of benzaldehyde did not lead to any significant change in hydrogenation rates under 1 bar N_2 (green) or 1 bar H_2 (blue) as depicted in Figure 4.1. The reaction performed in H_2 exhibited higher hydrogenation rates for all three tested ionic strength solutions compared to the reactions under N_2, which are attributed to additional hydrogenation occurring through dissociatively adsorbed hydrogen.

The effect of ionic strength variation was also studied under thermocatalytic hydrogenation of benzaldehyde at 1 bar H_2. The catalyst (10 mg of 5 wt. % Pd/C) was either thermally reduced in H_2 in a tubular furnace at 523 K for 1 h before transferring it to the buffer solution or the catalyst

was electrochemically reduced in the buffer with a Pt mesh at -40 mA applied for 1 h, while introducing 1 bar H_2 into the slurry. Following the detailed experimental description in section 2.5.1 and 3.5.1, TCH was performed by purging the slurry with 1 bar H_2 for 1 h and taking aliquots for quantification by GC-FID. Thereby, the thermally reduced reactions were performed in a beaker and the electrochemically reduced reaction in the two-compartment batch cell.

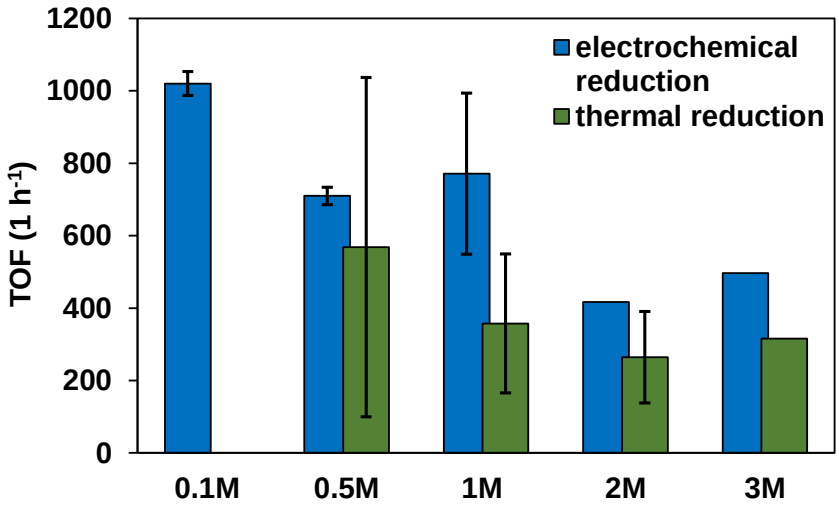

Figure 4.2. Thermocatalytic hydrogenation rates of benzaldehyde (20 mM) at 1 bar H_2 in sodium acetate buffer at various ionic strengths (0.1 M, 0.5 M, 1 M, 2 M and 3 M). Green – thermal prereduction in H_2 of catalyst in tubular furnace at 523 K for 1 h; blue – electrochemical prereduction of catalyst slurry with Pt mesh at -40 mA for 1 h. Standard deviations of the repeated measurements are depicted.

Increasing the ionic strength from 0.1 M to 3 M decreases thermocatalytic hydrogenation rates by up to half (Figure 4.2). This trend was observed for reactions using thermally and electrochemically pre-reduced catalysts (green and blue, respectively). The overall lower rates of the thermally reduced measurements could originate from agglomeration of the Pd particles during the heat treatment or their partial oxidation while transferring them into the buffer solution.

Activation energy measurements were conducted in acetate buffer of 0.5 M and 2 M ionic strength under ECH and TCH conditions (Figure 4.3). The 0.5 M ECH reactions were carried out in 1 bar H_2 while the 2 M ECH reaction were performed in 1 bar N_2. The reactions were performed analogous to the above reported measurements, just changing the reaction temperature for each experiment. For TCH reactions the reduction of Pd/C was done electrochemically.

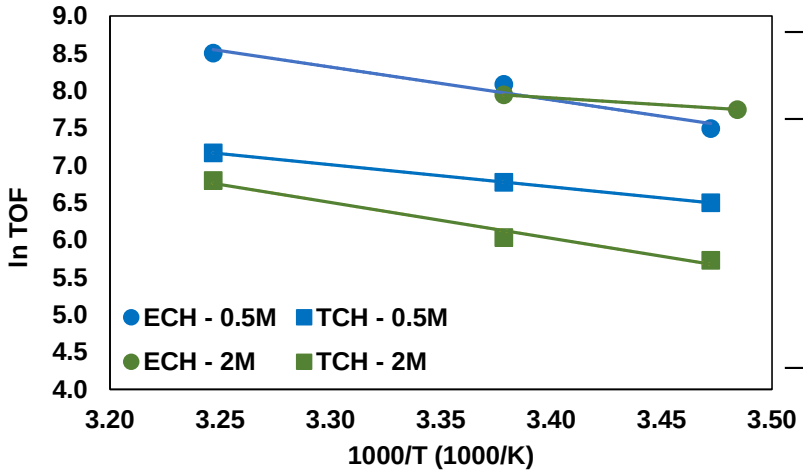

	E_A (kJ mol^{-1})
ECH – 0.5 M (H_2)	37
ECH – 2 M (N_2)	15
TCH – 0.5 M	25
TCH – 2 M	40

Figure 4.3. Activation energies of benzaldehyde hydrogenation in sodium acetate buffer (pH 5.2) with ionic strengths of 0.5 M (in 1 bar H_2) and 2 M (in 1 bar N_2) under applied potential of -0.1V_{RHE} (ECH) and under thermocatalytic hydrogenation with 1 bar H_2 (TCH).

Under ECH measurements, the activation energy in 2 M ionic strength NaOAc/HOAc and 1 bar N_2 shows a value of 15 kJ mol^{-1}, which is line with previous measurements (chapter 3.2.4) performed in 3 M acetate buffer (pH 5.2, 1 bar N_2) and 0.2 M phosphoric acid (pH 1.6, 1 bar N_2) exhibiting E_A of 14 kJ mol^{-1} and 13 kJ mol^{-1}, respectively. The E_A measurements in 0.5 M acetate buffer and 1 bar H_2 revealed a value of 37 kJ mol^{-1}. Assuming a decrease in E_A with higher ionic strength, this would in turn lead to an increase in ECH rates with increasing ionic strength. Higher ionic strength leads to an increase of non-ideality of the system, influencing ground state (GS) and transition state (TS) of the reaction. The ground state is a combination of the chemical potential of adsorbed benzaldehyde and adsorbed hydrogen ($\mu_{GS} = \mu_{BZH} + \mu_{H_3O^+}$). Stronger ionic environment increases μ_{BZH}^{excess} to a greater extent than as it decreases $\mu_{H_3O^+}^{excess}$, leading to an overall destabilization of the ground state. Presuming the proton coupled electron transfer mechanism for ECH, the TS will be charged, thus, more polar than the GS and be stabilized more compared to the GS as ionic strength increases. This would be reflected in a decrease of E_A and enhancement in reduction rates in higher ionic solutions. As this trend is not observed in Figure 4.1, it can be hypothesized that the applied potential influences the GS (and TS to some extent) balancing out any non-ideality influence of the ionic environment and/or the higher experimental error of ECH reactions covers any ionic strength effect. Thus, more reactions are needed to verify the phenomena.

During TCH reactions the activation energies increase from 25 kJ mol^{-1} to 40 kJ mol^{-1} when changing the ionic strength from 0.5 M to 2 M, respectively. The E_A for 0.5 M coincides with the TCH activation energy found in 0.2 M phosphoric acid of 18 kJ mol^{-1} in chapter 3.2.4. The increase in E_A with higher ionic strength explains the drop of hydrogenation rates during TCH with increasing ionic strength (Figure 4.2). As described above, high ionic strength leads to a destabilization of the GS. Under thermocatalytic condition, the transition state (TS) can be assumed to be more non-polar (neutral interaction of adsorbed benzaldehyde with adsorbed hydrogen) than the GS, causing a stronger destabilization, thus, increase of the TS than the GS with increasing ionic environment, explaining the change in E_A.

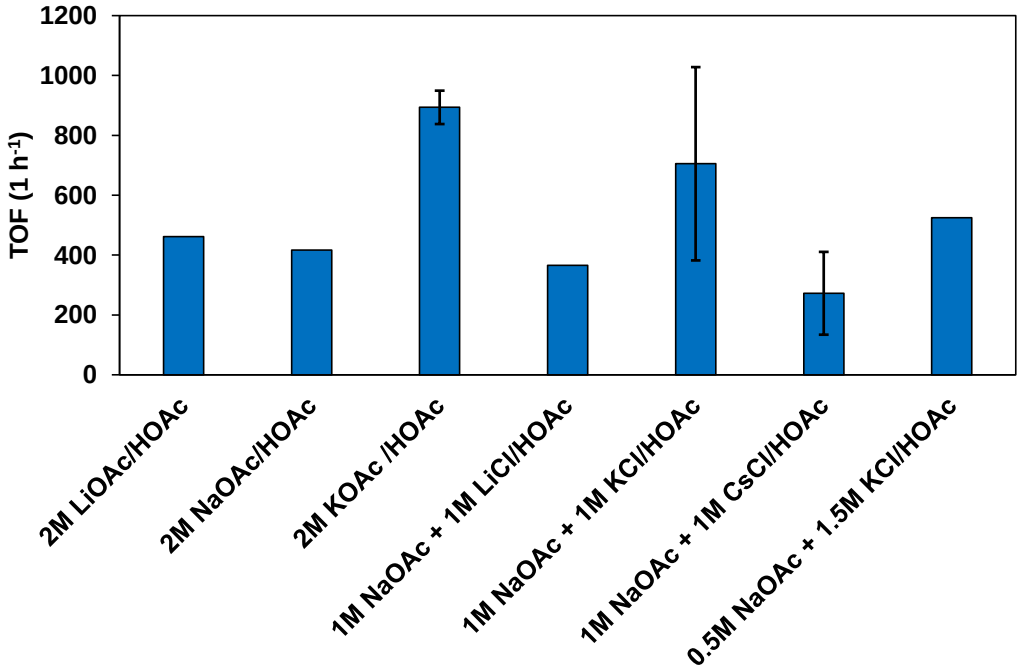

Figure 4.4. Rates of thermocatalytic benzaldehyde hydrogenation (1 bar H_2, 20 mM benzaldehyde) with changing cation species at constant 2 M ionic strength and pH 5.2. Standard deviations of repeated measurements are shown.

In Figure 4.4 the influence of alkali metal cation size on hydrogenation reactions is probed by TCH measurements of benzaldehyde varying the alkali cations in the electrolyte. The experiments were carried out according to the previously described procedure by electrochemically pre-reducing the catalyst and running the TCH reaction at 1 bar H_2 pressure. The acetic acid buffer was kept at 2 M ionic strength and pH 5.2. Only the cations of the acetate were changed (LiOAc/HOAc, NaOAc/HOAc, KOAc/HOAc) or 1 M alkali metal chloride (LiCl, KCl, CsCl) was added to 1 M

NaOAc/HOAc buffer. For the last reaction the ratio of KCl and NaOAc buffer was changed to 1.5 M KCl and 0.5 M NaOAc.

Following the hypothesis of OER and CO_2 reduction experiments, the lowest rates are expected from Li^+ ions, whereas the highest rates are predicted for Cs^+ ions. [3, 5] Figure 4.4 depicts the benzaldehyde TCH rates in acetate buffers with varying cation species. No significant influence of the cations on the reduction rates, except for K^+ containing electrolytes, was observed. Hydrogenation in 2 M potassium acetate buffer leads to highest rates, followed by 1 M sodium acetate with 1 M KCl. Increasing the KCl concentration to 1.5 M and decreasing the acetate buffer concentration to 0.5 M did not further increase the rates. Interestingly, the presence of chloride ions did not seem to effect reaction rates. Plotting the hydrogenation rates against the corresponding alkali metal cation sizes used in the measurements show a volcano like behavior of the rates, where K^+ seems to provide just the right interaction in the electric double layer to stabilize adsorbed reaction intermediates (Figure 4.5). Further repetitions and experiments are required to confirm the results.

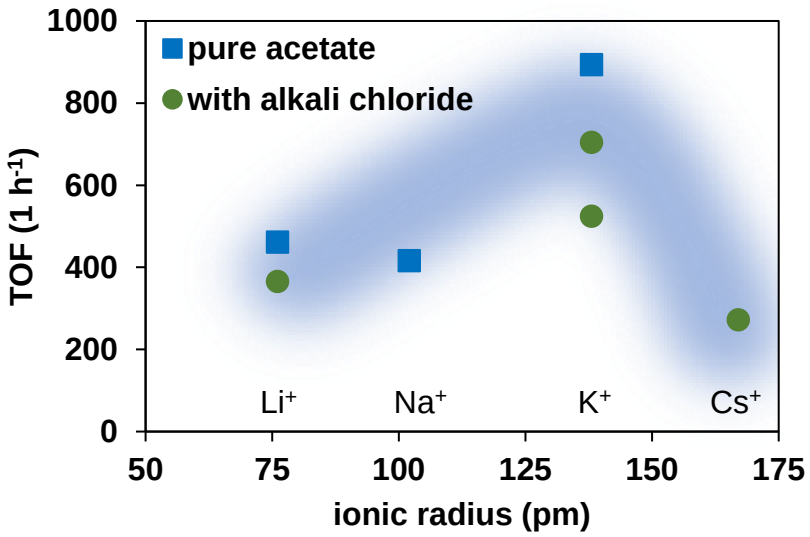

Figure 4.5. Rates of thermocatalytic benzaldehyde hydrogenation at 1 bar H_2 plotted against ionic radii of alkali metal cations used in each reaction of 2 M pure alkali metal acetate buffer or with added 1 M alkali metal chloride. Alkali metal cation radii are taken from Ref. [7].

4.2. References

1. Pfriem, N.; Hintermeier, P. H.; Eckstein, S.; Kim, S.; Liu, Q.; Shi, H.; Milakovic, L.; Liu, Y.; Haller, G. L.; Baráth, E.; Liu, Y.; Lercher, J. A., Role of the ionic environment in enhancing the activity of reacting molecules in zeolite pores. *Science* **2021,** *372* (6545), 952-957.
2. Milaković, L.; Hintermeier, P. H.; Liu, Y.; Baráth, E.; Lercher, J. A., Influence of Intracrystalline Ionic Strength in MFI Zeolites on Aqueous Phase Dehydration of Methylcyclohexanols. *Angewandte Chemie International Edition* **2021,** *60* (47), 24806-24810.
3. Resasco, J.; Chen, L. D.; Clark, E.; Tsai, C.; Hahn, C.; Jaramillo, T. F.; Chan, K.; Bell, A. T., Promoter Effects of Alkali Metal Cations on the Electrochemical Reduction of Carbon Dioxide. *Journal of the American Chemical Society* **2017,** *139* (32), 11277-11287.
4. Singh, M. R.; Kwon, Y.; Lum, Y.; Ager, J. W.; Bell, A. T., Hydrolysis of Electrolyte Cations Enhances the Electrochemical Reduction of CO2 over Ag and Cu. *Journal of the American Chemical Society* **2016,** *138* (39), 13006-13012.
5. Hou, S.; Xu, L.; Ding, X.; Kluge, R. M.; Sarpey, T. K.; Haid, R. W.; Garlyyev, B.; Mukherjee, S.; Warnan, J.; Koch, M.; Zhang, S.; Li, W.; Bandarenka, A. S.; Fischer, R. A., Dual In-situ Laser Techniques Underpin the Role of Cations in Impacting Electrocatalysts. *Angewandte Chemie International Edition n/a* (n/a).
6. Suntivich, J.; Perry, E. E.; Gasteiger, H. A.; Shao-Horn, Y., The Influence of the Cation on the Oxygen Reduction and Evolution Activities of Oxide Surfaces in Alkaline Electrolyte. *Electrocatalysis* **2013,** *4* (1), 49-55.
7. Sugiura, Y.; Saito, Y.; Endo, T.; Makita, Y., Effect of the Ionic Radius of Alkali Metal Ions on Octacalcium Phosphate Formation via Different Substitution Modes. *Crystal Growth & Design* **2019,** *19* (7), 4162-4171.

5. Summary and Conclusion

This thesis aims at providing a general fundamental understanding of electrocatalytic hydrogenation of carbonyl compounds and its correlation with thermocatalytic hydrogenation, where the applied electric potential is replaced by molecular hydrogen. This work showed that kinetic and thermodynamic parameters must be quantified to derive precise mechanisms of electrocatalytic reduction of organic compounds. Accordingly, this work studied the interaction of active metals with the reacting species under applied electric potential as well as the influence of reaction media, i.e., hydronium ion concentration (pH), cation species and concentration (ionic strength).

The results of this work led to a quantitative determination of the influence of molecular structure and applied cathodic potential on rates and selectivity of electrochemical hydrogenation (ECH) by probing the hydrogenation of a series of carbonyl compounds on Pd in aqueous phase. ECH and the concurrent H_2 evolution reaction (HER) rates follow disparate trends with varying applied potentials. Hydrogenation dominates at low overpotential but is surpassed in rate by HER with increasingly negative potential as the electrochemical potential of hydrogen increases and competes for active sites limiting the organic reactant coverage. Combination of spectroscopy, electrochemical characterization, and reaction kinetics revealed that the interaction strength of the organic compounds with Pd correlates with ECH rates in the order cyclohexanone < acetophenone < furfural < benzaldehyde and with the potential at which HER exceeds ECH rates. Particularly, strong interactions are associated with fast hydrogenation kinetics, hindering HER and the formation of H-rich bulk Pd hydride. Thus, the standard free energy of adsorption is the key factor influencing and enabling charge transfer at the metal, hydrogenation, competitive HER and even the state of the Pd bulk. A proton coupled electrons transfer was concluded to play a role in the electrochemical hydrogenation mechanism and to be favored over neutral hydrogen addition.

Increasing hydronium ion concentration in thermocatalytic (open circuit voltage - OCV) and electrocatalytic hydrogenation (using benzaldehyde and acetophenone as reactants) resulted in identical ECH and OCV rate increases i.e., up to four times. Acidic conditions also enabled hydrogenolysis reactions of the alcohol products. This pH effect is concluded to stem from weakening of the Pd-H binding energy with lower pH. The identical effects of hydronium ion

concentration on OCV and ECH conversions, via H binding energy, suggest that the reaction mechanisms are the same under both conditions. This is supported by similar activation energies of benzaldehyde hydrogenation under ECH and OCV and additional kinetic isotope and high-pressure experiments. We conclude that neutral and electrochemical hydrogenation steps are not mutually exclusive, both contribute to hydrogenation regardless of the origin of the reducing equivalents and are affected by hydronium ion concentration. The weakened metal-H bond leads to an easier transfer of hydrogen to the organic compound in case of the neutral mechanism, while for a PCET route the weakened metal-H binding energy shifts the hydrogen equilibrium to the side of the hydronium ion increasing the concentration of reducing equivalents at the outer Helmholtz plane. Fundamentally, the net contributions of both mechanisms depend on the applied potential of the system and on the coverage of hydrogen.

Variations in acetic buffer ionic strength during ECH led to negligible changes in hydrogenation rates, while in OCV reactions a decrease in reduction rates with increasing ionic strength was observed. These effects are explained on basis of the induced non-ideality of the system by the higher ionic strength and additional applied potential, overall destabilizing the ground state to a different extent in both cases and influencing the transition state in opposite directions for ECH and OCV. Changes in the cation size of the acetate buffer during OCV revealed an enhancement of hydrogenation rates with K^+ containing solutions, seeming to provide the right stabilization of adsorbed reaction intermediates.

List of Publications

Meyer, L. C.; Sanyal, U.; Stoerzinger, K.; Koh, K.; Fulton, J. L.; Camaioni, D. M.; Gutiérrez, O. Y.; Lercher, J. A., Influence of Molecular Structure on the Electrocatalytic hydrogenation of Carbonyl Groups and H_2 Evolution on Pd. Prepared for submission.

Cheng, G.*; Meyer, L. C.*; Sanyal, U.; Jentys, A.; Gutiérrez, O. Y.; Lercher, J. A., Role of Hydronium Ions in Electrocatalysis for Controlling and Enhancing Catalytic Hydrogenation in Aqueous Phase. Prepared for submission. (*contributed equally)

Chen, L.; Meyer, L. C.; Kovarik, L.; Meira, D.; Pereira Hernandez, X.; Shi, H.; Gutierrez-Tinoco, O.Y.; Szanyi, J., Disordered, Sub-nanometer Ru Structures on CeO2 are Highly Efficient and Selective Catalysts in Polymer Upcycling by Hydrogenolysis. *ACS Catalysis* 2022, 4618-4627.

Chen, L.; Zhu, Y.; Meyer, L. C.; Hale, L. V.; Le, T. T.; Karkamkar, A.; Lercher, J. A.; Gutiérrez, O. Y.; Szanyi, J., Effect of reaction conditions on the hydrogenolysis of polypropylene and polyethylene into gas and liquid alkanes. *Reaction Chemistry & Engineering* 2022, 7, 844.

Akhade, S. A.; Lee, M.-S.; Meyer, L. C.; Yuk, S. F.; Nguyen, M.-T.; Sanyal, U.; Egbert, J. D.; Gutiérrez, O. Y.; Glezakou, V.-A.; Rousseau, R., Impact of functional groups on the electrocatalytic hydrogenation of aromatic carbonyls to alcohols. *Catalysis Today* 2021, https://doi.org/10.1016/j.cattod.2021.11.047.

Chu, Y.; Sanyal, U.; Li, X. S.; Qiu, Y.; Song, M.; Engelhard, M. H.; Davidson, S. D.; Koh, K.; Meyer, L. C.; Zheng, J.; Xie, X.; Li, D.; Liu, J.; Gutiérrez, O. Y.; Wang, Y.; Shao, Y., Tuning proton transfer and catalytic properties in triple junction nanostructured catalyst. *Nano Energy* 2021, 86, 106046.

Sanyal, U.; Yuk, S. F.; Koh, K.; Lee, M.-S.; Stoerzinger, K. A.; Zhang, D.; Meyer, L. C.; Lopez-Ruiz, J. A.; Karkamkar, A.; Holladay, J. D.; Camaioni, D. M.; Nguyen, M.-T.; Glezakou, V.-A.; Rousseau, R.; Gutiérrez, O. Y.; Lercher, J. A., Hydrogen Bonding Enhances the Electrochemical Hydrogenation of Benzaldehyde in the Aqueous Phase. *Angewandte Chemie International Edition* 2021, 60 (1), 290-296.

Sanyal, U.; Koh, K.; Meyer, L. C.; Karkamkar, A.; Gutiérrez, O. Y., Simultaneous electrocatalytic hydrogenation of aldehydes and phenol over carbon-supported metals. *Journal of Applied Electrochemistry* 2021, 51 (1), 27-36.

List of Presentations

Meyer, L. C.; Sanyal, U.; Cheng, G.; Koh, K.; Gutiérrez, O. Y.; Lercher, J. A., Elucidating the hydrogenation of carbonyl compounds over Pd in aqueous phase under varying pH and potential. Oral presentation, *Northwest Regional Meeting of the American Chemical Society* 2021, Virtual, Western Washington University, Washington, USA.

Meyer, L. C.; Sanyal, U.; Camaioni, D. M.; Stoerzinger, K.; Fulton, J. L.; Gutiérrez, O. Y.; Lercher, J. A., Electrochemical reduction of carbonyl compounds over Pd in aqueous phase: role of interactions between metal and organic substrates. Oral presentation, *26th North American Catalysis Society Meeting* 2019, Chicago, USA.

Meyer, L. C.; Sanyal, U.; Stoerzinger, K. A.; Gutiérrez, O. Y.; Lercher, J. A., Elucidating the reaction networks and mechanisms in electrocatalytic hydrogenation of carbonyl compounds. Oral presentation, *257th American Chemical Society National Meeting & Exposition* Spring 2019, Florida, USA.

Meyer, L. C.; Sanyal, U.; Camaioni, D. M; Gutiérrez, O. Y.; Lercher, J. A., Competition between organic and H3O+ during electrochemical reduction explains efficiencies and high conversion rates of carbonyls on Pd. Poster presentation, *Pacific Coast Catalysis Society Meeting* 2018, Oregon, USA.

Meyer, L. C.; Sanyal, U.; Stoerzinger, K. A.; Gutiérrez, O. Y.; Lercher, J. A., Elucidating the reaction networks and mechanisms in electrocatalytic hydrogenation of carbonyl compounds. Oral presentation, *73rd Northwest Regional Meeting of the American Chemical Society* 2018, Pacific Northwest National Laboratory, Washington, USA.